

„Synthesis and Investigation of Phase-pure M1 MoVTaNbO_x Catalysts for Selective Oxidation of Propane to Acrylic Acid”

vorgelegt von
Dipl.- Ing. Chemikerin
Almudena Celaya Sanfiz
aus Lugo (Spanien)

Von der Fakultät II – Mathematik und Naturwissenschaften
der Technischen Universität Berlin
zur Erlangung des akademischen Grades
Doktorin der Ingenieurwissenschaften
- Dr. Dipl.-Ing. -

genehmigte Dissertation

Promotionsausschuss:

Vorsitzender:	Prof. Dr. R. Schomäcker
Berichter/Gutachter:	Prof. Dr. R. Schlögl
Berichter/Gutachter:	Prof. Dr. M. Lerch

Tag der wissenschaftliche Aussprache: 30. Mai 2008

Berlin 2008
D 83

Danksagung

Die vorliegende Arbeit wurde in der Zeit von Januar 2004 bis Dezember 2007 in der Abteilung Anorganische Chemie am Fritz-Haber-Institut der Max-Planck-Gesellschaft in Berlin und während zweier Aufenthalte am Combinatorial Technology and Catalysis Research Centre (COMBICAT), University Malaya in Kuala Lumpur/Malaysia angefertigt. Bei allen, die mich in dieser Zeit unterstützt und so zum Entstehen dieser Arbeit beigetragen haben, möchte ich mich herzlich bedanken.

Zunächst möchte ich den beiden Gutachtern dieser Arbeit danken, Prof. Dr. Robert Schlögl für die interessante Themenstellung und seine Unterstützung durch hilfreiche Anmerkungen und Diskussionen und Prof. Dr. Martin Lerch für seine Bereitschaft, diese Arbeit zu begutachten.

Prof. Dr. Reinhard Schomäcker danke ich, dass er sich so schnell bereit erklärt hat, den Vorsitz des Promotionsausschusses zu übernehmen.

Mein besonderer Dank gilt auch Dr. Annette Trunschke für die gute Zusammenarbeit, Motivation und Förderung und für ihre stete Diskussionsbereitschaft und konstruktive Kritik.

Weiterhin möchte ich all denen danken, die durch ihre Zusammenarbeit und ihre Unterstützung diese Arbeit ermöglicht haben: Dr. Andreas Furche für die thermogravimetrischen Analysen; Frau Dodo Lee für die Hilfe bei der Präparation am COMBICAT; Dr. Eva Rödel für die EXAFS-Untersuchung; Frau Edith Kitzelmann für die XRD Messungen; Dr. Frank Girgsdies für die Phasenzusammensetzungsanalysen (XRD&TOPAS); Frau Gisela Lorenz für die zahlreichen BET Messungen; Dr. Ming-Hong Looi und Dr. Sharifah B. A. Hamid für die katalytische Untersuchung am COMBICAT; Herr Peter Schnörch und Dr. Detre Teschner für die *in-situ* XPS Experimente; Dr. Olaf Timpe für die außergewöhnlichen chemischen Ideen und die vielen anregenden Diskussionen und Dr. Thomas W. Hansen für die Analysen der Mikrostruktur (TEM), der elementaren Zusammensetzung (EDX) und der Morphologie (SEM) der Katalysatoren.

Den jetzigen und ehemaligen Mitgliedern der Arbeitsgruppe „Präparation“ sowie allen Mitarbeitern der Abteilung Anorganische Chemie danke ich für die angenehme Arbeitsatmosphäre und die kontinuierliche Unterstützung.

Desde luego, llego al final de este doctorado gracias al gran apoyo y ayuda recibida de Philipp, y como no al cariño y al soporte moral que me otorgan mi madre y mis hermanos. Igualmente, quiero agradecer a mis dos amigas incondicionales de Berlín Maria y Georgia por sus ánimos constantes y su alegría contagiosa.

Synthesis and Investigation of phase-pure M1 MoVTaNbO_x Catalysts for Selective Oxidation of Propane to Acrylic Acid

by Almudena Celaya Sanfiz

Abstract

Hydrothermal synthesis of MoVTaNbO_x catalysts has been investigated. It has been shown that the phase composition of the crystalline catalyst strongly depends on the conditions of the hydrothermal process. The X-ray amorphous product of the hydrothermal synthesis shows a long-range order of structural motifs in [001] direction. Subsequent heat treatment of the precursor in inert atmosphere leads to crystallization. The target structure is an orthorhombic bronze-like structure, denominated as M1. M1 phase has been associated with high activity and selectivity in the direct oxidation of propane to acrylic acid. Other phases formed are, e.g. the orthorhombic M2 phase (isostructural to KW₃O₉ phase), Mo₅O₁₄, V_{0.95}Mo_{0.97}O₅ and TeMo₅O₁₆. Independent of the technical parameters of the autoclave used, phase-pure M1 has been successfully synthesized by optimization of the hydrothermal conditions (e.g. temperature and reaction time). As evidenced by SEM/EDX, precursor materials of M1 catalysts are characterized by a fairly homogeneous distribution of the elements and a significant higher Nb-content compared to that reported in the literature. According to EXAFS analysis, Nb is located into pentagonal bi-pyramidal units but also into octahedral coordinated positions, which is in contradiction to the established structural model. Furthermore, it was shown by XRD and TG/MS that the presence of ammonium containing phases in the precursor leads to the formation of phase mixture after the heat treatment.

Additionally, the impact of phase composition on the catalytic behavior of hydrothermally prepared MoVTaNbO_x catalysts in the selective oxidation of propane to acrylic acid has been investigated. Phase cooperation of M1 and M2 phase was not found in this contribution. For phase-pure M1 catalysts, the propane conversion increases with increasing the specific surface area. Other properties, such as chemical composition and aspect ratio of the needle-like M1 crystallites may influence the catalytic activity as well. In the present study the role of the (001) plane of the M1 phase in the propane oxidation is addressed by providing a M1 model catalyst that exposes preferentially this plane.

The molecular structure and dynamic nature of the active moiety on the M1 surface under conditions of propane oxidation, is the key for understanding the catalytic behaviour of these catalysts. X-ray photoelectron spectroscopic experiments in presence of the reactants propane, oxygen and water indicated re-distribution of the elements at the catalyst surface, in response to changes in the gas mixture. Furthermore, phase-pure M1 showed a reasonable stability under reaction conditions in laboratory-scale experiments, which is of a great importance for their potential industrial application.

The composition of multi-metal oxide catalysts has been varied. Metal substitution and/or addition of suitable diluents to the Mo-V-X-Nb (X=Te, P, Bi) oxides has been performed. The catalysts have been investigated in the selective oxidation of propane to acrylic acid. The results underlined the exceptional role of M1 phase. On the other hand, it has been proven that M1 is not necessarily required for acrylic acid formation.

*MoVTaNbO_x Katalysatoren für die selektive Oxidation von Propan zu Acrylsäure
Synthese und Untersuchung von phasenreinem M1*

vorgelegt von Almudena Celaya Sanfiz

Zusammenfassung

Die Hydrothermalsynthese von MoVTaNbO_x Katalysatoren ist untersucht worden. Es hat sich gezeigt, dass die Phasenzusammensetzung des kristallinen Katalysators stark von den Bedingungen des Hydrothermalprozesses (Temperature, Reaktionszeit) abhängt. Das Diffraktogramm des amorphen Syntheseprodukts (Precursor) zeigt, dass bereits hier eine langreichweitige Ordnung von strukturellen Elementen in [001] Richtung vorliegt. Die anschließende Temperung des Precursors in inerter Atmosphäre führt zur Kristallisation. Die Zielstruktur ist eine orthorhombische, bronzartige Phase, die als M1 bezeichnet wird und die mit der hohen Aktivität und Selektivität von MoVTaNb-oxid Katalysatoren in der direkten Oxidation von Propan zu Acrylsäure in Verbindung gebracht wird. Andere Phasen, die gebildet werden, sind z. B. die orthorhombische M2 Phase (isostrukturell mit KW₃O₉), Mo₅O₁₄, V_{0.95}Mo_{0.97}O₅ und TeMo₅O₁₆. Wie mittels SEM/EDX gezeigt, zeichnen sich Precursor Materialien von M1 Katalysatoren durch eine homogene Verteilung der Elemente und einen, im Vergleich zu Literaturangaben, erhöhten Nb-Gehalt aus. Basierend auf der EXAFS Analyse von phasenreinem M1 liegt Nb sowohl in pentagonal bipyramidaler Koordination, als auch oktaedrisch koordiniert vor, was im Widerspruch zu publizierten Strukturmodellen steht. Außerdem wurde durch XRD und TG/MS gezeigt, dass die Anwesenheit von ammoniumhaltigen Phasen im Precursor zur Bildung von Phasengemischen während der thermischen Behandlung führt.

Desweiteren ist der Einfluss der Phasenzusammensetzung auf die katalytischen Eigenschaften von hydrothermal hergestellten MoVTaNbO_x Katalysatoren in der Oxidation von Propan zu Acrylsäure untersucht worden. Eine Kooperation zwischen M1 und M2 Phase wurde in diesem Beitrag nicht gefunden. Für phasenreine M1 Katalysatoren, nimmt der Propanumsatz mit der Erhöhung der spezifischen Oberfläche zu. In der vorliegenden Untersuchung wird die Rolle der (001) Netzebene der M1-Phase in der Propanoxidation untersucht. Dazu wurde ein Modellkatalysator hergestellt, bei dem vorzugsweise (001) Ebenen exponiert sind, während die Seitenflächen der Nadeln mit SiO₂ passiviert wurden. Die Kenntnis der molekularen Struktur und der dynamischen Eigenschaften der M1 Oberfläche unter den Bedingungen der Propanoxidation ist der Schlüssel, um das katalytische Verhalten dieser Katalysatoren zu verstehen. Photoelektronenspektroskopische Experimente in Anwesenheit von Propan, Sauerstoff und Wasser zeigten, dass sich die chemische Zusammensetzung der Oberfläche stark von der des Volumens unterscheidet und dass diese darüber hinaus von der Zusammensetzung der Gasphase abhängt. Außerdem ist phasenreines M1 in der Propanoxidation über 50 Stunden stabil, was von Bedeutung für eine potentielle industrielle Anwendung des Katalysators ist.

Desweiteren wurde die Zusammensetzung der Multimetalloxidkatalysatoren variiert und SiO₂, ZrO₂, und Cr₂O₃ als Verdünnungsmittel zu MoVXNbO_x (X=Te, P, Bi) zugegeben. Die Katalysatoren wurden in der Oxidation von Propan zu Acrylsäure getestet. Die Ergebnisse unterstreichen die außergewöhnliche Bedeutung der M1 Phase für die selektive Aktivierung von Propan. Andererseits konnte gezeigt werden, dass die kristalline M1-Phase für die Acrylsäurebildung nicht notwendigerweise erforderlich ist.

List of Abbreviations

<i>ab</i> plane	(001) plane
at.- %	atome percentage
BESSY	Berliner Elektronenspeicherring – Gesellschaft für Synchrotronstrahlung
BET	Brunauer, Emmett and Teller method
<i>c</i> direction	[001] direction
$\Delta_f H^\circ$	standard enthalpy of formation
E_a	activation energy
EDX	Energy Dispersive X-ray Analysis
EXAFS	Extended X-ray Absorption Fine Structure
FT	Fourier Transform
GHSV	Gas Hour Space Velocity
HRTEM	High Resolution Transmission Electron Microscopy
HPCs	Heteropoly Compounds
i. d.	internal diameter
i. e.	that is
ICP	Inductively Coupled Plasma
ICSD	Inorganic Crystal Structure Database
IR	Infrared spectroscopy
JEMS	Jet Engine Maintenance Simulator
LEIS	Low Energy Ion Scattering
MS	Mass Spectrometry
m/e	mass/charge ratio

MMOs	multi-metal oxides
p	pressure
rpm	revolutions per minute
SEM	Scanning Electron Microscopy
S_l	specific surface area of the lateral of the needles
S_s	specific surface area of the cross-section of the needles
STP	Standard Temperature and Pressure
T	temperature
TCD	Temperature Control Device
TEM	Transmission Electron Microscopy
TG	Thermogravimetry
$t_{\text{synthesis}}$	time of synthesis
UV/VIS	Ultraviolet/Visible Spectroscopy
vol.-%	volume percentage
vs	very strong
vs.	versus
w	weak
XAFS	X-ray Absorption Fine Structure
XAS	X-ray Absorption Spectroscopy
XPS	X-ray Photoelectron Spectroscopy
XRD	X-ray Diffraction

Table of content

INTRODUCTION	1
1 Catalysis	1
1.1 Basic concepts	1
1.2 Catalytic oxidation of hydrocarbons	4
2 Acrylic acid	5
2.1 Applications and demand.....	6
2.2 Industrial manufacture.....	7
2.3 Future Technologies	8
3 Mo-V-Te-Nb mixed oxide catalyst	9
3.1 Historical development.....	10
3.2 Bulk structure of Mo-V-Te-Nb mixed oxides.....	10
3.3 Synthesis methods.....	12
3.3.1 <i>Precipitation-evaporation method (dry-up method)</i>	13
3.3.2 <i>Hydrothermal synthesis</i>	13
4 Motivation and Objectives	14
5 References.....	17
CHAPTER 1- Preparation of phase-pure M1 Mo-V-Te-Nb oxide catalysts by hydrothermal synthesis – Influence of reaction parameters on the structure and morphology.....	20
Abstract.....	20
1 Introduction	21
2 Experimental.....	24
2.1 Preparation of Mo-V-Te-Nb mixed oxides	24
2.2 Characterization	26
3 Results and discussion	28
3.1 Molecular species in the initial suspension.....	28
3.2 Hydrothermal synthesis.....	34
3.3 Homogeneity and microstructure of the precursor materials.....	41
3.4 Development of short-range order during hydrothermal synthesis and activation	42

3.5	Post-treatment of multi-phase precursors	45
3.6	Activation	46
4	Summary and conclusions.....	48
5	Acknowledgments	50
6	References.....	50
CHAPTER 2- Investigation of catalytic behavior of M1-phase catalyst in the selective oxidation of propane to acrylic acid. Correlation approach between catalytic performance and surface/bulk properties.....		
	Abstract.....	54
1	Introduction	55
2	Experimental.....	58
2.1	Catalysts preparation.....	58
2.2	Activity measurements	59
2.3	Catalysts characterization	59
3	Results	61
3.1	General properties of the Mo-V-Te-Nb mixed oxides.....	61
3.2	Selective oxidation of propane	62
3.3	Characterization of phase-pure M1 catalysts	65
3.3.1	<i>Morphology and shape analysis</i>	65
3.3.2	<i>Microstructure</i>	68
3.3.3	<i>Elemental dynamics and composition at the catalytic surface</i>	70
3.3.4	<i>Properties of the phase-pure catalysts after propane oxidation</i>	73
4	Discussion and conclusions.....	75
5	Acknowledgments	81
6	References.....	81
CHAPTER 3- How important is the (001) plane of M1 for selective oxidation of propane to acrylic acid		
	Abstract.....	84
1	Introduction	85
2	Experimental.....	87
2.1	Preparation of M1	87
2.2	Silylation of M1	88

2.3	Activity measurements	89
2.4	Catalysts characterization	89
3	Results	92
3.1	Silylation of M1	93
3.2	Phase composition of the Mo-V-Te-Nb oxides	95
3.3	Microstructure of the model catalysts.....	96
3.4	Catalytic properties of the model catalysts in propane oxidation	101
3.5	LEIS after catalysis.....	102
4	Discussion	104
5	Conclusions.....	110
6	Acknowledgments	111
7	References	111
CHAPTER 4- New synthesis routes of MMO catalysts by dilution of Mo-V-X-Nb (X=Te, Bi, and P) mixed oxides with SiO ₂ , Cr ₂ O ₃ or ZrO ₂ for the oxidation of propane to acrylic acid.		114
	Abstract.....	114
1	Introduction	115
2	Experimental.....	118
2.1	Catalysis preparation	118
2.2	Activity measurements	121
2.3	Catalyst characterization	121
3	Results	122
3.1	Bulk structure of precursors and catalysts	122
3.2	Catalytic performance.....	133
4	Discussion	138
5	Conclusion.....	147
6	Acknowledgments	150
7	References	150
CONCLUSION AND OUTLOOK		153
APPENDIX		157
	Curriculum Vitae.....	157
	Publication Index.....	159

INTRODUCTION

Steady increase of demand for manufactured products implicates a rise of world production of chemical intermediates. High amount of these valuable intermediates are industrially manufactured by means of chemical processes involving olefins. Since the raw materials constitute a large portion of the cost of production of the most commodity chemicals, low cost and abundant starting materials are of high importance. Therefore, the potential utilization of alkanes, which are more abundant and cheaper than the corresponding olefins, as feedstock in the industrial production of the organic chemicals, has recently generated a high interest. However, it is well-known that saturated hydrocarbons have a lower reactivity than unsaturated hydrocarbons, because of the little polarity of their C-H bonds and the absence of high polarizability associated with the π -bonding of the olefins. Design and development of new types of solid catalyst capable to activate and convert alkanes into desirable oxygen containing compounds in a selective manner at reasonable temperatures are therefore, challenging tasks.

1 Catalysis

Catalysis plays a remarkable role in industrial and environmental chemistry. More than 60% of all chemical products (including fuels, commodity and fine chemicals) and 90% of chemical processes are based on catalysis.

1.1 Basic concepts

In a reacting chemical system, two considerations are of importance: (i) the maximum attainable yield of products under specified conditions (chemical equilibrium), which is

matter of chemical thermodynamics and (ii) the rate of the reaction, i.e. how fast the equilibrium situation is attained. The answer of the last consideration is the concern of chemical kinetics. A chemical process is economically feasible if both, yields and rates are favorable. It is well-known that the rates of many chemical reactions can be affected by the presence of “alien” material – not included in the stoichiometric equation of the reaction. This material is denominated as catalyst and it is defined as *a substance which increases the rate* (i.e. the rate coefficient) *at which a chemical reaction approaches equilibrium, without being consumed in the process* (excluding physical deterioration and/or deactivation during use). As described either by the collision theory or by the transition-state theory [1], this phenomenon occurs by lowering the activation energy of the catalyzed reaction due to interaction with the catalyst (**Figure 1**). Lower activation energies and/or higher selectivities are achieved when the reactants find different pathways across the potential barrier separating them from the product state. Accordingly, a catalyst also has the effect of lowering the temperature at which a given rate is achieved, which is of a great advantage for many practical applications.

In heterogeneous catalysis the catalyst is in a different phase than the reactants, being the material state of the catalyst usually solid. The interaction between the reactants and the solid occurs on the surface of the catalyst. Therefore, heterogeneous catalysis is related to the specific chemical properties of the surface of the catalyst. However, the surface properties are determined by the chemistry of the bulk solid, and some useful insight into the catalytic activities of surfaces is also gained from knowledge of the bulk properties of the solid.

The chemical interaction during chemisorption of the reacting molecule on the surface of the catalyst lowers the activation energy that is needed in the non-catalyzed reactions. Two basic possible mechanisms are known in heterogeneous catalysts, depending on the mode of adsorption of the reactants: (i) Langmuir-Hinshelwood mechanism, which proposes that both reactants adsorb and the adsorbed reactants react on the surface of the catalyst, and (ii) Eley-Rideal mechanism, which proposes that only one reactant adsorbs and the other reacts with it directly, without adsorbing. One or more of the reactants diffuse to the catalyst surface and chemisorb on the active centers of the surface. Balanced bond strength in the adsorbate complex leads to activation and product formation by rearrangement of chemical bonds without poisoning the catalyst surface. Finally, products desorb and diffuse through the pore system away from the solid surface. The described mass transport of reactants and products from one phase to another can sometimes be the limiting step of the reaction.

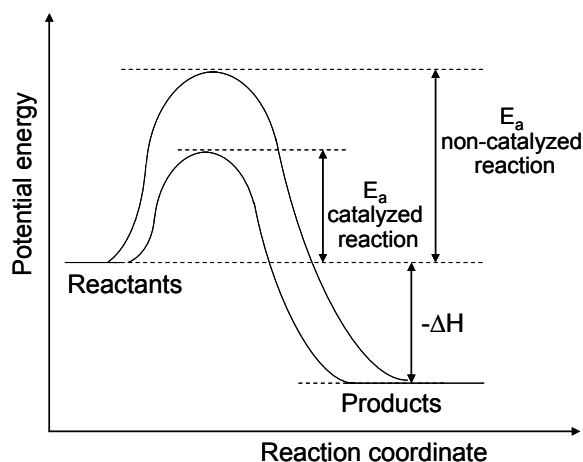


Figure 1. Potential-energy profile for an exothermic reaction, showing the lower activation energy of the catalyzed reaction.

1.2 Catalytic oxidation of hydrocarbons

Selective catalytic oxidation is a common method of functionalizing hydrocarbon molecules. In the chemical industry more than 60 % of the products obtained by catalytic routes are products of oxidation. Basically all monomers used in manufacturing artificial fibers and plastics are obtained by selective catalytic oxidation processes. Oxidation is not only essential in the production of a wide range of materials needed in the modern society but also in the removal of undesired by-products. Environmental pollution control may be achieved, e. g., by total catalytic oxidation.

In the particular case of selective oxidation of hydrocarbons involving metal oxide based catalyst, one possible reaction mechanism is the Mars and van Krevelen mechanism [2]. According to this mechanism, the oxidation of adsorbed hydrocarbons proceeds through lattice oxygen leaving reduced metal sites. The regeneration of the lattice oxygen vacancies occurs via reoxidation with molecular oxygen of the gas feed. Consequently, selective oxidation reaction is a dynamic process with respect to the catalyst. As far as the organic molecule is concerned, usually one or several H atom abstractions, O atom insertions and electron transfers are involved. Generally, the catalysts appropriate for selective oxidation reactions have the following common properties, summarized as the so-called “7 pillars” of the selective oxidation catalysis [3]:

- (i) lattice oxygen,
- (ii) metal-oxygen bonds,
- (iii) host structure,
- (iv) redox properties,
- (v) multifunctional active sites,

- (vi) site isolation and
- (vii) cooperation of phases.

Lattice oxygen, $[O^{2-}]$ (i), is more nucleophilic (less oxidizing power) than molecular oxygen delivered from the gas phase, reacting more selectively. The strength of the metal-oxygen bond (ii) of active oxygen determines the oxidizing power of lattice oxygen, being the intermediate strength the appropriate for selective oxidation. The host structure (iii) accommodates the appropriate metal-bond strength and the lattice oxygen, permitting the transfer of the electrons and vacancies as well as lattice oxygen diffusion. Once the lattice oxygen oxidizes the adsorbed hydrocarbon, the remaining reduced catalyst has to be re-oxidized (iv). Generally, the resulting vacancy is replenished via dioxygen of the gas phase, completing thus the redox cycle. The reactive surface lattice oxygen has to be isolated in defined groupings (vi) to achieve selectivity, and to avoid total combustion. As above-mentioned several functions are involved in the catalytic cycle: chemisorption of the reactant, abstraction of hydrogen, insertion of oxygen and desorption of the product. Therefore, multifunctionality of the active sites (v) of these catalysts is important. In case that the host structure of a single phase catalyst cannot incorporate such functions, intimate phase cooperation (vii) is required.

2 Acrylic acid

Acrylic acid is a widely used monomer for polymerization and its demand increases every year. Currently, acrylic acid is industrially produced by a two-stage oxidation process starting from propylene. Replacement of propylene by propane may provide an economic alternative for this commercial process. However, catalysts that are active and

selective enough to make this challenging process, reasonable from an economic point of view, have not yet been found.

2.1 Applications and demand

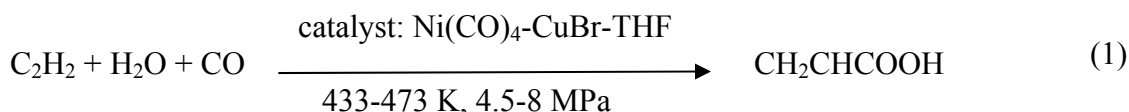
Acrylic acid, $\text{CH}_2=\text{CHCOOH}$, is the simplest unsaturated carboxylic acid possessing both a double bond ($-\text{C}=\text{C}-$) and a carboxyl group ($-\text{COOH}$).

Crude acrylic acid (99.7-99.8 % purity) is manufactured in a two stage oxidation process starting from propylene. By-products formed are maleic anhydride, propionic acid, acetic acid, furfural and sometimes traces of allyl acrylate and benzaldehyde. Crude acrylic acid is used in the production of commodity acrylates including methyl, ethyl, n-butyl, and 2-ethylhexyl acrylates. These acrylates are used to produce, e.g., coatings, adhesives, sealants, textiles, fibres, varnishes and polishes. Both crystallization and distillation are applied to purify crude acrylic acid. In its pure form, acrylic acid is a clear, colorless liquid with a characteristic acrid odor, presenting the following chemical properties: melting point at 285 K, boiling point at 412 K and $\Delta_f H^\circ_{\text{gas}} = -330.7 \pm 4.2 \text{ kJ}\cdot\text{mol}^{-1}$ [4]. Glacial acrylic acid normally contains about 200 ppm of methyl ethyl hydroquinone to prevent polymerization during storage and transportation. Acrylic acid in its glacial form is used to produce homo- and copolymers of acrylic and methacrylic acid (“polyacrylic acid”), superabsorbent polymers (based on sodium polyacrylate) and detergent co-builders (chelating agents for the removal of alkaline earth ions).

The global crude acrylic acid market reached around 3.2 million tons by the end of 2005. Since 1999, the market has grown at an average annual rate of around 4.6 percent. The forecast global demand growth lies in the range of 3.4 percent.

2.2 Industrial manufacture

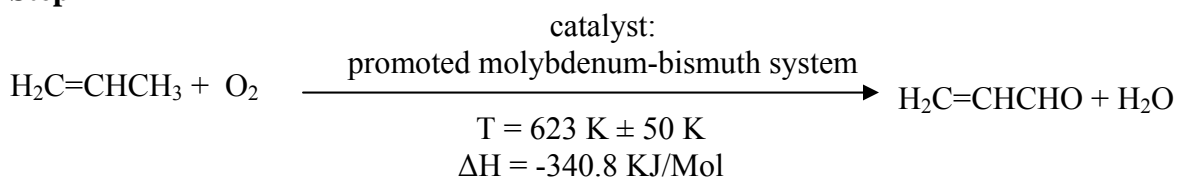
Acrylic acid synthesis dates back to the mid nineteenth century. However, the large scale production of acrylic acid did not begin until the 1930s. Acrylic acid has been produced in commercial processes starting from acetylene, ethylene or propylene, respectively. In the last century, acrylic acid was mainly manufactured by means of an acetylene-based process (1) developed by Reppe in the 1930s in Germany and commercialized by the BASF in Ludwigshafen, Germany, in the 1950s.

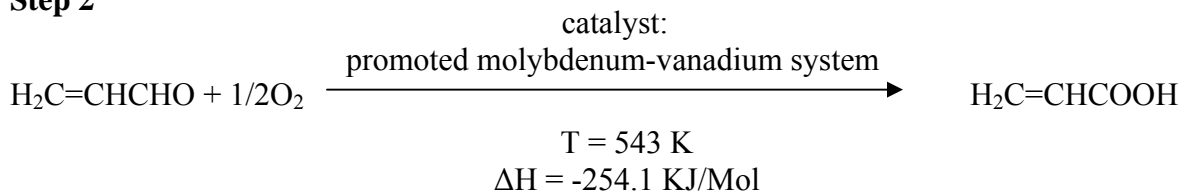


The BASF plant at Ludwigshafen, Germany, was the last acetylene-based acrylic acid plant to close in the 1990s, with the start-up of a new propylene-based plant in Antwerp, Belgium.

Today, acrylic acid is manufactured worldwide from propylene in two steps via acrolein in a gas phase oxidation process. The first stage is the oxidation of propylene to acrolein using promoted molybdenum-bismuth catalyst (promoters, e.g., Fe, Co, W, and Pt) at a reaction temperature of about $623 \text{ K} \pm 50 \text{ K}$. In the second stage, acrolein is passed over a promoted molybdenum-vanadium oxide catalyst (promoters, e.g., W, Cu, Sn, and Sb) at lower temperatures of about 543 K . The two oxidation steps are strongly exothermic.

Step 1



Step 2

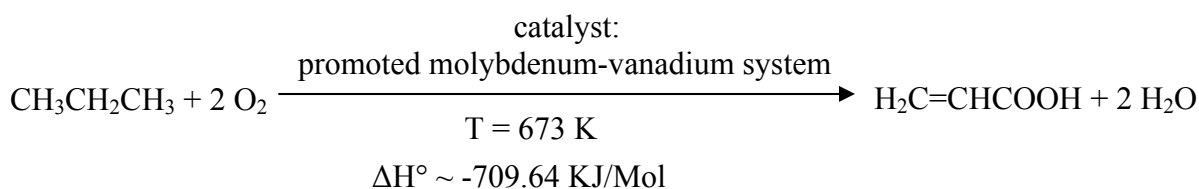
There is considerable variation in plant design. Reactors can be of tandem (two reactors in series) or combination design. In the latter case, the reactor consists of one tube sheet divided into two reaction zones operating under different conditions. The overall acrylic acid yield reaches 87 % [5]. Producers of acrylic acid are e. g., BASF, Rohm & Haas, Dow and Nippon Shokubai.

2.3 Future Technologies

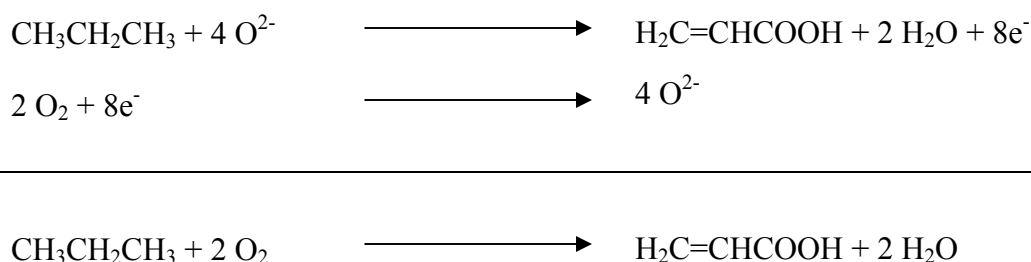
Current research activities are directed to substitute propylene as feedstock in the production of acrylic acid, focusing on the following processes:

- biotransformation processes (e.g., using lactic acid as an intermediate)
- oxidation of propane via propylene (oxidative dehydrogenation) and acrolein (three stage process), or
- direct oxidation of propane to acrylic acid in one step.

Due to the evident attractiveness of using propane as raw material, particularly, the latter pathway appears as potential route to acrylic acid in the future.



However, the direct catalytic oxidation of propane provides numerous challenges that face the further technical and commercial process development. Development of an efficient catalyst for this reaction is one of the major problems. The main difficulty regarding the selective conversion of propane is related to its low reactivity. Without proper catalysts, activation of propane needs significantly high temperatures (about 773 K). However, at such high temperatures, acrylic acid is not stable and totally oxidized products (CO_x) are obtained. The catalyst should activate stable C-H bonds of the saturated hydrocarbon at relatively low temperatures and selectively transform it into the desired oxygenated product avoiding its further oxidation. Furthermore, this reaction requires the transfer of more electrons (8 vs. 6) or oxygen atoms (4 vs. 3), as compared to the oxidative reaction starting from propylene.



Several types of catalysts, such as vanadium phosphorous oxides (VPO), heteropoly compounds (HPCs), and multi-component mixed oxides (MMOs) [6-8] have been investigated for this reaction.

3 Mo-V-Te-Nb mixed oxide catalyst

Reducible mixed metal oxides catalysts are currently the most promising catalytic materials for the selective oxidation of propane to acrylic acid. Among them, Mo-V-Te-

Nb mixed metal oxides, originally patented by Mitsubishi, achieve the maximum yields of acrylic acid of about 50 % [9].

3.1 Historical development

The application of mixed metal oxides as catalysts for propane oxidation to acrylic acid began in the late 1970s with Mo-V-Nb mixed oxides, previously reported as a catalyst for ethane oxidation [10]. Propane could be activated at 573 K producing only acetic acid, acetaldehyde, and carbon oxides. In 1993, Te was incorporated into the system and the patent concerning use of this system for ammoxidation of propane was published by Mitsubishi. In **Table 1**, several MMO catalysts applied in the oxidation of propane are shown. The highest yields have been obtained with Mo-V-Te-Nb mixed oxides.

Table 1
Propane oxidation over MMO catalysts

Catalyst	T _{Reaction} [K]	X _{C₃H₈} [%]	S _{AA} [%]	Y _{AA} [%]	Reference
BiMo ₁₂ V ₅ Nb _{0.5} SbK _{0.5} O _x	673	18	28	5	11
Mo ₁ V _{0.3} Te _{0.23} Nb _{0.12} O _n	653	84	63	53	12
Mo ₁ V _{0.3} Te _{0.23} Nb _{0.12} O _n	653	80	60	48	9, 13
Mo ₁ V _{0.3} Te _{0.23} Nb _{0.12} O _n	663	71	59	42	14
Mo ₁ V _{0.44} Te _{0.10} O _n	653	36.2	46.6	17	15
Mo ₁ V _{0.25} Te _{0.11} Nb _{0.12} O _n	653	33.4	62.4	21	15
Mo ₁ V _{0.3} Sb _{0.16} Nb _{0.05} O _n	653	50	32	16	16
Mo ₁ V _{0.3} Sb _{0.01} Nb _{0.1} O _n	673	39-40	43-42	17	17
Mo ₁ V _{0.3} Sb _{0.25} Nb _{0.12} K _{0.013} O _n	693	39	64	25	18
Mo ₁ V _{0.18} Sb _{0.15} K _{0.005} O _n	653	27	31	8.4	19
Ni ₁ Mo _{1.51} Te _{0.01} P _{0.02} O _x	733	12	23	3	20, 21
Te-Ni-Mo-O	693	40	41	16	22

3.2 Bulk structure of Mo-V-Te-Nb mixed oxides

Mo-V-Te-Nb oxide catalysts consist of mainly two orthorhombic phases, denoted as M1 (ICSD [55097], [23]) and M2 (ICSD [55098], [23]) [24], which are isostructural with

$\text{Cs}_{0.7}(\text{Mo}_{2.3}\text{Nb}_{2.7})\text{O}_{14}$ and KW_3O_9 , respectively. Both structures consist of basically the same layered structure [23], in which networks of corner-shared MO_6 ($\text{M}=\text{Mo}$, V , (Nb)) octahedra form slabs in the ab plane. The slabs are also connected by corner oxygen atoms forming linear infinite chains of octahedra along the c direction (**Figure 2a**). However, the arrangement of octahedra in the ab plane differs between both structures. In the M1 structure (**Figure 2b**), the network of MO_6 ($\text{M}=\text{Mo}^{5+}$, Mo^{6+} , V^{4+} , V^{5+}) octahedra generates pentagonal, hexagonal and heptagonal rings. The hexagonal and the heptagonal rings are reported to be partially occupied (80 % and 20 %, respectively) by TeO (Te^{4+} with a lone pair of electrons) units. Niobium (Nb^{5+}) has been reported to be exclusively located in the center of the pentagonal bipyramids. In the M2 structure (**Figure 2c**) the arrangement of octahedra in the ab plane is simpler. All MO_6 ($\text{M}=\text{Mo}^{6+}$, V^{4+} , Nb^{5+}) octahedra are corner sharing forming hexagonal rings, which are fully occupied by TeO units. Lattice parameters and formula of the unit cell of both structures are shown in the **Figure 2**. The M1 structure is richer in Te than M2, while M1 is especially poor in Nb.

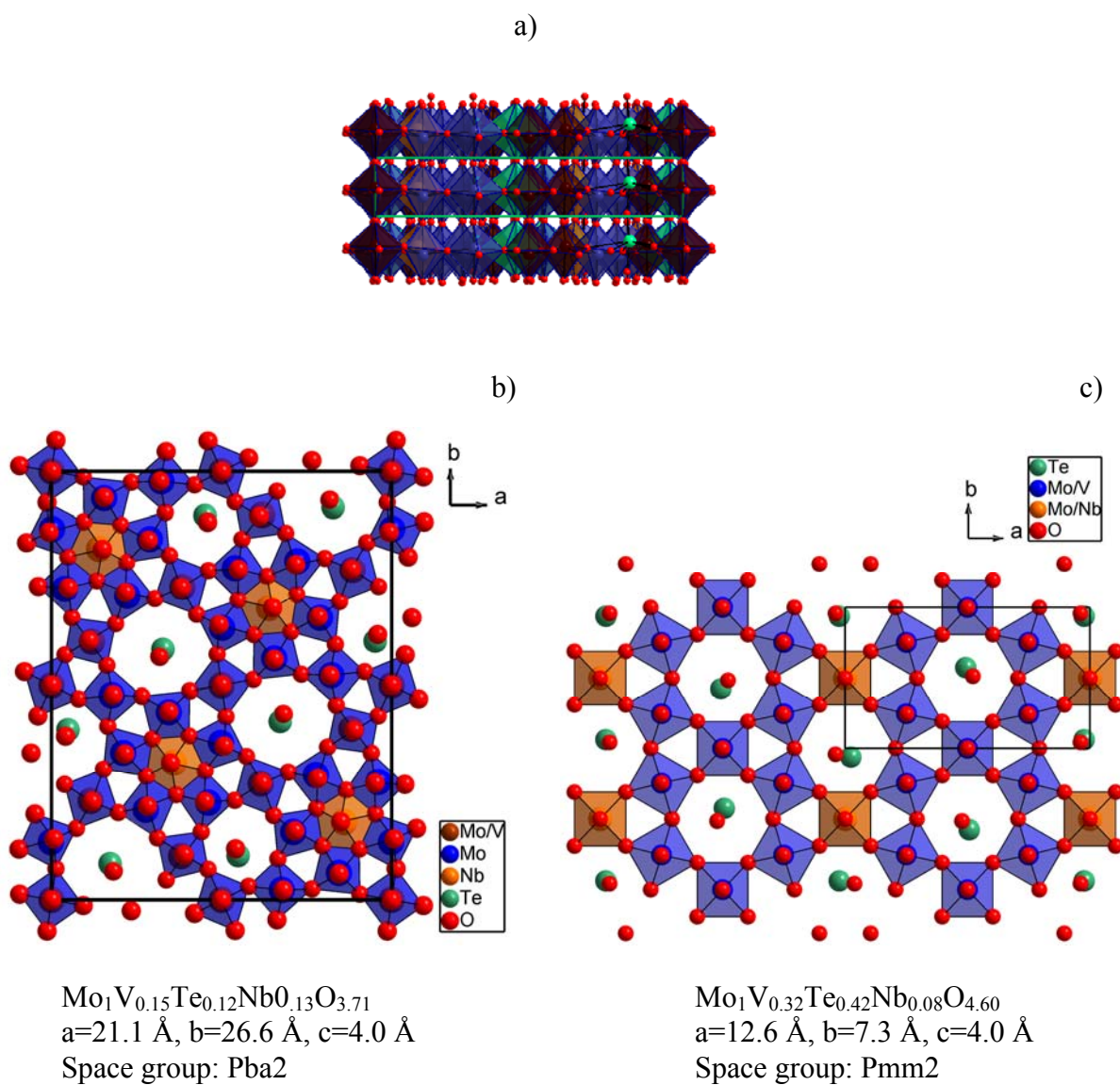


Figure 2. Crystal structures of Mo-V-Te-Nb oxides [23]. Schematic view of the M1 phase perpendicular to c direction (a), arrangement of octahedra in the ab plane of the M1 structure (b) and arrangement of octahedra in the ab plane of the M2 structure (c).

3.3 Synthesis methods

The most common preparation method of Mo-V-Te-Nb mixed oxide catalysts is the so-called “dry-method” [9, 25-28], which combines a precipitation and drying procedure

(freeze-dry, rotavap or spray-dry). Hydrothermal synthesis has also been applied [15, 29-32] in the preparation of these catalysts.

3.3.1 *Precipitation-evaporation method (dry-up method)*

The starting point of this method is the preparation of an aqueous suspension containing the metals in the required proportions to some extent in precipitated form. Generally, ammonium heptamolybdate, ammonium metavanadate, telluric acid, and ammonium niobium oxalate, have been used as starting salts. The slurry obtained is then spray dried. The resulting material is calcined first in air at 548 K in order to eliminate the counter ions of the starting salts. Finally, crystallization of the X-ray amorphous calcined material is carried out in inert gas at 873 K. The disadvantage of this method is that crystallization usually leads to phase mixtures.

3.3.2 *Hydrothermal synthesis*

The hydrothermal synthesis method starts also from an aqueous mixture of the corresponding salts. As in the dry-up method, ammonium heptamolybdate, telluric acid, and ammonium niobium oxalate are used. However, instead of ammonium metavanadate, vanadyl sulfate (VO_2SO_4) has been used in the hydrothermal synthesis. The initial mixture, which is partially precipitated, is introduced into the autoclave. The standard hydrothermal conditions generally applied are: $T = 448 \text{ K}$ (autogeneous pressure $\sim 9 \text{ bar}$) and $t_{\text{synthesis}} = 48 \text{ hours}$. The precursor obtained after the hydrothermal process is then activated in inert gas at 873 K, resulting in a crystalline material.

4 Motivation and Objectives

Direct synthesis of acrylic acid from propane is an alternative, challenging approach in view of displacing the current industrial two-stage oxidation process starting from propylene, reducing thus the price of the feedstock and the complexity of the process. Among the catalysts proposed to date for the selective oxidation of propane, mixed metal oxides of Mo, V, Te, and Nb, containing mainly two phases, designated as M1 and M2 phase [24], have shown the most promising catalytic properties [9]. However, this process has not yet reached a stage of commercialization. Deeper understanding of the characteristics of these materials with regard to catalytic applications is required to enable the design of efficient industrial catalysts.

The M1 phase has been suggested to be responsible for activation of propane and its selective conversion to acrylic acid. However, the nature of the active sites in selective oxidation of propane to acrylic acid and the potential cooperation of the M2 phase are still actively debated in the literature [24, 27, 28, 34-44]. Mixtures of M1 and M2 have been suggested to improve the yield of acrylic acid for operation at high propane conversions [24, 27, 34-42]. It is assumed that the M2 phase contributes to a slightly enhanced performance by converting the unreacted propylene generated on the M1 phase, to acrylic acid. In contrast to that, the M1 phase has been reported to achieve better catalytic performance than mixture of phases [43].

The unique catalytic properties of M1 have been attributed by Ueda *et al.* [45] and further by Grasselli *et al.* [38] to the specific arrangement of the elements in the *ab* plane (cross-section of the needle-like M1 crystals). This conclusion was drawn from experiments based on comparative catalytic tests of M1 materials before and after grinding. An

enhanced catalytic performance was exclusively attributed to the increased surface area of the basal plane presumably obtained after grinding [35, 45, 46] without providing any evidence for that and disregarding further impact of mechanical treatment, e.g., on nature and concentration of defects [47]. Based on the crystal structure of the M1 phase [23], Grasselli *et al.* has proposed a reaction mechanism of propane oxidation to acrylic acid [36], considering the atomic arrangement in the basal plane of the M1 structure as a rigid ensemble of active sites [36, 38]. Thereby, Grasselli *et al.* have been implicitly assumed that the chemical and structural assembly of the proposed active sites comprises an integral part of the catalyst surface. Contrary, it has been shown by Wagner *et al.* [44] that the surface of M1 is significantly different from the well-defined bulk structure. The M1 crystals are completely covered by a structurally disordered layer exhibiting no long-range order. Moreover, chemical and structural rearrangements of the catalyst surface as an effect of the chemical potential of the reaction gas mixture have not been considered in the hypotheses reported by Grasselli *et al.*. Generally, little is known regarding the surface properties of the MoVTenbO_x catalyst, particularly under operation conditions. Consequently, the mode of action of this promising catalyst as well as the reaction mechanism in the selective oxidation of propane to acrylic acid is still far from being understood.

López-Nieto *et al.* [48] have also proposed a reaction mechanism based on catalytic studies performed at different reaction temperatures and contact times on MoVTenbO_x catalysts. However, all the studied catalysts were composed of phase mixtures; thereby it is difficult to delineate the role played by the respective phases. Therefore, the reported correlations between structure and catalytic performance and consequently the suggested

reaction mechanism may be misleading. Access to single phases followed by a systematic investigation of each particular phase, is evidently required in order to shed some light to the catalytic behavior of such complex catalysts.

Therefore, the focus of the present contribution is a detailed investigation of the phase-pure M1 MoVTaNbO_x catalyst. Links between the M1 properties and its catalytic behavior will be discussed. However, as it has been previously shown [29, 31-32, 49-50], accessibility to phase-pure M1 materials is not a trivial task. Therefore, in the first step, the hydrothermal synthesis of the M1 phase has been investigated, achieving thus an improved control over the phase composition of the Mo-V-Te-Nb oxides finally obtained. Bulk and surface properties of the resulting phase-pure M1 catalysts have been examined. Specifically, a M1 model catalyst that preferentially exposes the *ab* plane to the reactants has been prepared, enabling thus the investigation of the catalytic relevance of this certain crystallographic plane. Moreover, in order to examine the dynamic nature of the M1 catalysts, *in-situ* XPS analysis has been carried out under different gas mixtures at reaction temperature.

Additionally, different mixed metal oxide catalysts (diluted and undiluted Mo-V-X-Nb (X=Te, Bi, P) oxides), exhibiting various final phase composition and different degrees of crystallinity, were synthesized and tested in propane oxidation. Comparing the catalytic properties of such catalysts with those of the phase-pure M1 catalysts, the significance of crystallinity in general, and the specific function of the M1 phase in particular will be discussed.

5 References

- [1] G. Ertl, H. Knözinger and J. Weitkamp, *Handbook of Heterogeneous Catalysis* (volume 3), VCH Verlagsgesellschaft mbH, 1997.
- [2] P. Mars, D. W. van Krevelen, *Chemical Engineering Science* 3 (1954), 41.
- [3] R. K. Grasselli, *Topics in Catalysis* 21 (2002), 1-3, 79.
- [4] Yu. Ya. Van-chin-syan, V. V. Kochubei, V. V. Sergeev, Yu. A. Raevskii, S. I. Gerasimchuk, Kh. Z. Kotovich, *Soviet Journal of Chemical Physic* (Engl. Transl.) 70 (1996), 1789.
- [5] D. Vitry, J-L Dubois, W. Ueda, *Journal of Molecular Catalysis A: Chemical* 220 (2004), 67.
- [6] E. K. Novakova, V. C. Védrine, *Propane Selective Oxidation to Propene and Oxygenates on Metal Oxides in J. L. G. Fierro, Metal Oxides, Chemistry and Applications*, CRC Press (2006), 414.
- [7] G. Centi, F. Cavani, F. Cavani, F. Trifiro, *Selective Oxidation by Heterogeneous Catalysis*, Kluwer Academic/Plenum Publishers (2001), 363.
- [8] M. M. Lin, *Applied Catalysis A: General* 207 (2001), 1.
- [9] T. Ushikubo, H. Nakamura, Y. Koyasu, S. Wajiki, US Patent 5 380 933 (1995); Mitsubishi Kasei Corporation.
- [10] E. M. Thorsteinson, T. P. Wilson, F. G. Young, P. H. Kasai, *Journal of Catalysis* 52 (1978), 116.
- [11] J. Bartek, A. Ebner, J. Brazdil, US Patent 5 198 580 (1993); The Standard Oil Company
- [12] T. Ushikubo, K. Oshima, JP Patent 10 036 311 (1998); Mitsubishi Kasei Corporation.
- [13] T. Ushikubo, *Catalysis Today* 78 (2003), 79.
- [14] M. Lin, L. M. Linsen, EP Patent 962 253 A2 (1999); Rohm & Haas.
- [15] D. Vitry, Y. Moriwaka, J. L. Dubois, W. Ueda, *Applied Catalysis A: General* 251 (2003), 411.
- [16] T. Ushikubo, Y. Koyasu, H. Nakamura, S. Wajiki, JP Patent 10 045 664 (1998); Mitsubishi Kasei Corporation.

- [17] J. N. Al-Saeedi, V. V. Guliants, O. Guerrero-Pérez, M. A. Bañares, *Journal of Catalysis* 215 (2003), 108.
- [18] M. Takahashi, S. To, S. Hirose, JP Patent 10 120 617 (1998); Toa Gosei Chemical Industry.
- [19] P. Botella, P. Concepción, J. M. López-Nieto, B. Solsona, *Catalysis Letters* 89 (2003), 249.
- [20] C. Mazzocchia, E. Tempesti, R. Anouchinsky, A. Kaddouri, FR Patent 2 693 384 (1994); Atochem Elf.
- [21] A. Kaddouri, C. Mazzocchia, E. Tempesti, *Applied Catalysis A: General* 180 (1999), 271.
- [22] N. Fujikawa, K. Wakui, K. Tomita, N. Ooue, W. Ueda, *Catalysis Today* 71 (2001), 83.
- [23] P. DeSanto, D. J. Buttrey, R. K. Grasselli, C. G. Lugmair, A. F. Volpe, B. H. Toby, T. Vogt, *Zeitschrift für Kristallographie* 219 (2004), 3, 152.
- [24] T. Ushikubo, K. Oshima, A. Kayou, M. Hatano, *Studies in Surface Science and Catalysis* 112 (1997), 473.
- [25] M. M. Lin, *Applied Catalysis A: General* 250 (2003), 305.
- [26] M. M. Lin, *Applied Catalysis A: General* 250 (2003), 287.
- [27] J. M. Oliver, J. M. López-Nieto, P. Botella, A. Mifsud, *Applied Catalysis A: General* 257 (2004), 67.
- [28] P. Beato, A. Blume, F. Girgsdies, R. E. Jentoft, R. Schlögl, O. Timpe, A. Trunschke, G. Weinberg, Q. Basher, F. A. Hamid, S. B. A. Hamid, E. Omar, L. Mohd Salim, *Applied Catalysis A: General* 307 (2006), 137.
- [29] H. Watanabe, Y. Koyasu, *Applied Catalysis A: General* 194-195 (2000), 479.
- [30] H. Hibst, F. Borgmeier, F. Rosowski, K. J. Müller-Engel, DE 102004027999A1 (2005); BASF.
- [31] W. Ueda, D. Vitry, T. Kato, N. Watanabe, Y. Endo, *Research on Chemical Intermediates* 32 (2006), 3–4, 217.
- [32] F. Ivarsa, P. Botella, A. Dejoz, J. M. López-Nieto, P. Concepción, M. I. Vázquez, *Topics in Catalysis* 38 (2006), 1–3, 59.
- [33] H. Tsuji, Y. Koyasu, *Journal of the American Chemical Society* 124 (2002), 5680.

- [34] M. Baca, A. Pigamo, J. L. Dubois, J. M. M. Millet, *Topics in Catalysis* 23 (2003), 1–4, 39.
- [35] R. K. Grasselli, D. J. Buttrey, P. DeSanto, Jr., J. D. Burrington, C. G. Lugmair, A. F. Volpe, Jr., T. Weingand, *Catalysis Today* 91–92 (2004), 251.
- [36] R. K. Grasselli, *Catalysis Today* 99 (2005), 23.
- [37] T. Ushikubo, *Catalysis Today* 57 (2000), 331.
- [38] R. K. Grasselli, J. D. Burrington, D. J. Buttrey, P. DeSanto Jr., C. G. Lugmair, A. F. Volpe Jr., T. Weingand, *Topics in Catalysis* 23 (2003), 1–4, 5.
- [39] J. Holmberg, R. K. Grasselli, A. Andersson, *Topics in Catalysis* 23 (2003), 1–4, 55.
- [40] J. Holmberg, R. K. Grasselli, A. Andersson, *Applied Catalysis A: General* 270 (2004), 121.
- [41] R. K. Grasselli, D. J. Buttrey, J. D. Burrington, A. Andersson, J. Holmberg, W. Ueda, J. Kubo, C. G. Lugmair, A. F. Volpe Jr., *Topics in Catalysis* 38 (2006), 1–3, 7.
- [42] E. García-González, J. M. López-Nieto, P. Botella, and M. M. González-Calbet, *Chemistry of Materials* 14 (2002), 4416.
- [43] D. Vitry, Y. Morikawa, J. L. Dubois, W. Ueda, *Topics in Catalysis* 23 (2003), 1–4, 47.
- [44] J. B. Wagner, O. Timpe, F. A. Hamid, A. Trunschke, U. Wild, D. S. Su, R. K. Widi, S. B. A. Hamid, R. Schlögl, *Topics in Catalysis* 38 (2006), 51.
- [45] K. Oshihara, T. Hisano, W. Ueda, *Topics in Catalysis* 15 (2001), 153.
- [46] V. V. Gulians, R. Bhandari, R. S. Soman, O. Guerrero-Pérez, M. A. Bañares, *Applied Catalysis A: General* 274 (2004), 213.
- [47] G. Mestl, N. F. D. Verbruggen, H. Knözinger, *Langmuir* 11 (1995), 3034.
- [48] P. Botella, J. M. López-Nieto, B. Solsona, A. Mifsud, F. Márquez, *Journal of Catalysis* 209 (2002), 445.
- [49] H. Hibst, F. Rosowski, G. Cox, *Catalysis Today* 117 (2006), 234.
- [50] M. Baca, J. M. M. Millet, *Applied Catalysis A: General* 279 (2005), 67.

CHAPTER 1- Preparation of phase-pure M1 Mo-V-Te-Nb oxide catalysts by hydrothermal synthesis – Influence of reaction parameters on the structure and morphology.

Abstract

This work presents a detailed investigation of the preparation of MoVTenbO_x catalysts by hydrothermal synthesis. Phase-pure synthesis of M1 has been achieved applying the metals in a molar ratio Mo/V/Te/Nb = 1/0.25/0.23/0.12. Raman, UV/Vis spectroscopy, and SEM/EDX analysis show that the elements are inhomogeneously distributed in the initial suspension that is formed after mixing the metal salts in an aqueous medium. Iso- and heteropoly anions of molybdenum, free telluric acid as well as supra-molecular polyoxometalate clusters are observed in the solution, whereas all metals have been found in the precipitate. Complete rearrangement of molecular building blocks under hydrothermal conditions is essential for formation of phase-pure materials. Optimized synthesis conditions with respect to temperature and time result in the formation of a precursor consisting of nano-structured M1 characterized by an extended periodic organization in the [001] direction and a fairly homogeneous distribution of the elements. Residual ammonium containing supra-molecular species in the precursor result in the formation of phase mixtures during the subsequent crystallization by heat treatment in inert gas. Phase-pure M1 exhibits a distinct degree of flexibility with respect to the chemical composition that becomes obvious by incorporating Nb not exclusively into pentagonal bi-pyramidal units, but also into octahedral coordinated positions as shown by EXAFS. Anisotropic growth of the needle-like M1 crystals has been observed during the final heat treatment performed at 873-923 K in inert atmosphere disclosing a potential method to control the catalytic properties of MoVTenbO_x catalysts.

Keywords: Hydrothermal synthesis, MoVTenbO_x catalyst, M1 phase, propane oxidation

1 Introduction

Multi-metal oxides based on molybdenum, vanadium, tellurium, and niobium have been reported to achieve outstanding performance in the direct oxidation of propane to acrylic acid [1]. Despite their considerable chemical complexity, such materials basically consist of two orthorhombic phases known as M1 and M2 [2]. Minority phases like $(\text{Mo}_{0.93}\text{V}_{0.07})_5\text{O}_{14}$, MoO_3 , and $\text{TeMo}_5\text{O}_{16}$ [3, 4] are also formed depending on the preparation method and the activation procedure applied. In the M1 phase (ICSD 55097 [5]), corner-linked MO_6 ($\text{M}=\text{Mo}, \text{V}$) octahedrons are assembled forming 6- and, 7-membered rings, partially accommodating TeO units [6-9]. Niobium has been postulated to be exclusively located in the center of a MO_7 pentagonal bipyramidal unit sharing edges with the surrounding octahedrons [6, 9]. The (001) planes are congruently stacked along the [001] direction, forming a bronze-like structure similar to the structure of $\text{Cs}_{0.7}(\text{Nb}_{2.7}\text{W}_{2.3})\text{O}_{14}$ (ICSD 67974 [5]) [10]. The M2 phase differs from M1 by the absence of the pentagonal bi-pyramidal unit, and the 7-membered ring [6]. The formulae of the refined unit cells have been determined to be $\text{Mo}_{7.8}\text{V}_{1.2}\text{Te}_{0.937}\text{NbO}_{28.9}$ for M1 and $\text{Mo}_{4.31}\text{V}_{1.36}\text{Te}_{1.81}\text{Nb}_{0.33}\text{O}_{19.81}$ for M2, respectively [6].

Symbiosis between the two phases has been suggested to be responsible for maximum yield of acrylic acid or acrylonitrile in the oxidation or ammoxidation of propane, respectively [11, 12]. Selective oxidation of propane has been assigned to M1. M2 on its own does not activate propane, but selectively oxidizes the propylene intermediate. Correlations between phase composition and catalytic properties are still actively debated [13-16]. However, it has been generally accepted that the high selectivity towards acrylic acid is associated with the M1 phase [3, 17]. Based on chemical experience, the unique

catalytic properties of M1 have been attributed to the specific geometric arrangement of the metal centers in the (001) plane [18, 19]. However, the molecular structure and dynamic nature of the active moiety on the M1 surface under conditions of propane oxidation, (673 K and up to 50 vol.- % steam in the feed) still remain to be elucidated experimentally. For that purpose, synthesis of phase-pure M1 in larger batches is a basic prerequisite.

Generally, two different preparation methods have been used to synthesize Mo-V-Te-Nb mixed oxides. By precipitation and fast evaporation of water from the precipitate suspended in the mother liquor, orange colored precursors are obtained. Subsequent calcination in air followed by annealing in inert atmosphere at high temperatures usually results in catalysts composed of several phases [2, 14, 20]. Purification by post-treatment with nitric acid [16] or H_2O_2 [21], gives access to phase-pure M1. However, the chemical composition of M1 might be affected by leaching [15].

Hydrothermal synthesis represents an alternative synthesis route to Mo-V-Te-Nb oxide catalysts [22]. Usually the synthesis is performed at $T = 448$ K in nitrogen atmosphere applying a synthesis time of 48 h [23-29].

López-Nieto and co-workers conducted the synthesis under these conditions in a Teflon-lined stainless-steel autoclave using different metal-containing compounds and various nominal metal stoichiometries [23, 24, 27-29]. Generally, phase mixtures including $\text{Mo}_5\text{TeO}_{16}$, MoO_3 , M_5O_{14} ($\text{M}=\text{Mo}, \text{V}, \text{Nb}$), $\text{Te}_2\text{M}_{20}\text{O}_{57}$ ($\text{M}=\text{Mo}, \text{V}, \text{Nb}$), and $\text{Te}_{0.33}\text{MO}_{3.33}$ ($\text{M}=\text{Mo}, \text{V}, \text{Nb}$) were obtained after heat treatment for 2 h at 873 K in nitrogen of the hydrothermally prepared precursor. The latter two phases correspond to M1 and M2, respectively, as originally denominated by Ushikubu *et al.* [2]. M1 has been achieved as

the predominant phase using a nominal metal stoichiometry of Mo/V/Te/Nb = 1/0.2/0.17/0.17 and oxalate/molybdenum molar ratios in the range between 0.2 and 0.6 [29]. The as-synthesized metal stoichiometry of the M1-rich materials correspond to Mo/V/Te/Nb = 1/0.20-0.27/0.19-0.22/0.19-0.21.

Applying a synthesis temperature of 448 K and a synthesis time of 48 h, Ueda and co-workers prepared orthorhombic Mo-V-Te-Nb mixed oxides in a stainless steel autoclave equipped with a 70 ml Teflon inner beaker without stirring using a nominal stoichiometry of the metals of Mo/V/Te/Nb = 1/0.3/0.16/0.12 and a molybdenum concentration of 0.76 M [25]. The XRD patterns of the resulting dark blue powder indicate the formation of a basically amorphous material. However, one sharp peak close to $30^\circ 2\theta$ probably due to elemental tellurium has also been observed. Heat treatment of the precursor in nitrogen at 873 K for 2 h resulted in the formation of a crystalline solid. The XRD patterns displayed all reflections of the orthorhombic M1 phase. Polycrystalline orthorhombic Mo-V-Te [30] and Mo-V [31] oxides have also been prepared operating at the same synthesis temperature, but applying different metal ratios, molybdenum concentrations, and synthesis times, as well as separating undesired phases by manual sorting [30].

Selective synthesis of phase-pure M1 requires precise control of preparation parameters, such as temperature, metal salt concentration, metal stoichiometry, batch size, pressure, and redox potential of the synthesis mixture. The latter is determined by pH, solvent, organic additives, and the nature of metal salt precursors. Moreover, different characteristics of a specific autoclave, e.g. wall material, volume, and heating/cooling regime have substantial influence on the crystallization behavior. These factors are well known in the synthesis of crystalline aluminosilicates but have not yet been considered in

the preparation of Mo-V-Te-Nb oxides. In the present work, a systematic investigation of the hydrothermal preparation procedure of Mo-V-Te-Nb mixed oxides has been undertaken. The arrangement of molecular building blocks in aqueous solution has been studied by Raman and UV/Vis spectroscopy. The development of short-range order during hydrothermal synthesis has been investigated by X-ray absorption spectroscopy, while the bulk and microstructure of precursors and heat-treated crystalline synthesis products have been analyzed by X-ray diffraction and electron microscopy, respectively. The hydrothermal synthesis was revealed to be the crucial synthesis step in the formation of nano-structured M1. The morphology of the final catalyst is governed by the conditions of the thermal treatment.

2 Experimental

2.1 Preparation of Mo-V-Te-Nb mixed oxides

Mo-V-Te-Nb mixed metal oxide catalysts have been prepared by hydrothermal synthesis using two different autoclaves. The technical parameters of these autoclaves are summarized in **Table 1**. The general preparation procedure is illustrated in **Scheme 1**.

Table 1
Specifications of the autoclaves used

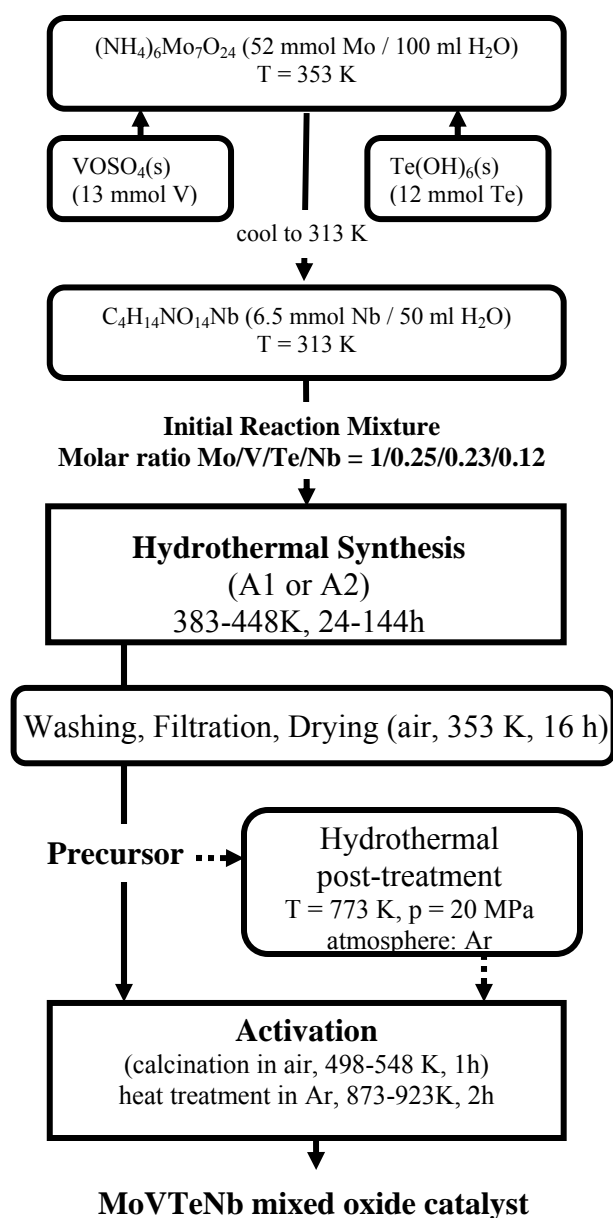
Parameter	Autoclave 1 (A1)	Autoclave 2 (A2)
Volume	200 ml	300 ml
Wall material	Hastelloy C276	Teflon
Stirring	250 rpm	no control
Cooling	water cooling (1.6 K/min)	manually (6.0 K/min)

Ammonium heptamolybdate $(\text{NH}_4)_6\text{Mo}_7\text{O}_{24}\cdot 4\text{H}_2\text{O}$ (Merck), vanadyl sulfate $\text{VOSO}_4\cdot 5\text{H}_2\text{O}$ (Riedel-deHäen), telluric acid $\text{Te}(\text{OH})_6$ (Aldrich), and ammonium niobium

oxalate $(\text{NH}_4)[\text{NbO}(\text{C}_2\text{O}_4)_2(\text{H}_2\text{O})_2] \cdot 3\text{H}_2\text{O}$ (Aldrich) were used as starting materials to prepare the initial suspension that contains the metals in a molar ratio of $\text{Mo/V/Te/Nb} = 1/0.25/0.23/0.12$. After replacing residual air by nitrogen, hydrothermal synthesis was carried out at temperatures between 373 and 448 K for 24 to 144 h, producing

Scheme 1

Hydrothermal synthesis of MoVTeNbO_x



autogeneous pressures between 4 and 9 bars. The obtained suspensions were centrifuged for 20 minutes; the precipitate was washed with 100 ml of bidistilled water for 10 minutes and filtered under vacuum. Finally, the solid material was dried in a muffle furnace at 353 K for 16 hours in air, resulting in the precursor material, referred to as “P” followed by a consecutive number.

Starting from the precursors, crystalline products have been obtained by heat treatment of 3 g of the precursor in inert gas with a flow of 100 ml/min for 2 hours at 873 or 923 K (heating rate 15

K/min), either with or without previous calcination in synthetic air (100 ml/min) for 1 hour at 548 or 598 K (heating rate 10 K/min). The heat treatments were carried out in a rotating oven. The crystalline reaction products are denominated as “C” followed by the consecutive number of the corresponding precursor.

2.2 Characterization

Molecular species in the initial solutions and precipitates were studied by Raman spectroscopy performed on a Labram I (Dilor) instrument equipped with a confocal microscope (Olympus). A notch filter (Kaiser Optical) was applied to cut off the laser-line and the Rayleigh scattering up to 150 cm^{-1} . The spectrometer is equipped with a CCD camera (1024*298 diodes) that is Peltier cooled to 243 K to reduce the thermal noise. A He/Ne laser (Melles Griot) was used to excite the Raman scattering at 632 nm. Using a slit width of 200 μm and a 1800 grating gives a spectral resolution of 2.5 cm^{-1} . For the solution experiments the laser beam was directed through the glass reaction vessel into the solution. UV/Vis spectra have been recorded on a PerkinElmer Lambda 950 UV/Vis-NIR spectrometer.

Phase composition of the catalysts was determined by X-ray diffraction performed on a STOE STADI-P transmission diffractometer equipped with a focussing primary Ge (111) monochromator and a position sensitive detector, using Cu-K α_1 radiation. The diffraction patterns of the activated materials were analyzed with the “TOPAS” software (v.2.1, Bruker AXS).

The short-range order in the M1 precursor and in crystalline M1 has been investigated by X-ray absorption spectroscopy. The XAS measurements were performed in transmission mode at the Mo K edge (19.999 keV), Nb K edge (18.986 keV), V K edge (5.465 keV),

and Te L_{III} edge (4.314 keV) at beamlines X1 and E4 at the Hamburger Synchrotronstrahlungslabor, HASYLAB. For investigation of Mo and Nb, 30 mg of boron nitride was mixed with ca. 8 mg sample, ground, and pressed into a pellet of 5 mm in diameter under one ton of pressure. For investigation of V and Te, 100 mg of polyethylene was mixed with 5 mg sample, ground and pressed at a force of 2 tons into a pellet 13 mm in diameter. The resulting edge jump amounted to $\Delta\mu \sim 0.5$ at the Mo K edge and Nb K edge, $\Delta\mu \sim 0.02$ at the V K edge, and $\Delta\mu \sim 0.1$ at the Te L_{III} edge. Data processing and analysis were performed with the software package WinXAS 3.1 [32].

Morphology studies and shape analysis were performed using scanning electron microscopy. A Hitachi S-5200 with a PGT Spirit EDX system and a Hitachi S-4800 with an EDAX Genesis EDX detector were used. EDX studies in the SEMs were carried out with an accelerating voltage of 10 kV while images were acquired at 2 kV to optimize surface resolution. For SEM investigations, the samples were deposited on carbon tape without any pretreatment. From the SEM images, size distributions of the M1 needles have been obtained by measuring the lengths and diameters of more than 300 M1 needles.

Nitrogen physisorption at 77 K was measured using an AUTOSORB-1-C physisorption/chemisorption analyzer (Quantachrome). Specific surface areas have been calculated from the adsorption isotherms using the BET method.

Thermal analysis was performed using a STA 449C Jupiter apparatus (Netzsch). Precursors have been heated in He atmosphere (flow rate 100 ml/min) applying a heating rate of 10 K/min. The produced gases were analyzed using an OmniStar quadrupole mass spectrometer (Pfeiffer Vacuum).

3 Results and discussion

3.1 Molecular species in the initial suspension

Metal salt concentration and metal stoichiometry strongly influence the phase composition of molybdenum based mixed oxides prepared by hydrothermal synthesis [22, 24, 25, 28, 29, 31, 33]. These parameters have been kept constant, because the present study mainly addresses the thermodynamic and kinetic parameters of M1 synthesis. The preparation procedure (**Scheme 1**) differs slightly from the routines described in the literature [22]. Ammonium heptamolybdate was dissolved in bidistilled water at 353 K, resulting in a colorless solution with a pH of 5.3. Subsequently, vanadyl sulfate as a powder was added at 353 K. The color of the mixture (pH = 3.05) changed into dark violet. Finally, solid telluric acid was added at the same temperature, forming a light brown slurry (pH = 2.18). Afterwards, the MoVTe slurry was cooled to 313 K and a solution of ammonium niobium oxalate in bidistilled water (313 K, pH = 0.8) was added, resulting in further precipitation. Before introduction into the autoclave, the dispersion (313 K, pH = 1.69) was stirred for 10 minutes. The observation of color changes and precipitation processes during the preparation procedure described above reflects the formation and rearrangement reactions of molecular building blocks happening in this early stage of the synthesis. Raman spectra of reference solutions and the binary MoV solution are shown in **Figure 1**. The spectrum of the colorless telluric acid solution (296 K, pH = 3.7, [Te] = 0.138 M) exhibits a single peak at 644 cm^{-1} due to $\nu(\text{Te-O})$ vibrations (**Figure 1a**) [34]. The aqueous solution of vanadyl sulfate (298 K, pH = 1.86, [V] = 0.198 M) (**Figure 1b**) displays a strong band at 980 and a shoulder at 996 cm^{-1} associated to superimposed V=O and S=O stretching vibrations of solvated vanadyl ions [35]. The Raman spectrum of ammonium heptamolybdate in aqueous solution (333 K, pH = 5.2,

[Mo] = 0.6 M) is characterized by bands at 937 and 893 cm^{-1} due to the presence of $[\text{Mo}_7\text{O}_{24}]^{6-}$ species (**Figure 1c**) [36]. Bands at 942, 919, and 570 cm^{-1} assigned to Nb=O and Nb-O stretching vibrations, respectively, were observed with the ammonium niobium oxalate solution (296 K, pH = 0.8, [Nb] = 0.5 M) (**Figure 1d**) [37].

When vanadium and tellurium are added successively to the solution of ammonium heptamolybdate, significant changes in the Raman spectra are observed. **Figure 1e** shows the Raman spectrum taken after addition of 0.11 mmol vanadium as vanadyl sulfate in 10 ml bidistilled water (Mo/V = 1/0.03). The bands due to ammonium heptamolybdate are

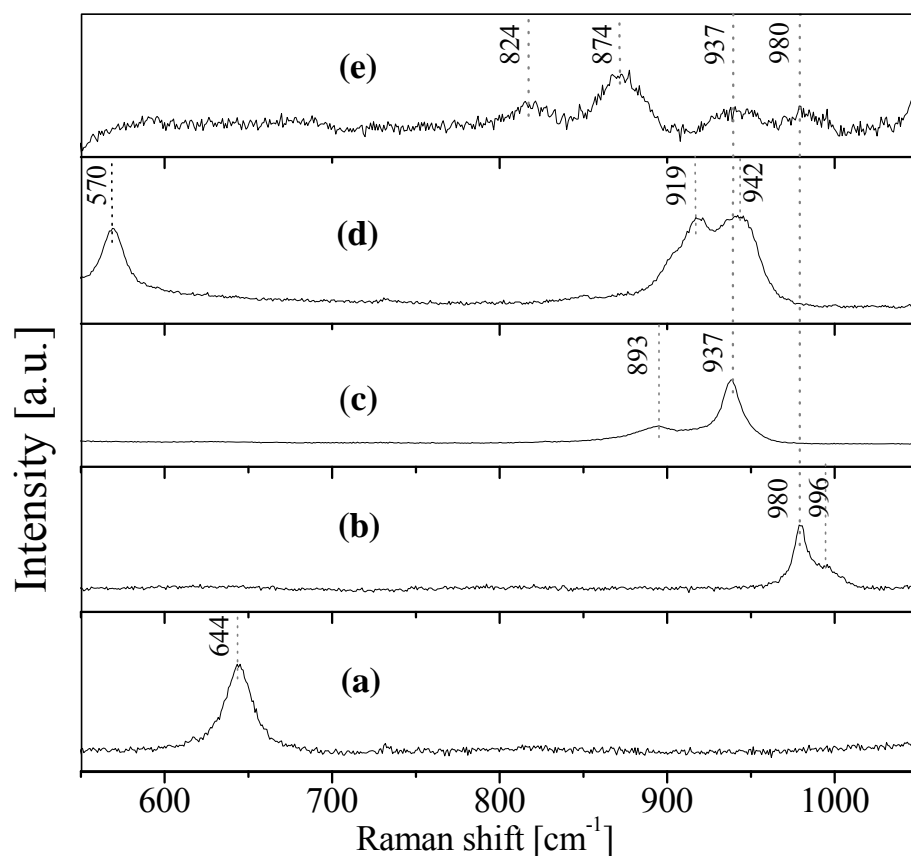


Figure 1. Raman spectra of aqueous solutions of (a) $\text{Te}(\text{OH})_6$ (296 K, pH = 3.7, $[\text{Te}] = 0.138 \text{ M}$), (b) $\text{VOSO}_4 \cdot 5\text{H}_2\text{O}$ (298 K, pH = 1.86, $[\text{V}] = 0.198 \text{ M}$), (c) $(\text{NH}_4)_6\text{Mo}_7\text{O}_{24} \cdot 4\text{H}_2\text{O}$ (333 K, pH = 5.2, $[\text{Mo}] = 0.6 \text{ M}$), (d) $\text{NH}_4[\text{NbO}(\text{C}_2\text{O}_4)_2(\text{H}_2\text{O})_2] \cdot 3\text{H}_2\text{O}$ (296 K, pH = 0.8, $[\text{Nb}] = 0.5 \text{ M}$), and (e) $(\text{NH}_4)_6\text{Mo}_7\text{O}_{24} \cdot 4\text{H}_2\text{O} + \text{VOSO}_4 \cdot 5\text{H}_2\text{O}$ (T = 298 K, $[\text{Mo}] = 0.33 \text{ M}$, molar ratio Mo/V = 1/0.03).

reduced in intensity and two new bands at 824 and 874 cm^{-1} appear. The band at 874 cm^{-1} is reminiscent of the peaks observed in Raman spectra of supra-molecular polyoxomolybdates or mixed molybdenum-vanadium clusters [38, 39]. Such clusters are composed of $\{(\text{Mo})\text{Mo}_5\}$ structural units, which can be regarded as structural building block of the M1 structure. These units consist of a central pentagonal bipyramidally coordinated Mo atom surrounded by five edge-sharing MoO_6 octahedrons. The UV/Vis spectrum of the supra-molecular polyoxometalate cluster $\text{Mo}^{\text{VI}}_{72}\text{V}^{\text{IV}}_{30}$ in aqueous solution is characterized by two bands at 689 (w) and 510 (vs) nm [39]. A related spectrum has also been observed during preparation of a mixed Mo-V oxide [40]. The binary MoV solution shows similar bands at about 690 and 530 nm (**Figure 2b**) providing further evidence for the formation of mixed MoV polyoxometalates.

The Raman spectrum of the final binary solution that contains molybdenum and vanadium in a molar ratio of $\text{Mo}/\text{V} = 1/0.25$

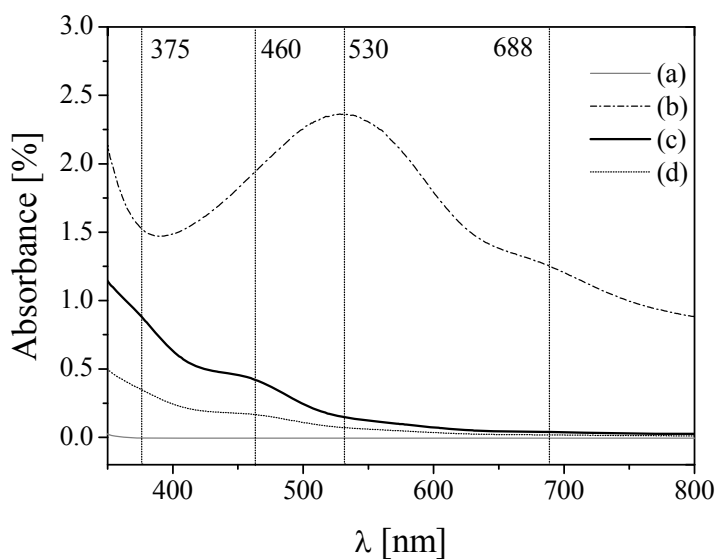


Figure 2. UV/Vis spectra of aqueous solutions of (a) $(\text{NH}_4)_6\text{Mo}_7\text{O}_{24}\cdot 4\text{H}_2\text{O}$ (298 K, $\text{pH}=5.2$, $[\text{Mo}]=0.3$ M), (b) $(\text{NH}_4)_6\text{Mo}_7\text{O}_{24}\cdot 4\text{H}_2\text{O} + \text{VOSO}_4\cdot 5\text{H}_2\text{O}$ ($T=298$ K, $\text{pH}=3.05$, $[\text{Mo}]=0.3$ M, molar ratio $\text{Mo}/\text{V}=1/0.25$), (c) MoVTe-filtrate, and (d) MoVTeNb-filtrate.

(not shown) is of very low quality due to the dark color of the solution. However, the general spectroscopic patterns and, therefore, the nature of the molecular species in solution are not changed with increasing vanadium concentration.

After the addition of tellurium, precipitation occurs, making interpretation of the Raman spectrum difficult due to superposition of bands originating from both solution and precipitate. Therefore, the solid was removed by filtration.

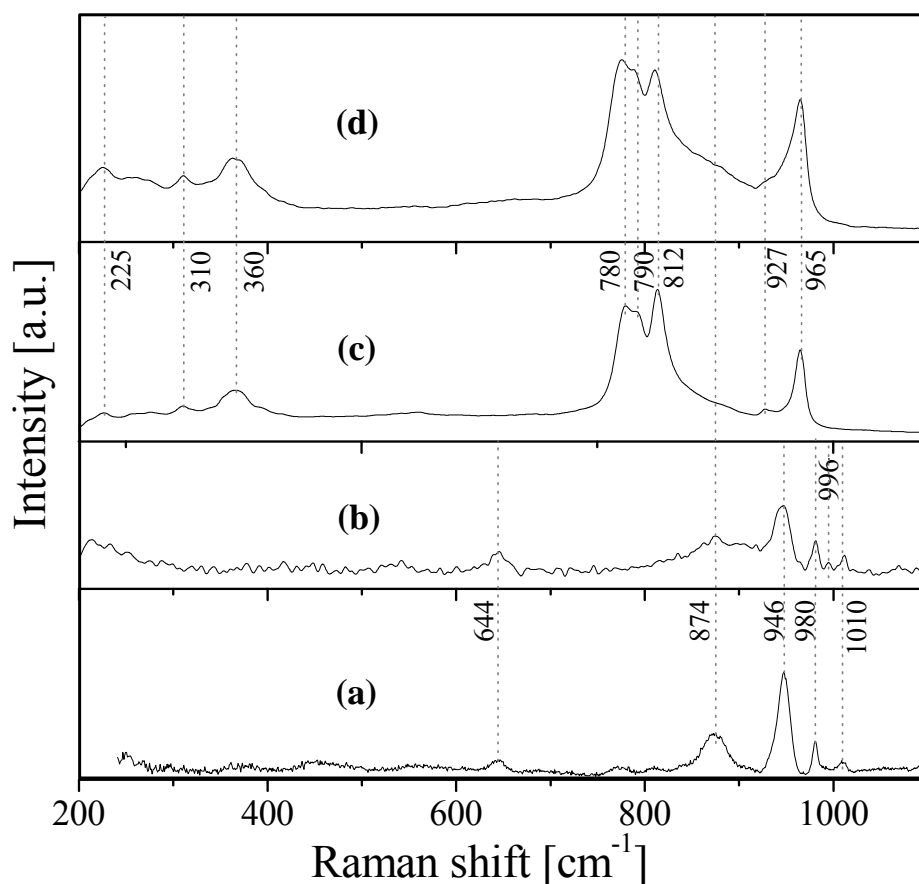


Figure 3. Raman spectra of the (a) MoVTe filtrate, (b) MoVTeNb filtrate, (c) MoVTe precipitate, and (d) MoVTeNb precipitate.

The Raman spectrum of the MoVTe filtrate is shown in **Figure 3a**. In addition to the bands at 874 and 980 cm^{-1} due to the presence of polyoxometalate clusters and vanadyl sulfate, respectively, bands at 644, 946 and 1010 cm^{-1} appear. The band at 946 cm^{-1} could

be attributed to the formation of $[\text{TeMo}_6\text{O}_{24}]^{6-}$ Anderson-type heteropolyanions [14, 41, 42]. The band at 1010 cm^{-1} may indicate partial substitution of Mo by V in the Anderson anion [42], which is also supported by a shift of the absorption maximum in the UV/Vis spectrum to lower energies (**Figure 2c**). Molybdo-tellurates containing vanadium have been reported to show absorption below 400 nm in the UV/Vis spectrum [42]. However, due to similar band positions and intensity ratios in the Raman spectra of $[\text{Mo}_7\text{O}_{24}]^{6-}$ and $[\text{TeMo}_6\text{O}_{24}]^{6-}$, the coexistence of heptamolybdate anions in the solution cannot be excluded. On the other hand, mixed $\text{Mo}^{\text{V}}/\text{Mo}^{\text{VI}}$ polyoxomolybdate clusters, such as $(\text{NH}_4)_{42}[\text{Mo}^{\text{VI}}_{72}\text{Mo}^{\text{V}}_{60}\text{O}_{372}(\text{CH}_3\text{COO})_{30}(\text{H}_2\text{O})_{72}]$ ca. 300 H_2O ca. 10 $\text{CH}_3\text{COONH}_4$ exhibit bands at 215, 260, and 450 nm in the UV/Vis spectrum [38]. The spectrum of the MoVTe filtrate (**Figure 2c**) showing a band at 450 nm and absorption below 300 nm, could therefore also be interpreted in terms of the formation of molybdenum-blue-type clusters. The latter interpretation would be in agreement with the existence of the band at 874 cm^{-1} in the Raman spectrum, which is also characteristic for such clusters [38]. Finally, the peak at 644 cm^{-1} indicates the presence of free telluric acid in the MoVTe filtrate.

The dried white precipitate that has been separated from the MoVTe filtrate was also analyzed by Raman spectroscopy (**Figure 3c**) and SEM-EDX (**Figure 4a**, **Table 2**). A Mo/Te molar ratio of ~ 6 was measured at different spots of the white solid (**Figure 4a**), which is consistent with the metal ratio in an Anderson-type heteropolyanion $[\text{TeMo}_6\text{O}_{24}]^{6-}$. Particles containing substantial amounts of vanadium have also been detected. The Raman spectrum of the solid shows bands at 225, 310, 360, 780, 790, 812, 927, and 965 cm^{-1} .

After addition of the ammonium niobium oxalate solution to the ternary MoVTe mixture, further precipitation occurs. Raman spectra of the filtrated solution and the precipitate have been recorded separately (**Figure 3b and 3d**). The Raman spectrum of the MoVTeNb solution shows similarities to that of the MoVTe solution (**Figure 3a**). Bands due to Nb-O stretching vibrations are absent in the spectrum of the filtrate, indicating that most of the added niobium was precipitated. **Figure 3d** shows the Raman spectrum of the MoVTeNb precipitate that is similar to the spectrum of the MoVTe precipitate.

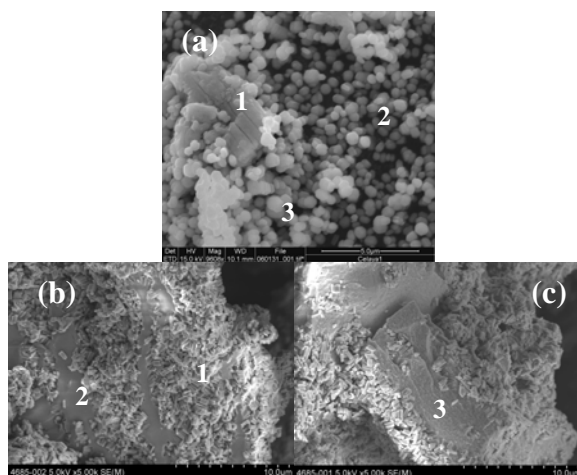


Figure 4. SEM images of (a) the MoVTe precipitate obtained after filtration of the ternary slurry (synthesis with molar ratio Mo/V/Te = 1/0.25/0.23), and (b and c) of the MoVTeNb precipitate obtained after filtration of the final mixture (synthesis with molar ratio Mo/V/Te/Nb = 1/0.25/0.23/0.12). Elemental composition at the spots marked is shown in **Table 2**.

In summary, Raman and UV/Vis spectroscopy, together with SEM-EDX analysis indicate that the individual elements are distributed rather inhomogeneously in the initial suspension. Although the interpretation of Raman and UV/Vis spectra of the complex mixture is not unambiguous, giant polyoxometalate clusters containing the pentagonal bipyramidal structure, iso- and heteropolyanions of molybdenum and free telluric acid are

Table 2

Elemental analysis (at.-%) of the MoVTe and MoVTeNb precipitate by EDX at different spots. SEM images of both materials are shown in **Figure 4**

	Spot	Mo	V	Te	Nb	Mo/Te ratio
MoVTe precipitate	1	67	26	7	0	9.0
	2	84	2	14	0	5.6
	3	85	2	13	0	6.5
MoVTeNb precipitate	1	80	1	15	14	5.3
	2	66	8	13	13	5.1
	3	54	7	13	26	4.2

supposed to be present in the solution. The pre-formed precipitate contains all the elements.

3.2 Hydrothermal synthesis

Catalyst synthesis aimed at the formation of a desired crystal structure is preferably performed under hydrothermal conditions. Although the structural rearrangements occurring during hydrothermal synthesis are concealed by the “black box” autoclave, the synthesis can be optimized by applying different reaction conditions and appropriate adjustment of the chemical properties of the reaction medium. Moreover, it is well known that technical parameters of a specific autoclave, such as wall material, vessel size, stirring system, cooling and heating facilities, exert significant influence by affecting heat transfer, wall effects, homogeneity, and crystallization behavior. Until now, less attention has been paid to the hydrothermal conditions in preparation of Mo-V-Te-Nb mixed oxides. However, these parameters might have a crucial influence on phase and chemical composition of the resulting catalysts and finally on their catalytic properties, particularly due to the considerable chemical flexibility of the orthorhombic M1 structure [22].

Table 3

Hydrothermal conditions and phase composition of the activated catalysts; the nominal stoichiometry applied in hydrothermal synthesis corresponds to Mo/V/Te/Nb = 1/0.25/0.23/0.124, with the exception of P7 (Mo/V/Te/Nb = 1/0.25/0.15/0.124)

Precursor/ Catalyst	Code	Autoclave	Hydrothermal conditions	Phase composition [%]
P1/C1	1760/1761	A1	448 K, 48 h	M1 100
P2/C2	929/939			
P3/C3	1885/1886			
P4/C4	1422/1434			
P5/C5	1422/1650			
P6/C6	2431/2501	A2	448 K, 48 h	M1 58
				M2 37
				Mo ₅ O ₁₄ 5
P7/C7	2445/2488		448 K, 48 h	M1 47
				M2 11
				Mo ₅ O ₁₄ 25
				V _{0.95} Mo _{0.97} O ₅ 17
P8/C8	3961/3984		403 K, 24 h	M1 53
				M2 14
				Mo ₅ O ₁₄ 23
				TeMo ₅ O ₁₆ 10
P9/C9	3791/3792		403 K, 48 h	M1 51
				M2 23
				Mo ₅ O ₁₄ 26
P10/C10	3241/3673		403 K, 96 h	M1 100
P11/C11	3648/3779		403 K, 144 h	M1 90
				M2 10
P12/C12	3665/3695		383 K, 96 h	M2 29
				Mo ₅ O ₁₄ 60
				TeMo ₅ O ₁₆ 11
P13/C13	3777/3778		423 K, 96 h	M1 86
				M2 14
P14/C14	3298/3303		448 K, 96 h	M1 38
				M2 41
				Mo ₅ O ₁₄ 8
				V _{0.95} Mo _{0.97} O ₅ 13

In the following, the impact of temperature, reaction time, and technical parameters of the autoclave on M1 synthesis has been studied. For this purpose, the initial reaction mixture,

prepared as described above, was transferred into two different autoclaves, referred to as A1 and A2, respectively. The technical parameters of the two autoclaves differing in wall material, batch size and cooling system are summarized in **Table 1**. An overview of the experimental conditions applied and the final phase composition of the activated mixed oxides obtained is given in **Table 3**. Precursor materials are denominated as “P” and the corresponding activated catalysts are denominated as “C”.

The phase composition of the final crystalline material differs depending on autoclave, synthesis temperature and reaction time used (**Table 3**). Applying standard hydrothermal

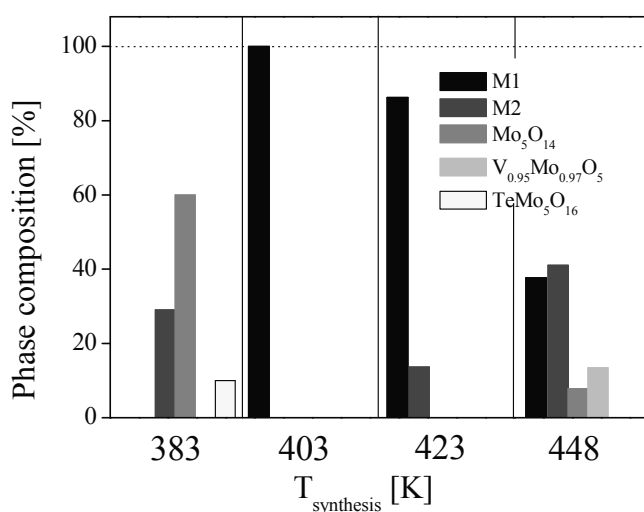


Figure 5. Phase composition of catalysts prepared in A2 at different temperatures; synthesis time = 96 h.

conditions (T = 448 K, t = 48

h) in autoclave A1, precursor

materials P1–P5 have been

obtained, which could repro-

ducibly be crystallized into

phase-pure M1 (C1–C5). If the

same reaction conditions were

applied in autoclave A2, the

synthesis results in a precursor

of a phase mixture (P6/C6 in

Table 3). However, synthesis of phase-pure M1 succeeded in A2 after optimization of the reaction temperature. The latter was varied between 383 and 448 K (autogeneous pressures between 4 and 9 bar) (**Figure 5**), keeping the synthesis time constant at 96 h. The optimum synthesis temperature in A2 was found to be 403 K (P10). At this temperature, phase-pure M1 has been obtained after activation (C10). Below this

temperature, M1 is not formed, but M2, Mo_5O_{14} , and $\text{TeMo}_5\text{O}_{16}$. Increasing the temperature further to 423 and 448 K, results in the formation of M1/M2 (C13), and M1/M2/ Mo_5O_{14} / $\text{V}_{0.95}\text{Mo}_{0.97}\text{O}_5$ phase mixtures (C14), respectively.

Furthermore, the synthesis time of the hydrothermal treatment has been varied between 24 and 144 h, keeping the optimized synthesis temperature constant at 403 K (**Figure 6**). The complexity of the crystalline phase mixtures decreases with increasing reaction time resulting in phase-pure M1 after 96 h (C10). However, an extended reaction time of 144 h, again results in a M1/M2 phase mixture (C11).

The diffraction patterns of the various precursor materials obtained under the different hydrothermal reaction conditions show different characteristics. Generally, XRD patterns of the precursor materials

synthesized in A1 exhibit a broad peak at $22^\circ 2\theta$, a peak of very low intensity at $45^\circ 2\theta$, and two ill-defined features around 8° and $27^\circ 2\theta$ (see for example P2 in **Figure 7a**). The reflection at $22^\circ 2\theta$ indicates the presence of long-range ordering of either, M1, M2, or a Mo_5O_{14} -type phase in the

[001] direction. Ordering along other crystallographic directions is hardly developed as indicated by the width of the other features, which are observed at diffraction angles where the reflections of the M1 structure are expected (**Figure 8**) [5, 8]. Activation of the

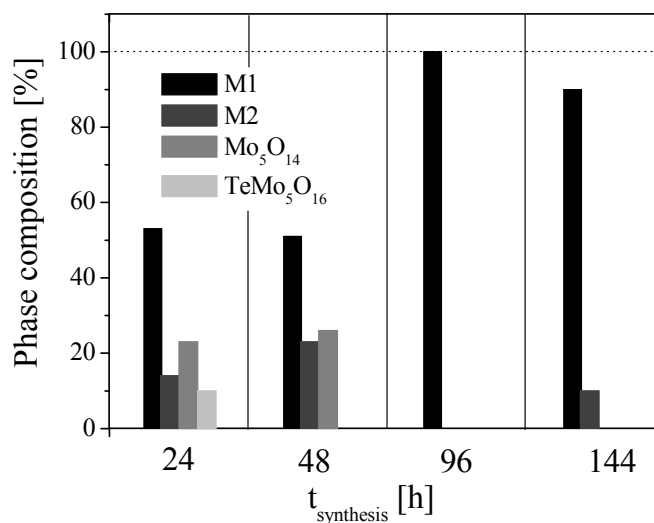


Figure 6. Phase composition of catalysts prepared in A2 at 403 K and different synthesis times.

precursor prepared in A1 leads to highly crystalline phase-pure M1 (see for example C2 in **Figure 8a**). The XRD patterns of crystalline M1 materials C1-C5 fit satisfactorily with the structural model of M1 refined by DeSanto *et al.* (ICSD 55097) [5], showing differences only with respect to the peak intensities, which indicates deviant metal site occupancy (**Figure 8c**).

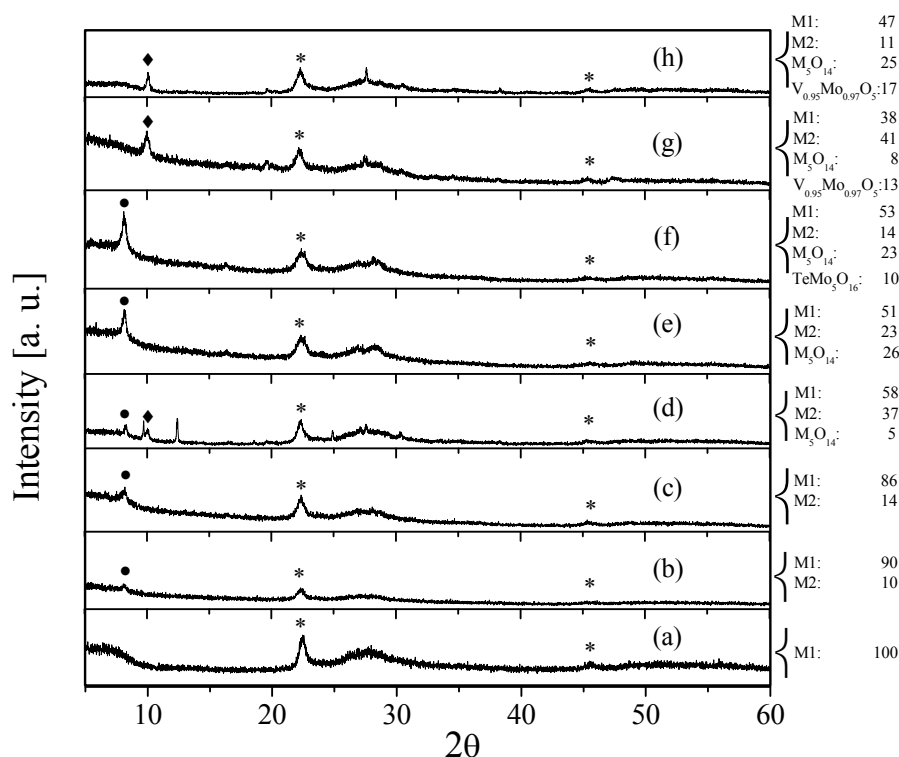


Figure 7. XRD patterns of precursors, (a) P2, (b) P11, (c) P13, (d) P6, (e) P9, (f) P8, (g) P14, and (h) P7.

● $(\text{NH}_4)_8(\text{V}_{19}\text{O}_{41}(\text{OH})_9)(\text{H}_2\text{O})_{11}$, ◆ $(\text{NH}_4)_6\text{Mo}_8\text{O}_{27} \cdot 4\text{H}_2\text{O}$, * M1 precursor.

The resulting phase-composition of each precursor after activation is indicated right in the figure in [%].

In addition to the peaks described above for the M1 precursor materials, sharp peaks at 8.3° , 9.7° , 10.0° , 12.4° , 18.6° , 24.9° , 27.1° , 27.6° , 30.4° , and 38.3° 2θ appear in the XRD patterns of precursor materials leading to phase mixtures of M1, M2, M_5O_{14} -type ($\text{M}=\text{Mo}$, V and/or Nb) structures, and/or $\text{V}_{0.95}\text{Mo}_{0.97}\text{O}_5$ (**Table 3**, **Figure 7b-h**). The peak

at $8.3^\circ 2\theta$ may be assigned to a supra-molecular vanadium compound $(\text{NH}_4)_8(\text{V}_{19}\text{O}_{41}(\text{OH})_9)(\text{H}_2\text{O})_{11}$ (ICSD 063213) [43], and the peak at $10.0^\circ 2\theta$ may indicate the formation of ammonium octamolybdate $(\text{NH}_4)_6\text{Mo}_8\text{O}_{27}\cdot 4\text{H}_2\text{O}$ (ICSD 2017) [44]. The peaks at 9.7° , 12.4° , 18.6° , and $30.4^\circ 2\theta$ can be assigned to $(\text{NH}_4)_2(\text{Mo}_4\text{O}_{13})$ (ICSD 068562), whereas the peaks at 27.6° and $38.3^\circ 2\theta$ are due to the presence of elemental tellurium. Furthermore, the presence of $\text{Nb}_2\text{Te}_4\text{O}_{13}$ (ICSD 90371) cannot be excluded due to the presence of additional peaks at 24.9° and $27.1^\circ 2\theta$.

Precursors P8, P9, P11, and P13 (**Figure 7b, c, e, and f**) have identical XRD fingerprints, differing only in the intensity of the peak at $8.3^\circ 2\theta$. As mentioned above, this peak may originate from a residual supra-molecular vanadium compound with NH_4^+ as the counter ion. The variety of phases in the activated catalysts increases with increasing intensity of

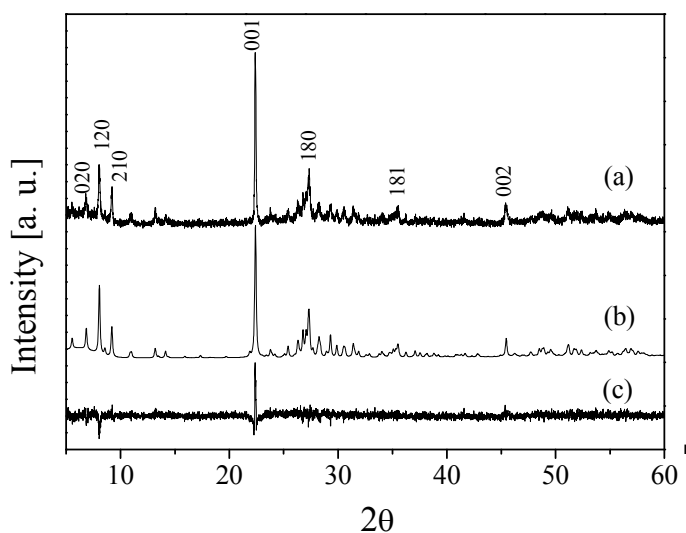


Figure 8. XRD patterns of the phase-pure M1 catalyst C2: (a) measured, (b) calculated based on [5], and (c) difference a-b; the lattice parameters of C2 are $a = 21.2044(23)$, $b = 26.6785(30)$ and $c = 4.00466(33)$.

this peak in the patterns of the precursor.

Figure 7g and h show a slightly different XRD fingerprint with a peak at $10.0^\circ 2\theta$ assigned to crystalline ammonium octamolybdate. The presence of this phase in the precursor may correlate with the formation of $\text{V}_{0.95}\text{Mo}_{0.97}\text{O}_5$, which is obtained after the activation process in both cases (C14, C7).

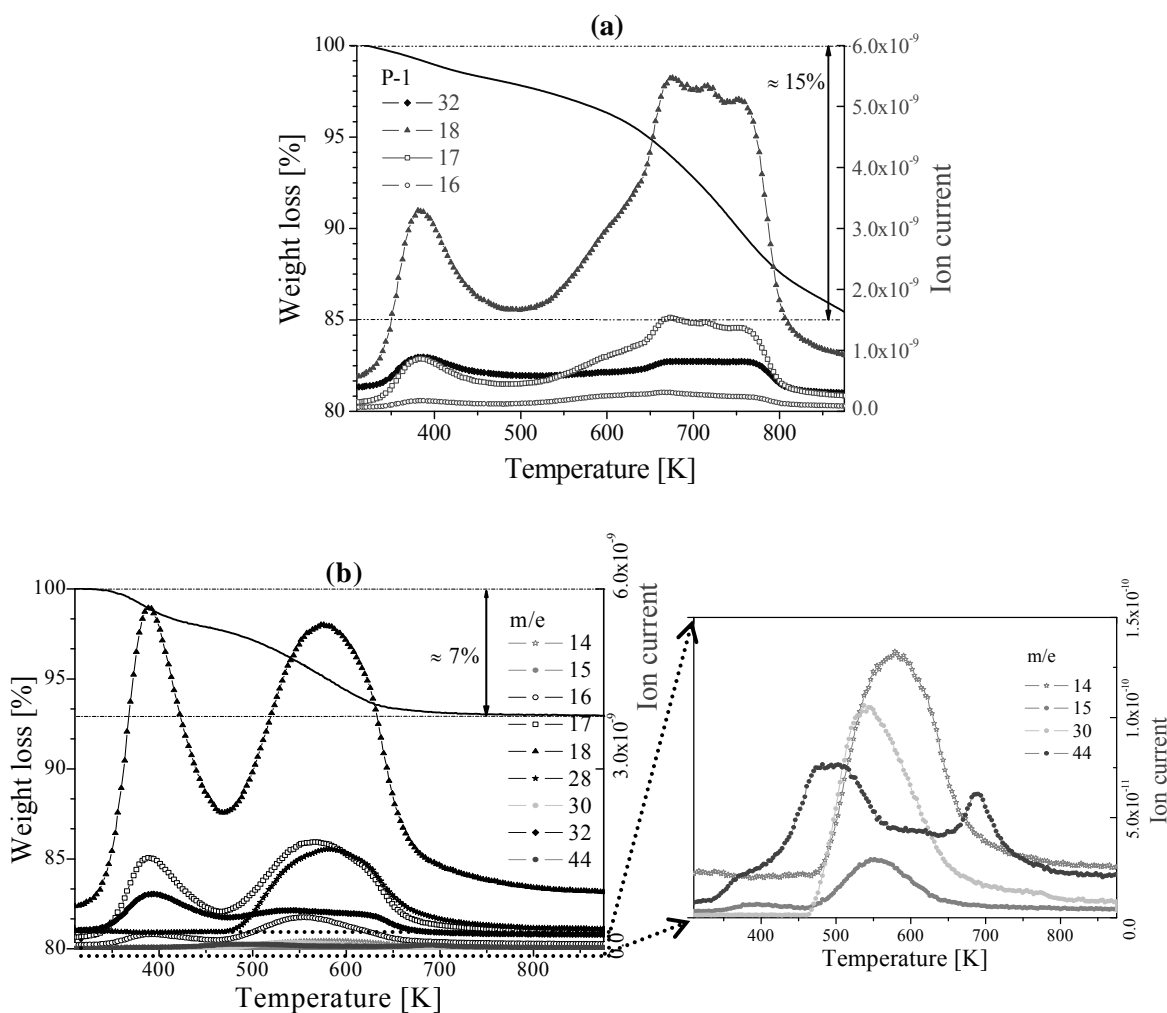


Figure 9. TG-MS of precursor materials; (a) M1 precursor P4 and (b) precursor of a phase mixture P8.

The presence of ammonium containing phases in the precursor materials leading to phase mixtures after activation is supported by thermoanalysis of the M1 precursor P4 and the multi-phase precursor P8, respectively. Two steps of mass loss appear in the TG curves of both precursors (**Figure 9**). The mass loss of 15 % of P4 is exclusively due to release of water. Traces of nitrogen containing compounds were not detected. In contrast, the mass loss of 7 % observed in case of P8 is partially due to desorption of ammonia. The two losses observed at 388 K and 578 K are mainly associated with the release of water

and oxygen. However, the second mass loss is also due to the decomposition of residual nitrogen containing compounds (N_2 ($m/e = 28$), NO ($m/e = 30$)). Traces of CO_2 ($m/e = 44$) are released at 490 K and 690 K.

Obviously, nanostructure and phase composition of the precursor material predetermine the final phase composition of the catalyst obtained after activation in inert gas at high temperatures. The entire disruption of the metal-ligand coordination in the initial metal salts and complete rearrangement of the coordination geometry around the central metal atoms are presumably necessary requirements for crystallization of phase-pure M1 during the subsequent activation step. As long as, e.g., ammonium containing phases are observed in the precursor, the crystallization into a phase-pure M1 catalyst fails and additional phases are formed.

3.3 Homogeneity and microstructure of the precursor materials

Phase-pure crystalline mixed oxides characteristically exhibit a high spatial homogeneity in their chemical composition. The homogeneous distribution of elements in phase-pure M1 is already reflected in the precursor as evidenced by EDX in the scanning electron microscopy. The standard deviation of the elemental analysis by EDX including numerous spots is lowest for the precursor of single-phase M1 (**Figure 10a**). As expected, the standard deviation increases with increasing phase variety. Therefore, in addition to the XRD patterns, the analysis of the local bulk elemental distribution can also be used in evaluating the potential of as-synthesized precursor materials in view of the expected phase purity after activation. Compared to precursors leading to phase mixtures, the M1 precursor shows a strikingly increased niobium content. This increased Nb content is also evident from SEM/EDX analysis of the activated catalyst (**Figure**

10b). Since the activated material is highly crystalline, the presence of Nb in amorphous fractions of the material can be excluded. The metal stoichiometry in the activated M1 corresponds to $\text{Mo}_{6.24}\text{V}_{1.41}\text{Te}_{1.76}\text{Nb}_{2.35}\text{O}_x$ for the catalyst C1. Compared to the unit cell formula normalized to niobium $\text{Mo}_{7.8}\text{V}_{1.2}\text{Te}_{0.94}\text{Nb}_1\text{O}_{28.9}$ given in the literature [5], the Nb content of M1 prepared in this work is more than two times higher than in the M1 phase analyzed by DeSanto *et al.*. This increased Nb content is exclusively observed for the phase-pure M1 catalysts, but not for the phase mixtures and their precursors.

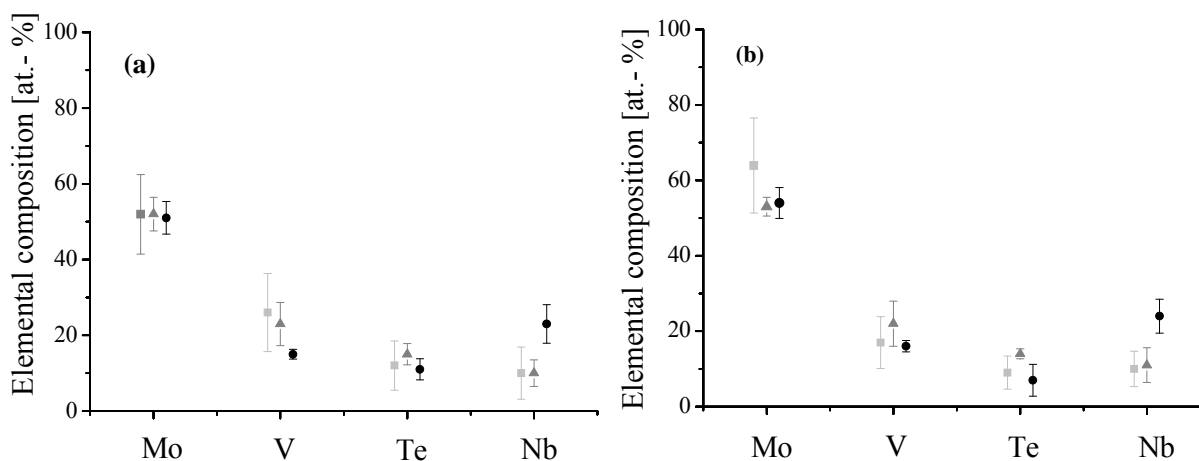


Figure 10. Elemental composition of (a) single-, bi- and multi-phase precursors and (b) single, bi, multi-phase activated catalysts as determined by EDX.
 ● phase-pure M1; ▲ bi-phase materials; ■ multi-phase materials
 The bars represent the standard deviation.

3.4 Development of short-range order during hydrothermal synthesis and activation

The M1 structure contains 13 crystallographic metal sites (**Figure 11**). According to combined neutron and synchrotron powder diffraction data, the four metals occupy certain sites either preferred or exclusively [5]. EXAFS analysis has been performed on

phase-pure M1 C1. The data quality obtained at the V K edge and Te L_{III} edge was not sufficient for reliable analysis, but local coordination of Mo and Nb in both precursor and

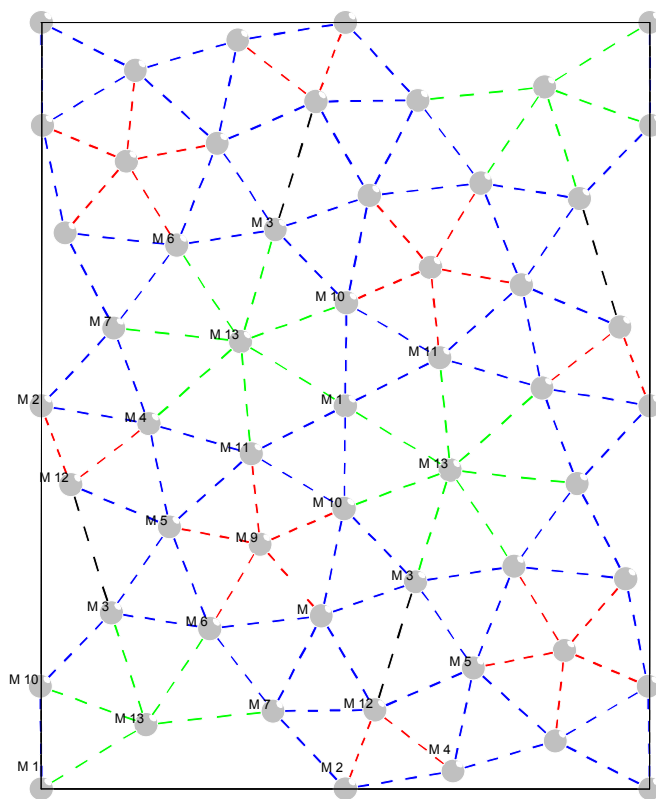


Figure 11. Classification of average metal-metal distances in the M1 structure [6] (oxygen positions not shown): red: 2.9-3.5 Å, blue: 3.5-4.0 Å, green: 4.0-4.5, black: 4.5-5.0 Å.

activated materials have been investigated. Of particular interest is the metal-metal shell in the EXAFS spectra, because this is directly correlated to the distance between neighboring metals and characteristic for the coordination geometry. An approximate classification of metal-metal distances in the M1 structure is given in

Figure 11. As observed in the EXAFS spectra at the Mo and Nb K edges, the

characteristic bond length distribution of the metal-oxygen and the metal-metal shell of the M1 phase is already established in the precursor (**Figure 12**). The pseudo-radial distribution functions shown in **Figure 12** are not phase-shift corrected, and, therefore, the peaks are shifted by approximately -0.4 Å with respect to the crystallographic distances. The Fourier transform of the EXAFS signal at the Nb K edge of the precursor material has a large peak at about 3 Å that corresponds to the short metal-metal distance

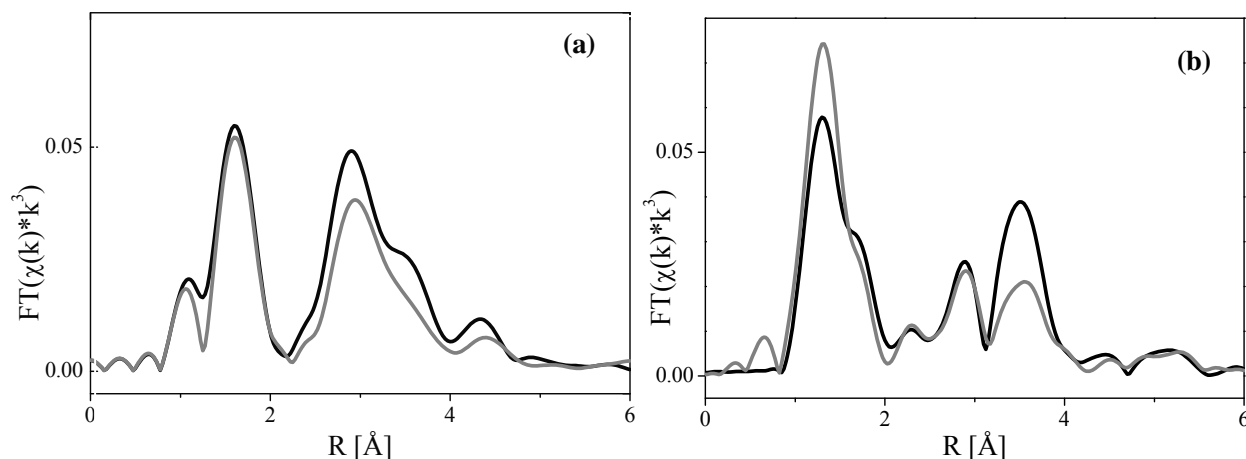


Figure 12. Fourier transformed (not phase-shift corrected) of (a) the Nb K edge $\chi(k)*k^3$ and (b) the Mo K edge $\chi(k)*k^3$ of the precursor (gray) and activated phase-pure M1 (black). The peaks are shifted by approx. -0.4 Å with respect to crystallographic distances.

between the pentagonal bipyramidal coordination and the center of the surrounding octahedrons (**Figure 12a**). In agreement with XRD, the higher amplitude in the metal-metal shells of the activated material compared to the precursor can be attributed to ongoing crystallization. At the Mo K edge (**Figure 12b**), a second peak is observed at about 3.8 Å, which corresponds to longer metal-metal distances, typical for either distances between central atoms in octahedrons, or the interlayer Mo-M distance in $[001]$ direction. In EXAFS spectra measured at the Nb K edge, the strong amplitude in the metal-metal shell around the Nb centers at about 3 Å indicates the presence of many short metal-metal distances implying preferential pentagonal bipyramidal coordination of niobium. Additionally, a broad shoulder appears at about 3.8 Å, which is present in the precursor and more pronounced in the activated material (**Figure 12a**). This shoulder is much stronger than in simulations assuming exclusive pentagonal bi-pyramidal coordination of Nb. Taking the high niobium content of C1 into account, which is inconsistent with the unit cell formula of a M1 containing Nb only in pentagonal

bipyramidal positions [5, 8], EXAFS supplementary indicates that Nb is additionally located in octahedral positions.

3.5 Post-treatment of multi-phase precursors

Decomposition of the metal salts and complete rearrangement of molecular building blocks has been shown to be essential in hydrothermal synthesis of phase-pure M1. Control of process parameters is required to achieve this. Under standard conditions ($T = 448$ K, $t = 48$ h), the reconstruction succeeds more or less efficiently depending on the technical parameters of the autoclave. In **Figure 13a**, diffraction patterns of a multi-phase precursor with a content of residual ammonium octamolybdate is shown. In the absence of oxygen, this precursor has been subjected to steam at 773 K and a pressure of 20 MPa for 2 hours. The resulting material shows the typical X-ray diffraction patterns of nano-structured M1 (**Figure 13b**). Performing the usual thermal activation in argon at 673 K,

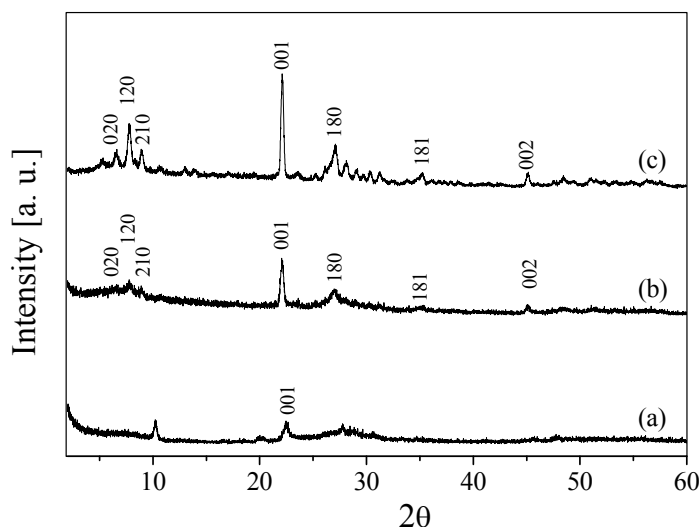


Figure 13. XRD patterns of (a) a multi-phase precursor (catalyst code 2392) that crystallizes during heat treatment in Ar at 873 K into 55 % M1, 31 % M2, and 14% Mo_5O_{14} , (b) the precursor after hydrothermal post-treatment at 773 K in presence of steam (catalyst code 2902) and (c) the activated steam-treated material (catalyst code 3057).

the steam-treated precursor crystallizes into phase-pure M1 (**Figure 13c**) indicating a comparatively high thermodynamic stability of M1 under the high temperature and high pressure applied, compared to other phases, such as M_5O_{14} -type (M=Mo, V and/or Nb) structures, or M2.

3.6 Activation

Table 4

Influence of the heat treatment on BET surface area of crystalline phase-pure M1 catalysts synthesized in A1

Catalyst	Calcination in synthetic air	Activation in Ar	BET [m ² /g]
C1	548K, 1h	873K, 2h	1
C2	-	873K, 2h	2
C4	598K, 1h	923K, 2h	4

Activation in inert atmosphere at high temperatures is necessary, on the one hand, to obtain long-range order of the material and, on the other hand, to create catalytic activity. In the present work, different activation conditions have been applied to precursors prepared in A1 in order to study the influence of the activation conditions on the microstructure of the final catalyst. Irrespective of the temperature applied in the thermal treatment in an inert atmosphere (873 or 923 K), and whether preceding calcination in air (548 or 498 K) was performed, the bulk of the final catalyst is exclusively composed of M1, confirming the observation described above that the M1 phase is established during hydrothermal synthesis. To a certain extent, the specific surface area may be adjusted by the thermal activation parameters (**Table 4**). Different from the general expectation, the BET surface area increases with increasing activation temperature. In **Figure 14**, SEM images of two phase-pure M1 catalysts activated at 873 or 923 K, respectively, are

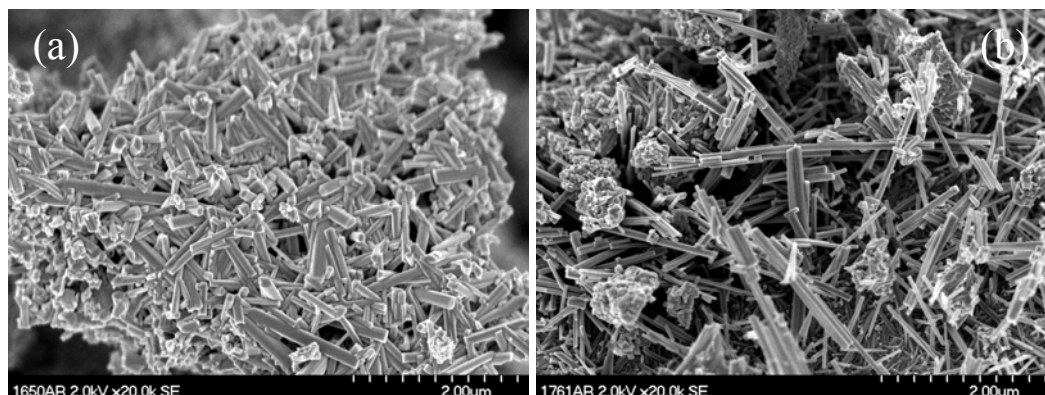


Figure 14. SEM images of phase-pure catalysts treated at different temperatures; (a) calcination in air at 598 K followed by activation in argon at 923 K (C5) and (b) calcination in air at 548 K followed by activation in argon at 873 K (C1).

shown. From these images, the typical needle-shape morphology of the M1 crystals is evident. The results of a shape-analysis based on measuring approximately 400 needles are presented in **Figure 15**. The distribution of the length of the needles in the two catalysts (**Figure 15a**) is very similar. Evidently, in the present experiments the length was predetermined by the hydrothermal synthesis. This observation is consistent with the

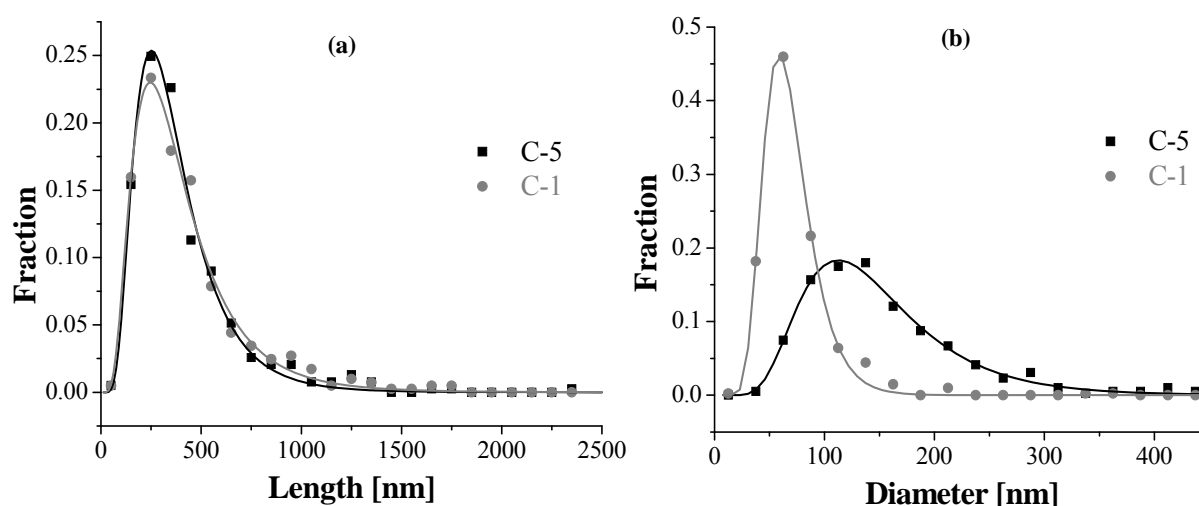


Figure 15. Shape analysis of two single-phase catalysts heat-treated at different temperatures: distribution of (a) length and (b) the diameter of the M1 needles. ● single-phase activated at lower temperatures (C1), ■ single-phase activated at higher temperatures (C5).

XRD results indicating that long-range ordering in the [001] direction is already established in the precursor material. Further growth of the needles in the [001] direction during the activation step cannot be excluded. However, in the temperature range applied (873-923 K), no influence of the temperature on the length of the needles was observed. In contrast, an anisotropic growth of the basal (001) plane has been observed. This is reflected in an increased mean diameter of the needles in phase-pure M1 activated at higher temperature (**Figure 15b**). Apparently, the parameters of the heat treatment could be used to control the aspect ratio in the final phase-pure catalyst, which may have implications on the catalytic activity in propane oxidation. However, the effect observed for the two catalysts needs further systematic elucidation.

4 Summary and conclusions

In the last decade, MoVTaNbO_x catalysts, and specifically the M1 phase have generated great academic interest due to the exceptional catalytic performance achieved in the selective oxidation of propane to acrylic acid. The accessibility of phase-pure M1 on a large scale is a key issue that needs to be solved in order to systematically investigate the catalytic properties of M1 and to elucidate the function of its structure in propane activation and oxygenate formation [3, 12, 15, 17, 24]. Hydrothermal synthesis of the chemically and structurally complex M1 phase requires precise control of the preparation parameters. In this study, the influence of reaction temperature, reaction time, and the technical parameters of the autoclave on morphology, and bulk and local structure of the resulting MoVTaNbO_x catalysts has been investigated, achieving a better understanding of the formation mechanism of the M1 phase, and enabling an improved control over the final catalyst structure.

Hydrothermal reaction is the crucial step in the synthesis of M1. The individual elements are inhomogeneously distributed in the reaction mixture initially introduced into the autoclave as shown by Raman and UV/Vis spectroscopy together with SEM-EDX analysis. In solution, iso- and heteropolyanions of molybdenum and giant polyoxometalate clusters have been identified. Pre-precipitation is not necessarily detrimental for formation of phase-pure M1. Investigation of the resulting precursor materials proves that the structural elements required for crystallization of M1 are already established in the course of the hydrothermal process. The reaction could take place by a dissolution-precipitation mechanism involving dissolution or rearrangement of polyoxometalate building blocks followed by precipitation of an ill-crystallized nano-structured product from solution. A complete reorganization of counter-ion-containing phases is essential, which has been shown to be accelerated in presence of steam at very high temperatures and pressures. Residual ammonium containing supra-molecular species in the precursor result in formation of phase mixtures during the subsequent heat treatment. Precursor materials of phase-pure M1 catalysts show long-range order in the [001] direction as confirmed by XRD and EXAFS analysis. Ordering along the other crystallographic directions is less developed. Crystallization occurs during the subsequent heat treatment of the precursor in an inert gas in the temperature range between 823 and 923 K. The spatial homogeneity of elements in crystalline M1 is already reflected in the corresponding precursor. Remarkably, phase-pure M1 prepared in the present work shows a niobium content twice as high as the Nb content in the M1 phase analyzed by DeSanto *et al.* [6], which confirms observations that the M1 structure has a considerable chemical flexibility. There is some indication that the specifics of the needle-like

morphology of the final catalyst can be controlled by the conditions of the activation process. An anisotropic growth of the basal (001) plane of the M1-phase has been observed, which is reflected in an increased mean diameter of the needles in materials activated at higher temperature.

In summary, precise control of the hydrothermal reaction conditions is required to obtain the desired crystal structure. The proper conditions can be achieved by optimizing particularly reaction temperature and reaction time. Technical parameters of the autoclave influencing the hydrothermal synthesis have to be taken into account. The present study shows that application of identical reaction parameters does not necessarily mean that identical materials with comparable catalytic properties will be produced when the reaction is performed in different autoclaves. This has to be taken into account when the catalytic behavior of MoVTenbO_x catalysts is compared. The availability of *in-situ* techniques is required and currently under development to monitor the hydrothermal reaction inside the autoclave and to generate quantitative kinetic information.

5 Acknowledgments

The authors thank Mrs. Gisela Lorenz, Mrs. Edith Kitzelmann, and Mrs Gisela Weinberg for technical assistance. Dr. Andreas Furche is acknowledged for performing the thermal analysis. We are grateful to HASYLAB/Hamburg for providing beam time for this work.

6 References

- [1] T. Ushikubo, H. Nakamura, Y. Koyasu, S. Wajiki, US Patent 5380 933A (1995); Mitsubishi Kasei Corporation.
- [2] T. Ushikubo, K. Oshima, A. Kayou, M. Hatano, *Studies in Surface Science and Catalysis* 112 (1997), 473.

- [3] M. Baca, A. Pigamo, J.-L. Dubois, J. M. M. Millet, *Topics in Catalysis* 23 (2003), 39.
- [4] J.M. López-Nieto, P. Botella, B. Solsona, J. M. Oliver, *Catalysis Today* 81 (2003), 87.
- [5] Inorganic Crystal Structure Database, Fachinformationszentrum (FIZ) Karlsruhe, Germany.
- [6] P. DeSanto, D. J. Buttrey, R. K. Grasselli, C. G. Lugmair, A. F. Volpe, B. H. Toby, T. Vogt, *Zeitschrift für Kristallographie* 219 (2004), 152.
- [7] J. M. M. Millet, H. Roussel, A. Pigamo, J. L. Dubois, J. C. Jumas, *Applied Catalysis A: General* 232 (2002), 77.
- [8] H. Tsuji, K. Oshima, Y. Koyasu, *Chemistry of Materials* 15 (2003), 2112.
- [9] H. Murayama, D. Vitry, W. Ueda, G. Fuchs, M. Anne, J.L. Dubois, *Applied Catalysis A: General* 318 (2007), 137.
- [10] M. Lundberg, M. Sundberg, *Ultramicroscopy* 52 (1993), 429.
- [11] J. Holmberg, R. K. Grasselli, A. Andersson, *Applied Catalysis A: General* 270 (2004), 121.
- [12] R. K. Grasselli, D. J. Buttrey, P. DeSanto, Jr., J. D. Burrington, C. G. Lugmair, A. F. Volpe, Jr., T. Weingand, *Catalysis Today* 91-92 (2004), 251.
- [13] D. Vitry, Y. Morikawa, J. L. Dubois, W. Ueda, *Topics in Catalysis* 23 (2003), 47.
- [14] P. Beato, A. Blume, F. Girgsdies, R. E. Jentoft, R. Schlögl, O. Timpe, A. Trunschke, G. Weinberg, Q. Basher, F. A. Hamid, S. B. A. Hamid, E. Omar, L. Mohd Salim, *Applied Catalysis A: General* 307 (2006), 137.
- [15] J. B. Wagner, O. Timpe, F. A. Hamid, A. Trunschke, U. Wild, D. S. Su, R. K. Widi, S. B. A. Hamid, R. Schlögl, *Topics in Catalysis* 38 (2006), 51.
- [16] H. Hibst, F. Rosowski, G. Cox, *Catalysis Today* 117 (2006), 234.
- [17] W. Ueda, D. Vitry, T. Katou, *Catalysis Today* 99 (2005), 43.
- [18] P. DeSanto Jr., Douglas J. Buttrey, R. K. Grasselli, C. G. Lugmair, A. F. Volpe, B. H. Toby, T. Vogt, *Topics in Catalysis* 23 (2003), 23.
- [19] P. DeSanto Jr., D. J. Buttrey, R. K. Grasselli, W. D. Pyrz, C. G. Lugmair, A. F. Volpe Jr., T. Vogt, B. H. Toby, *Topics in Catalysis* 38 (2006), 31.

- [20] T. Ushikubo, I. Sawaki, K. Oshima, K. Inumaru, S. Kobayakawa, K. Kiyono, US Patent 5 422 328 (1995); Mitsubishi Kasei Corporation.
- [21] M. Baca, J. M. M. Millet, *Applied Catalysis A: General* 279 (2005), 67.
- [22] W. Ueda, D. Vitry, T. Kato, N. Watanabe, Y. Endo, *Research on Chemical Intermediates* 32 (2006), 217.
- [23] P. Botella, B. Solsona, A. Martínez-Arias, J. M. López-Nieto, *Catalysis Letters* 74 (2001), 149.
- [24] P. Botella, J. M. López-Nieto, B. Solsona, A. Mifsud, F. Márquez, *Journal of Catalysis* 209 (2002), 445.
- [25] D. Vitry, Y. Morikawa, J. L. Dubois, W. Ueda, *Applied Catalysis A: General* 251 (2003), 411.
- [26] W. Ueda, D. Vitry, T. Katou, *Catalysis Today* 96 (2004), 235.
- [27] P. Botella, E. García-González, J. M. López-Nieto, J. M. González-Calbet, *Solid State Sciences* 7 (2005), 507.
- [28] P. Botella, P. Concepción, J. M. López-Nieto, Y. Moreno, *Catalysis Today* 99 (2005), 51.
- [29] F. Ivars, P. Botella, A. Dejoz, J. M. López-Nieto, P. Concepción, M. I. Vázquez, *Topics in Catalysis* 38 (2006), 59.
- [30] W. Ueda, K. Oshihara, *Applied Catalysis A: General* 200 (2000), 135.
- [31] T. Katou, D. Vitry, W. Ueda, *Chemistry Letters* 32 (2003), 11.
- [32] T. Ressler, *Journal of Synchrotron Radiation* 5 (1998), 118.
- [33] K. Oshihara, T. Hisano, W. Ueda, *Topics in Catalysis* 15 (2001), 153.
- [34] J. Gupta, *Nature* 140 (1937), 685; H. Siebert, *Zeitschrift für anorganische und Allgemeine Chemie* 301 (1959), 11.
- [35] J. C. Evans, *Inorganic Chemistry* 2 (1963), 373.
- [36] K.-H. Tytko, B. Schönfeld, *Zeitschrift für Naturforschung B* 30 (1975), 471.
- [37] J.-M. Jehng, I. E. Wachs, *Journal of Raman Spectroscopy* 22 (1991), 83.
- [38] A. Müller, E. Krickemeyer, H. Bögge, M. Schmidtman, F. Peters, *Angewandte Chemie International Edition* 37 (1998), 3360.

-
- [39] A. Müller, A. M. Todea, J. van Slageren, M. Dressel, H. Bögge, M. Schmidtmann, M. Luban, L. Engelhardt, M. Rusu, *Angewandte Chemie International Edition* 44 (2005), 3857.
- [40] M. Sadakane, N. Watanabe, T. Katau, Y. Nodasaka, W. Ueda, *Angewandte Chemie International Edition* 46 (2007), 1493.
- [41] M. T. Pope, Y. Jeannin, M. Fournier, *Heteropoly and Isopoly Oxometalates*, Springer-Verlag, Berlin Heidelberg, New York, Tokyo (1983), 21.
- [42] S. Yuhao, L. Jingfu, W. Enbo, *Inorganica Chimica Acta* 117 (1986), 23.
- [43] A. Mueller, M. Penk, E. Krickemeyer, H. Boegge, H. J. Walberg, *Angewandte Chemie* 100 (1988), 1787.
- [44] I. Boeschen, B. Buss, B. Krebs, *Acta Crystallographica B* 30 (1974), 48.

CHAPTER 2- Investigation of catalytic behavior of M1-phase catalyst in the selective oxidation of propane to acrylic acid. Correlation approach between catalytic performance and surface/bulk properties.

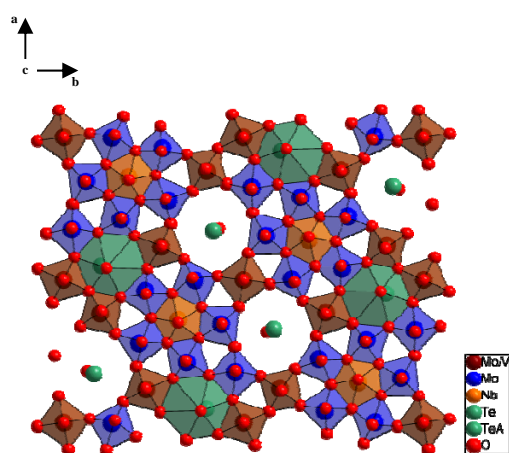
Abstract

Hydrothermally synthesized single-, bi-, and multi-phase MoVTaNbO_x catalysts were studied in the selective oxidation of propane to acrylic acid. Phase-pure M1 catalysts showed high formation rates of acrylic acid. Phase cooperation between the M1 and M2 phases has not been observed. Single-phase M1 catalysts show different catalytic properties, which are mainly related to differences in the BET surface areas. Shape analysis of the needle-like M1 crystals has been presented as a suitable method to elucidate the correlation between the surface area of a certain crystallographic plane, such as the *ab* plane, and the formation rate of acrylic acid. In-situ XPS experiments under different reaction media over time confirmed the elemental re-distribution at the catalytic surface. Tellurium enrichment at the expense of molybdenum is observed at the surface of phase-pure M1 depending on the reactant mixture. Depth profile analysis of the catalytic surface reveals tellurium migration to the surface from subsurface layers in response to changes in the reactive gas mixture. Furthermore, phase-pure M1 exhibited reasonable stability under reaction conditions, which is of a great importance for any potential industrial application.

Keywords: MoVTaNbO_x catalyst, M1-phase, hydrothermal synthesis, in-situ XPS, SEM-EDX, TEM, propane oxidation

1 Introduction

Direct selective oxidation of propane into acrylic acid is an alternative and challenging approach [1-3] with the view of displacing the current industrial two-stage oxidation process, in which propylene is used as feedstock [4, 5]. Efficient catalysts for such a reaction should be able simultaneously to activate the stable C-H bonds of the saturated hydrocarbon, provide lattice oxygen atoms and accommodate the suitable acid-base properties, which may control the desorption of the desired reaction product avoiding its further oxidation. Among all catalysts proposed to date [1-3], Mo-V-Te-Nb mixed metal oxides have been found to be the most promising, achieving yields of acrylic acid of about 50 % [6]. These multi-component metal oxide catalysts consist of mainly two orthorhombic phases called “M1” and “M2” [7]. In the M1 phase (**Scheme 1**),



Scheme 1. M1 phase [8].

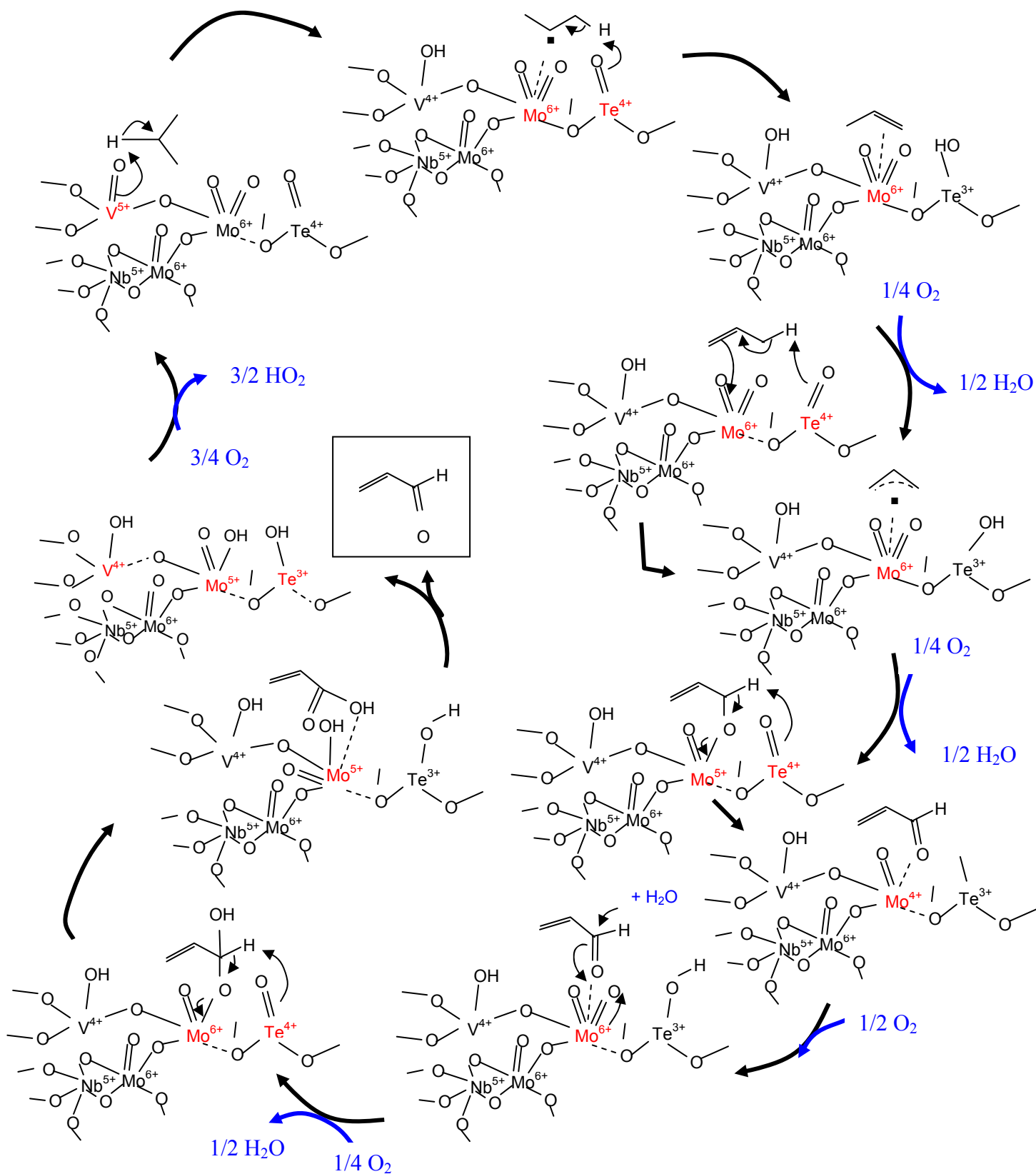
corner-linked MO_6 ($\text{M}=\text{Mo}, \text{V}$) octahedrons are two-dimensionally assembled in the ab plane forming 6- and, 7-membered rings which are partially occupied by TeO units [8, 9]. Niobium has been reported to be exclusively located in the centre of a MO_7 pentagonal bipyramidal motif sharing edges with the surrounding octahedrons [8]. The

ab planes are congruently stacked along the c direction by sharing corner oxygen atoms, resulting in a needle-like crystal morphology in which the ab planes are perpendicular to the length axis. The M2 phase is less complex [8]. In this structure, only 6-membered rings are formed by arrangement of corner-linked octahedrons in the ab plane. The

formula of the refined unit cell has been determined to be $\text{Mo}_{7.8}\text{V}_{1.2}\text{NbTe}_{0.937}\text{O}_{28.9}$ for M1 and $\text{Mo}_{4.31}\text{V}_{1.36}\text{Te}_{1.81}\text{Nb}_{0.33}\text{O}_{19.81}$ for M2, respectively [8].

It is generally accepted that propane activation and the high selectivity to acrylic acid are due to the M1 phase [10-12]. It has been suggested that the *ab* plane in particular is responsible for this high activity. This conclusion was drawn from experiments based on mechanical grinding of M1 phase catalysts [13-15]. It was postulated that this mechanical treatment resulted in exclusively the creation of new surface belonging to the *ab* plane.

Grasselli *et al.* have proposed a propane oxidation mechanism based on structural considerations (**Scheme 2**), supposing that the *ab* plane of the M1 phase is the carrier of the active centers, and general concepts of organic chemistry [16]. According to this mechanism, the first step is the activation and abstraction of a methylene hydrogen atom from propane at a V^{5+} site. Subsequently, α -H abstraction and oxygen insertion occur on Te^{4+} and Mo^{6+} sites, respectively. The resulting σ -O-allylic species is attacked by water, leading to a surface bound acrolein hemiacetal intermediate which is then readily further oxidized and desorbed as acrylic acid. The function of Nb is attributed to spatial separation of the active centers - according to the concept of site isolation. Increased selectivity to acrylic acid is thus obtained by minimizing unwanted total oxidation. On the other hand, the specific arrangement of transition metal atoms in the model suggested by Grasselli *et al.* is, however, not essential since catalysts of completely different chemical composition, e.g. without Te, show catalytic activity in selective oxidation of propane to acrylic acid [17, Chapter 4]. Moreover, the mechanism reported by Grasselli *et al.* [16] is based on the addition of half an atom of oxygen ($1/4 \text{ O}_2$), which is physically meaningless.



Scheme 2. Mechanism of the selective oxidation of propane to acrylic acid reported by Grasselli *et al.* [16].

On the other hand, the M2 phase is regarded as being unable to activate propane but as being efficient in the oxidation of propylene to acrylic acid [10]. Correlations between phase composition and catalytic performance are still actively debated [7, 10, 11, 15, 16, 18-26]. It has been suggested that a mixture of M1 and M2 is required for operation at high propane conversions. Phase cooperation was reported in case of bi-phase catalysts synthesized in one pot [7, 10, 11, 15, 18, 19], as well as in case of intimate physical mixtures of both orthorhombic single-phases [16, 20-23]. On the contrary, hydrothermally synthesized phase-pure M1 was found to produce higher acrylic acid yields compared to physical mixture of M1 with M2 prepared by hydrothermal synthesis and solid-state reaction, respectively [24].

The present contribution is an attempt to shed some light on the debate regarding the correlation between phase composition and catalytic properties. For this propose, single-phase M1 and multi-phase MoVTenbO_x catalysts have been prepared by hydrothermal synthesis and studied in the selective oxidation of propane to acrylic acid. Phase-pure M1 proved to be highly active and selective to acrylic acid. Therefore, in this study a series of differently prepared phase-pure M1 catalysts was investigated. The bulk and surface properties were examined with emphasis on surface composition under different reaction conditions and morphological analysis was carried out in order to elucidate whether the exposure of a certain crystal plane correlates with catalytic performance.

2 Experimental

2.1 Catalysts preparation

The catalysts have been prepared by hydrothermal synthesis as described previously [27].

Ammonium heptamolybdate (NH₄)₆Mo₇O₂₄·4H₂O (Merck), vanadyl sulfate

$\text{VOSO}_4 \cdot 5\text{H}_2\text{O}$ (Riedel-deHäen), telluric acid $\text{Te}(\text{OH})_6$ (Aldrich) and ammonium niobium oxalate $\text{C}_{10}\text{H}_8\text{N}_2\text{O}_{33}\text{Nb}_2$ (Aldrich) were used as starting materials. A slurry was prepared by mixing the aqueous solutions of the metal salts in a Mo/V/Te/Nb molar ratio of 1/0.25/0.23/0.124. After the hydrothermal synthesis at 403-448 K during 24-48 h, the dark blue slurry obtained was filtered, washed with bidistilled water and dried for 16 hours at 353 K. Starting from the dried precursors, 3 g of the crystalline products were obtained by heat-treatment in inert gas with a flow of 100 ml/min for 2 h at 873 K or at 923 K (ramp 15°/min), either with or without previous calcination in air for 1 h at 548 K or at 598 K (ramp 10°/min). The activation was carried out in a rotating furnace.

2.2 Activity measurements

For testing the catalysts in selective oxidation of propane to acrylic acid, 0.5 g of the material was loaded into a quartz fixed bed reactor with an inner diameter of 4 mm. The feed was composed of propane/oxygen/nitrogen/steam in a molar ratio of 2.8/6.4/50.8/40. A GHSV of 1200 h^{-1} and a reaction temperature of 673 K have been applied. The products were analyzed by gas chromatography. Inorganic gases and $\text{C}_1\text{-C}_3$ hydrocarbons have been analyzed with a TCD detector using a molecular sieve column and a Porapak Q column, respectively, for separation. Oxygenated products have been detected applying a HP-FFAP column and a flame ionization detector.

2.3 Catalysts characterization

Bulk and microstructure were studied by X-ray Diffraction (XRD) and Transmission Electron Microscopy (TEM). XRD measurements were performed with a STOE STADI-P transmission diffractometer equipped with a focusing primary Ge (111)

monochromator and a position sensitive detector, using Cu-K α_1 radiation. For data analysis, the program TOPAS (v.2.1, Bruker AXS) was used to fit the diffraction patterns of the activated materials. Transmission electron microscopy was carried out on a Philips CM 200 FEG TEM operated at 200 kV. The microscope is equipped with a Gatan CCD camera for image acquisition and an EDAX Genesis EDX system. For TEM, the specimens were prepared by dry dispersing the catalyst powder on a standard copper grid coated with holey carbon film. HRTEM image simulations were calculated using JEMS. Morphology studies and shape analysis were performed applying Scanning Electron Microscopy (SEM). A Hitachi S-5200 with a PGT Spirit EDX system and a Hitachi S-4800 with an EDAX Genesis EDX detector were used. EDX (Energy Dispersive X-ray) studies in the SEMs were carried out with an accelerating voltage of 10 kV while images were acquired at 2 kV to optimize surface resolution. For SEM investigations the samples were deposited on carbon tape. From the SEM images, the length and diameter of more than 300 M1 needles was measured for each sample. Based on these measurements, the surface area was separately calculated for the lateral surface area, and the surface area of the *ab* facets assuming that the needles can be approximated as cylinders and that all material is in the form of needles.

A depth profile of the elemental composition was studied by X-ray Photoelectron Spectroscopy (XPS). By varying the kinetic energy between 170 eV and 470 eV, information depths of ca. 0.5 and ca. 1.5 nm were examined. The experiments have been performed in the presence of 0.3-0.5 mbar of the reaction mixtures, at the beamline U49-/2-PGM1, at the synchrotron source BESSY II (Berlin, Germany). Details of the setup have been published earlier [29].

Specific surface areas of the catalysts were measured by nitrogen physisorption using an AUTOSORB-1-C physisorption/chemisorption analyzer. All the samples were degassed at 353 K for 2 hours prior to nitrogen adsorption. Generally, 11 points have been considered in the linear range of the adsorption isotherm to calculate the surface area according to the BET method.

3 Results

3.1 General properties of the Mo-V-Te-Nb mixed oxides

Single-, bi-, and multi-phase Mo-V-Te-Nb mixed oxide catalysts have been prepared by

Table 1

Notation, phase composition and specific surface areas of the prepared catalysts

ID	Notation	Phase composition [%]	BET [m ² /g]
1761	SP-1	M1 100	1.0
1886	SP-2	M1 100	1.4
939	SP-3	M1 100	2.0
1650AR	SP-4	M1 100	2.5
1434	SP-5	M1 100	4.0
3906	MP-1	M1 85 M2 15	1.0
3982	MP-2	M1 59 M2 33 V _{0.95} Mo _{0.97} O ₅ 8	3.2
1464	MP-3	M1 58 M2 42	5.1
3984	MP-4	M1 53 M2 14 Mo ₅ O ₁₄ 23 TeMo ₅ O ₁₆ 10	0.8
3303	MP-5	M1 38 M2 41 Mo ₅ O ₁₄ 8 V _{0.95} Mo _{0.97} O ₅ 13	6.3
3695	MP-6	M2 32 Mo ₅ O ₁₄ 68	1.0

hydrothermal synthesis at different temperatures and reaction times [27]. Phase composition as determined by XRD and the specific surface area of the prepared catalysts are shown in **Table 1**. Single-phase M1 materials, denominated as “SP”, have a specific surface area between 1 and 4 m²/g. The specific surface area decreases in the sequence, SP-1 < SP-2 < SP-3 < SP-4 < SP-5. Bi- and multi-phase materials, denominated as “MP”, contain

Table 2

Bulk composition of phase-pure M1 catalysts as determined by EDX before and after propane oxidation. The numbers in parenthesis represent molar ratios of the metals normalized to molybdenum

Notation	Before/After reaction	Mo [%]	V [%]	Te [%]	Nb [%]
SP-1	Before reaction	53 ± 1.9	12 ± 0.9	15 ± 2.6	20 ± 1.7
	After reaction	52 ± 2.7	14 ± 2.0	14 ± 3.2	20 ± 4.1
SP-2	Before reaction	58 ± 3.0	13 ± 1.1	12 ± 2.6	17 ± 1.6
	After reaction	55 ± 1.0	14 ± 0.8	13 ± 1.3	18 ± 0.8
SP-3	Before reaction	51 ± 4.3	15 ± 1.3	11 ± 2.8	23 ± 5.1
SP-4	After reaction	58 ± 0.9	15 ± 0.5	10 ± 1.6	17 ± 1.4
SP-5*	Before reaction	54	16	10	20
Average composition before reaction		54 (1)	13 (0.24)	13 (0.24)	20 (0.37)
Average composition After reaction		55 (1)	14 (0.25)	12 (0.22)	19 (0.35)

* ICP

different amounts of M1. In addition to the M1 phase, other phases, such as M2, $V_{0.95}Mo_{0.97}O_5$, M_5O_{14} (M=Mo, V) or $TeMo_5O_{16}$ are present. The M1 content decreases with increasing number of the samples notation. The bulk composition of the phase-pure catalysts is summarized in **Table 2**.

3.2 Selective oxidation of propane

The hydrothermally synthesized single-, bi-, and multi-phase $MoVTenbO_x$ catalysts have been studied in the selective oxidation of propane to acrylic acid. Propane conversion, selectivity to acrylic acid and acrylic acid yield of all tested catalysts are shown in the **Table 3**. The phase-pure M1 catalysts (SP-1-5) convert propane with ca. 70-80 % selectivity into acrylic acid. Such value is significantly higher as compared with those reported in the literature (73 % vs. 62 % at comparable propane conversion of ~ 35 %) [28]. The activity and the formation rate of acrylic acid per unit of catalyst mass, as well

as, per unit surface area are also included in **Table 3**. M1 catalysts show similar but not identical values of their activity calculated per unit surface area, indicating that the

Table 3

Catalytic properties of Mo-V-Te-Nb mixed oxides in the selective oxidation of propane to acrylic acid

Notation	$X_{C_3H_8}$ [%]	S_{AA} [%]	Y_{AA} [%]	Rate [mmol/g _{cat} ·h]		Rate [mmol/m ² ·h]	
				C ₃ H ₈ consumption	Formation of AA	C ₃ H ₈ consumption	Formation of AA
SP-1	18	70	13.0	0.27	0.19	0.27	0.19
SP-3	38	73	28.0	0.57	0.42	0.29	0.21
SP-4	56	79	44.0	0.84	0.66	0.34	0.27
SP-5	52	79	41.0	0.78	0.62	0.20	0.15
MP-1	9	62	5.3	0.14	0.08	0.14	0.09
MP-2	33	58	18.9	0.50	0.29	0.15	0.09
MP-3	61	47	29.0	0.92	0.43	0.18	0.08
MP-4	6	65	3.6	0.09	0.06	0.11	0.07
MP-5	19	49	9.3	0.29	0.14	0.05	0.02
MP-6	2	44	0.6	0.03	0.01	0.03	0.01

activity of these catalysts is mainly but not exclusively dependent on their specific surface area. As it is also shown in **Table 3**, by normalizing the activity and the formation rate of acrylic acid to the specific surface area of the catalysts it is revealed that phase-pure M1 catalysts show higher activity and enhanced formation rates as compared with the mixed-phase materials. In **Figure 1**, the corresponding catalytic data are plotted against the M1 content of the catalysts. Both the trend of the normalized propane consumption as well as the trend of the normalized formation rate of acrylic acid increase with increasing M1 content.

In **Figure 2**, the catalytic behavior of single-phase catalyst (SP-1) and multi-phase catalysts with different M1 content (MP-1, MP-2 and MP-5) are plotted against the time on stream. The single-phase catalysts have been tested for 9 hours, whereas the other

catalysts were subjected to the feed for 50 hours. All the catalysts are stable under reaction conditions. No deactivation of the catalysts is observed during the reaction times applied. It should be noted at this point that propylene has never been observed as a reaction product on the phase-pure M1 catalysts under the conditions applied in this study. The bulk and surface characterization of the post-reaction samples will be presented in **section 3.3.4**.

As was mentioned above, the discrepancies observed between the catalytic activities of the phase-pure M1 catalysts are not exclusively due to the differences in their specific

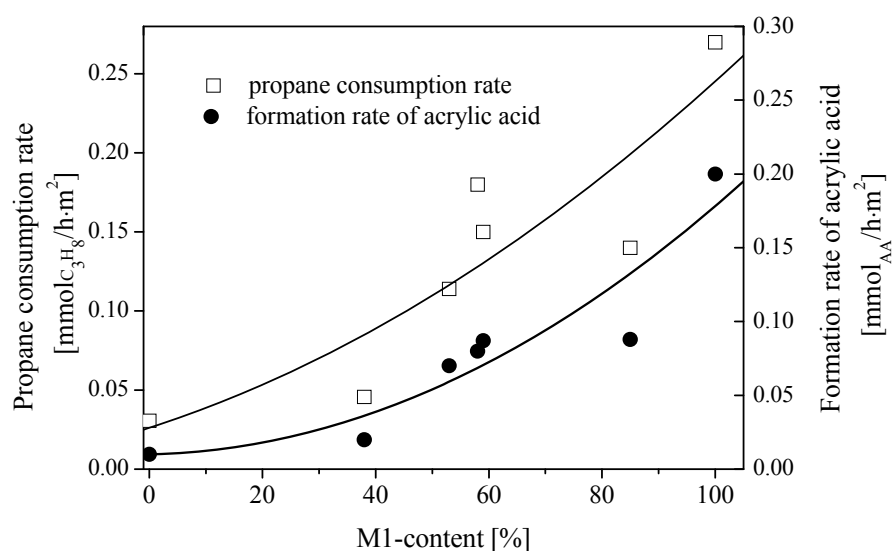


Figure 1. Rates of propane consumption and acrylic acid formation per unit of surface area of single-, bi-, and multi-phase MoVTenbO_x catalysts containing different amounts of M1.

surface areas. Therefore, the bulk and surface properties of these materials were investigated in order to evaluate the effects of bulk and surface composition as well as morphological factors on the catalytic properties.

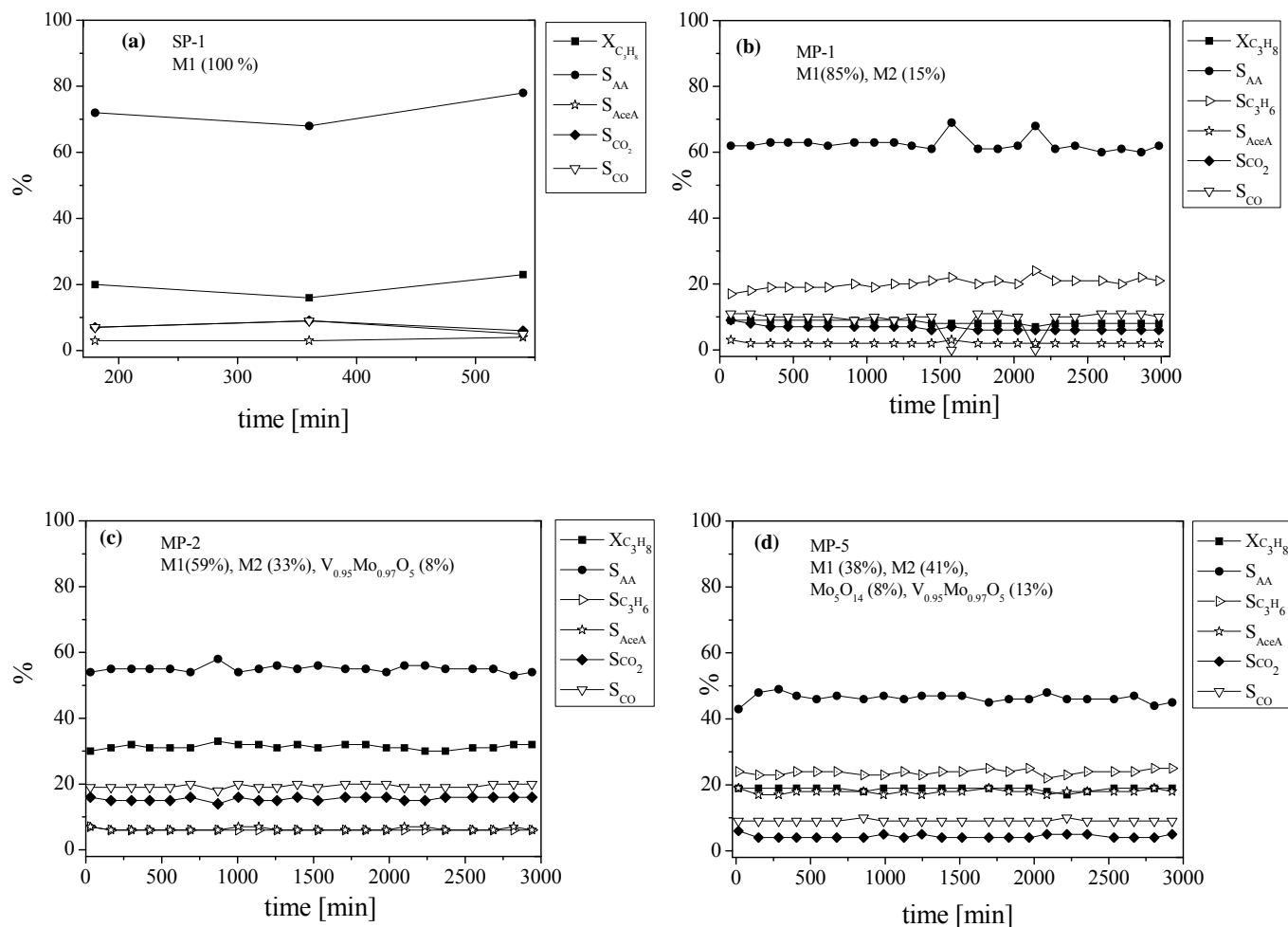


Figure 2. Catalytic behavior of (a) SP-1 (b) MP-1 (c) MP-2 and (d) MP-5 against time on stream.

3.3 Characterization of phase-pure M1 catalysts

3.3.1 Morphology and shape analysis

SEM images of the phase-pure $MoVTeNbO_x$ catalyst (**Figure 3**) revealed that the material mainly crystallized in a high aspect ratio needle-like morphology. The needle-shaped crystals are not isolated entities. They form agglomerates and the crystals are in

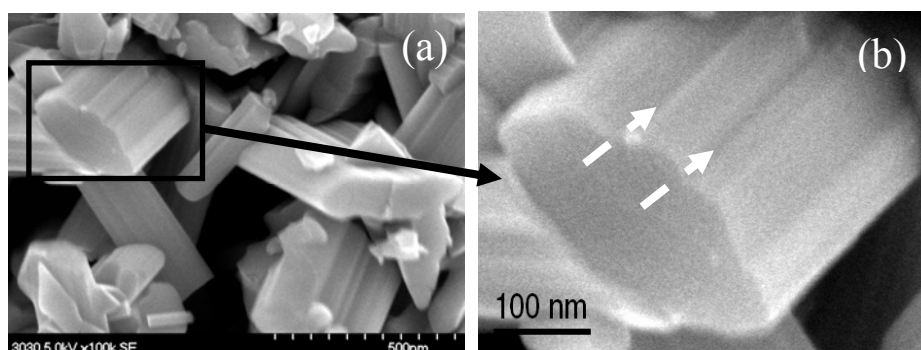


Figure 3. SEM images of phase-pure M1 materials, (a) needle shape and (b) steps on the sides of the needles parallel to c direction.

some cases fused together (**Figure 3a**). This high aspect ratio structure possesses a limited amount of exposed ab plane (section surface, S_s) whereas the surface area is mainly accounted for by the sides of the needles (lateral surface, S_l). Along the sides, steps of different dimensions parallel to the length axis (c direction) are observed. The largest steps amount tens of nanometers comprising several unit cells of M1 (arrows in

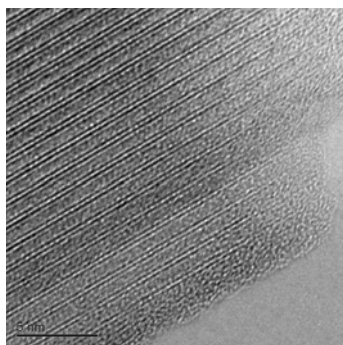


Figure 4. HRTEM (view of the steps).

Figure 3b). On the terraces, contrast variations are observed which are assumed to be steps of sub-unit cell dimensions. In the HRTEM (**Figure 4**), these surface steps are indeed revealed as crystallographic steps propagating along the length axis of the needle structures. Such steps provide sites of high coordination traditionally assumed to be centers of catalytic activity.

The diameter and length of the needles of different M1 materials were determined from SEM images. From this data, the aspect ratio was calculated as the ratio of diameter to length. **Table 4** summarizes the measurements from the samples investigated in this

study. The materials were analyzed after propane oxidation in the fixed bed reactor over 9 hours time on stream (SP-1AR and SP-4AR). Length distributions of both materials overlap, whereas the diameter distributions differ from each other considerably (Figure 15 of chapter 1). SP-4R shows a bigger mean diameter of the needles as compared with SP-1R (**Table 4**).

Table 4

Shape analyses of three phase-pure catalysts and their corresponding propane consumption rate and formation rate of acrylic acid

Notation	NP	Length [nm]	Diameter [nm]	S_s [m ² /g]	S_l [m ² /g]	Rate [mmol/g _{cat} ·h]	
						C ₃ H ₈ consumption	Formation of AA
SP-1AR	407	437 ± 308	75 ± 46	0.6	6.0	0.27	0.19
SP-4AR	389	411 ± 276	152 ± 71	0.9	4.4	0.84	0.66

NP: number of particles analysed

Based on the shape analysis of the materials, two different surface areas were calculated: the surface areas of the *ab* plane (S_s) and the surface areas of the sides of the needles (S_l) (**Table 4**). These calculations were done under the assumption that (i) the material is 100 % crystalline, (ii) each crystal is cylindrically needle shaped, and (iii) the density of the material is the density of the unit cell reported in the literature (4.4 g/cm³) [8]. XRD patterns (not shown) and SEM images (**Figure 3**) confirm the high crystallinity of the materials, justifying the first postulate. SEM images of the needles (**Figure 3**) show that a cylindrical shape is just a rough estimation that leads especially to an underestimation of the surface area of the sides of the needles. In case of the *ab* planes, the calculation error is significantly smaller, justifying the second postulate. As observed from **Table 2**, the elemental composition of the synthesized materials differs from that reported in the

literature [8]. However, these discrepancies mainly involve Mo and Nb. As the atomic mass of these elements is close, these discrepancies are expected to have only a minor influence on the real density justifying the third postulate. In **Table 4**, the catalytic properties of the two samples are compiled together with the calculated surface areas of the *ab* planes and the sides of the needles. The catalytic activity of the M1-phase catalysts decreases in the following sequence: SP-1 < SP-4. The corresponding calculated S_s of both catalysts follow the same trend (**Table 4**). However, correlation between catalytic properties and the calculated S_s can not be confirmed, since only two catalysts were investigated. Morphological analyses of a series of phase-pure M1 catalysts are required. Furthermore, functionality of the *ab* plane of the M1 phase in the selective oxidation of propane is thoroughly investigated in our next work [30]. Such investigation is based on the preparation of a model M1 catalyst, which exposes preferentially MoVTenbO_x surface area, belonging to the *ab* plane of this structure.

3.3.2 Microstructure

The microstructure of the phase-pure M1 was studied by HRTEM. **Figure 5a** shows the M1 phase of MoVTenbO_x viewed in the direction of $\langle 001 \rangle$ zone axis. The observed structure matches that reported in the literature [8], with arrangements of octahedra forming pentagonal (**Figure 5b**), heptagonal (**Figure 5c**) and hexagonal rings (**Figure 5d**). The contrast variation between the heptagonal and hexagonal channels indicates the difference in tellurium occupancy. Lattice spacings observed in the images agree with those of the M1 phase reported by DeSanto *et al* [8]. **Figure 6** shows the HRTEM image of a M1 needle viewed along the $\langle 127 \rangle$ direction. No contrast variations are observed along the needle indicating that it is of uniform thickness. Structures of different

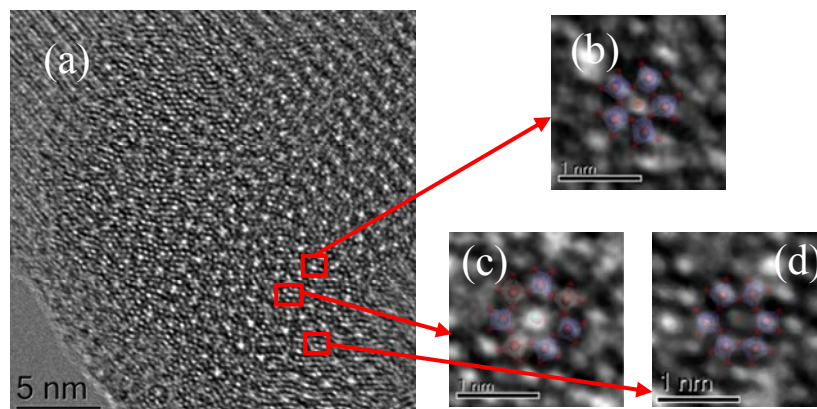


Figure 5. Microstructure examined by TEM, (a) *ab* plane of M1-phase; Structure features – overlapping simulation with experimental- of (b) pentagonal bipyramids, (c) heptagonal channels and (d) hexagonal channels.

thicknesses were simulated by using the JEMS program. In the inset of the HRTEM image, a simulation of the thickness of 1.6 nm is shown in the same orientation as in the experimental image. The contrast variations on the simulated image closely match that of the experimental image, confirming the simulated thickness.

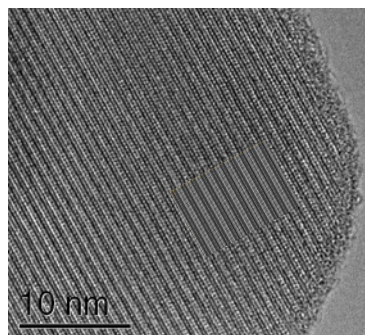


Figure 6. HRTEM image of M1 overlapped with that of M1 simulation.

As previously reported [25], Mo-V-Te-Nb mixed oxides show a characteristic complex termination clearly observed in the HRTEM images. To verify that the formation of this terminal layer is not an artifact of the electron beam, a region of the sample was irradiated with electrons over an extended period of time (**Figure 7**). The thickness of

the surface layer was measured at different times and plotted as a function of irradiation time (**Figure 8**). A constant growth rate of the surface layer ($\sim 0.06 \text{ nm}\cdot\text{min}^{-1}$) was

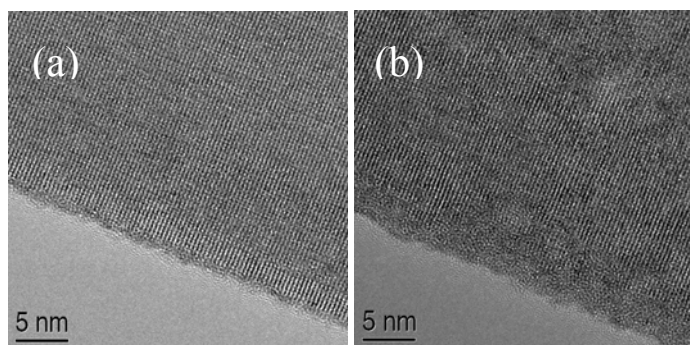


Figure 7. TEM images after (a) 1 minute (b) 31 minutes exposure time.

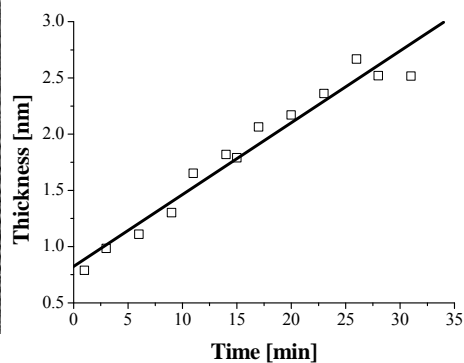


Figure 8. Thickness of the complex termination of the M1 phase against the exposure time of the beam.

observed, indicating that the layer is in part an effect of the electron beam. However, extrapolating to $t = 0$, a positive thickness value is obtained, indicating that there is a terminating structure different than that of the bulk M1 structure prior to electron beam exposure. The thickness of this surface layer is roughly 0.7 nm, which is within the range of surface sensitive X-ray photoelectron spectroscopy.

3.3.3 Elemental dynamics and composition at the catalytic surface

The terminating layer that covers the surface of M1 crystallites has been investigated by *in-situ* X-ray photoelectron spectroscopy in the presence of a reactant gas mixture. A depth profile of single-phase M1 catalyst was analyzed by applying different excitation energies, corresponding to a depth of approximately 0.5 nm (denominated as *surface*) or 1.5 nm (denominated as *subsurface*), respectively. In-situ experiments were performed on SP-1 in presence of 0.25-0.3 mbar of the reactants (**Figure 9**) in order to elucidate the influence of the reaction medium on the surface composition. Additionally, SP-1 has been also investigated after the catalytic test in a fixed bed reactor at 1 bar (SP-1AR), in the presence of 0.3 mbar of oxygen at 298 K (**Figure 9**).

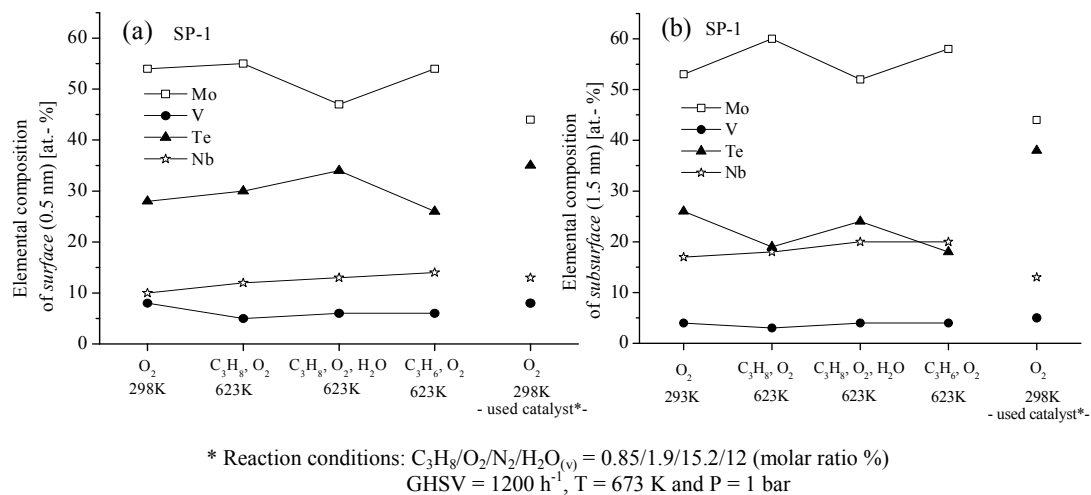


Figure 9. *In-situ* XPS results at different layer depth, (a) *surface* (information depth of ca. 0.5 nm) and (b) *subsurface* (information depth of ca. 1.5 nm).

The *surface* of SP-1 in 0.3 mbar of O₂ before admission of propane is mainly composed of molybdenum and tellurium. Furthermore, a considerable enrichment of tellurium at the expense of niobium is observed at the *surface* in comparison to the bulk (**Table 2**). After admission of propane, the *surface* concentration of tellurium is enhanced at the expense of molybdenum, which is even more noticeable in the presence of steam. As the steam is removed from the feed and propane is replaced by propylene keeping the temperature constant at 623 K, the tellurium fraction decreases in favor of molybdenum, close to the initial composition measured in O₂. The concentration of vanadium and niobium remain relatively constant under the different reaction media. Consequently, a reversible enrichment of the M1 *surface* with tellurium is observed in presence of the reactants (C₃H₈, O₂ and H₂O at 623 K). Such tellurium enrichment at the *surface* is also observed in the used SP-1 (SP-1AR).

The *subsurface* composition of the M1 catalyst is similar to the *surface* composition. In contrast to what occurs on the *surface*, the tellurium content decreases after the addition of propane to the oxidative atmosphere in favor of molybdenum. Apparently, the *subsurface* supplies tellurium to the *surface* and is, therefore, depleted in tellurium.

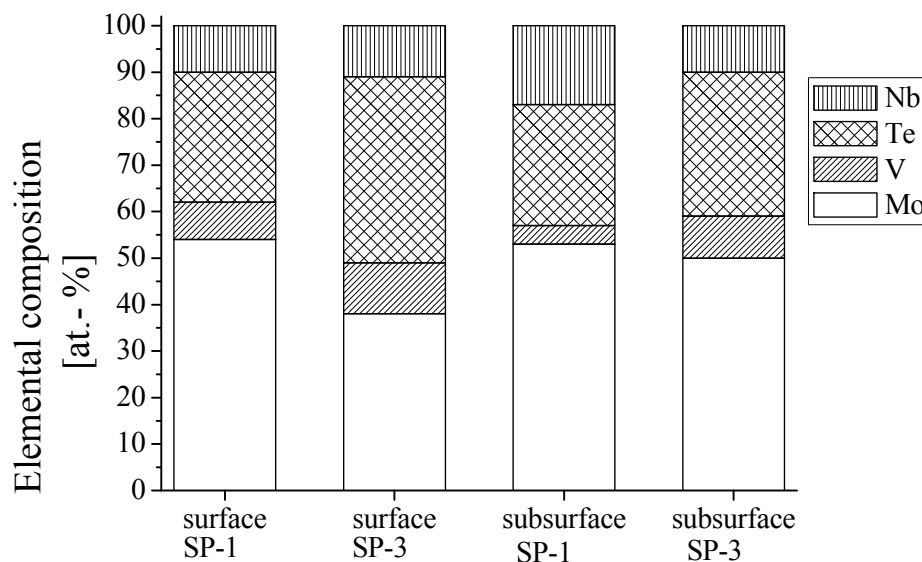


Figure 10. Depth profile composition of two single-phase catalysts (SP-1 and SP-3).

However, following the addition of steam the tellurium content increases again at the expense of molybdenum, as is the case at the surface. The observations reflect the mobility of tellurium that migrates through the hexagonal and heptagonal channels towards the *surface*, particularly in wet reaction atmosphere conditions.

In **Figure 10**, the depth profiles of two single-phase catalysts (SP-1 and SP-3) that show different catalytic properties are compared in presence of 0.3 mbar of O₂. SP-3 is more active and shows a higher formation rate of acrylic acid than SP-1 (**Table 3**). The enhanced tellurium content on the *surface* as well as on the *subsurface*, observed in the

more active catalyst (SP-3) might suggest that tellurium is essential for an improved catalytic efficiency.

3.3.4 Properties of the phase-pure catalysts after propane oxidation

Bulk structure, elemental composition and morphology of used SP-1 and SP-2 have been investigated after 9 hours time on stream. In both cases the reaction was performed at 673 K and the feed was composed of propane/oxygen/nitrogen/steam in a molar ratio of 2.8/6.4/50.8/40. However, different GHSVs, 1200 h^{-1} and 4800 h^{-1} , were applied.

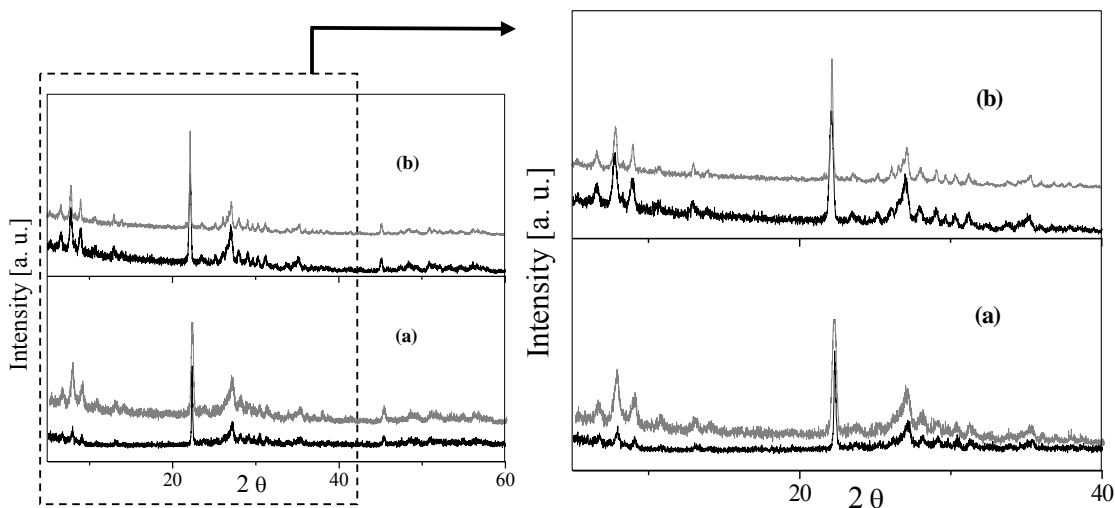


Figure 11. XRD patterns of (a) SP-1 and (b) SP-2; before (black line) and after reaction (grey line).

XRD patterns of both catalysts before and after reaction are shown in **Figure 11**. No evident changes in the bulk structure are observed after the catalytic reaction even in case of the more severe conditions (SP-2). However, SP-2 shows sharper reflections after reaction, indicative of an increase on crystallinity and/or growth of the crystals during reaction. Last affirmation is in agreement with the crystallite size (Crystallite Size

Table 5

Crystallite size values of SP-2 before and after reaction calculated from XRD data. The standard deviations are indicated in brackets

	SP-2	SP-2AR
Crystallite Size Lorentz [nm]	70(4)	72(2)
Crystallite Size Gauss [nm]	42(2)	93(5)

Lorentz/Gauss) calculated from the XRD data (**Table 5**). The unit cell sizes (lattice parameters) of both M1 materials have not suffered significant modifications after reaction as it is observed in **Table 6**.

Table 6

Lattice parameters of the samples SP-1 and SP-2 before and after reaction. The standard deviations are indicated in brackets.

Lattice parameters	SP-1	SP-1AR	SP-2	SP-2AR
a [Å]	21.234(6)	21.208(5)	21.199(3)	21.1957(16)
b [Å]	26.749(7)	26.740(6)	26.710(4)	26.700(2)
c [Å]	4.0030(7)	4.0016(6)	4.0131(4)	4.0108(3)

Bulk elemental composition also remains unchanged (**Figure 12**). The shape analyses of the catalyst tested at 1200 h⁻¹ (SP-1) before and after reaction (**Figure 13**), confirmed that the dimensions of the needles, the diameter (**Figure 13a**) as well as the length (**Figure 13b**), are not modified during catalytic reaction. In case of the catalyst exposed to high space velocities (SP-2), the inspection of the SEM images indicates that the morphology also remains unchanged after the catalytic reaction (**Figure 14**).

The absence of bulk structural and morphological changes indicates a structural stability of the M1 phase under the reaction conditions applied.

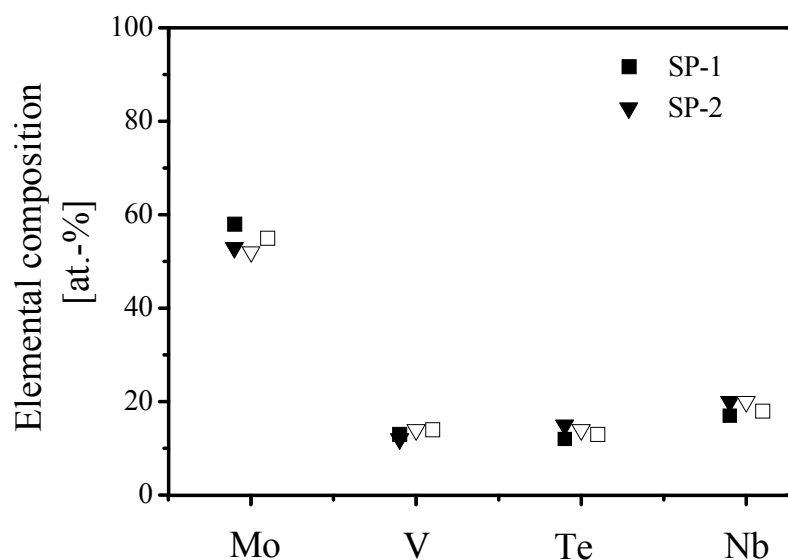


Figure 12. Elemental composition of SP-1 (■) and SP-2 (▼), before reaction (filled symbol) and after reaction (empty symbol). Reaction conditions: C_3H_8 : O_2 : N_2 : steam (% molar) = 0.85: 1.9: 15.2: 12; $T = 673\text{ K}$ and a GHSV of 1200 h^{-1} and 4800 h^{-1} for SP-1 and SP-2, respectively.

4 Discussion and conclusions

Catalysts composed exclusively of the M1 phase show a higher catalytic activity per unit surface area (**Figure 1**, **Table 3**) and a higher selectivity to acrylic acid (**Table 3**) compared to bi-, and multi-phase catalysts. However, normalization of the surface area shown in **Table 3** and **Figure 1** is problematic, since different phases present in the multi-phase catalysts could contribute differently to the total specific surface area of the catalyst. Thus, correlating the catalytic data per unit surface area with the M1 content of the catalysts may be misleading. This potential inconsistency could be the reason for the lack of a linear trend in the catalytic properties versus M1 content. In any case, no evidence of M1/M2 phase cooperation, as it is reported in the literature [7, 10, 11, 15, 16, 18-23], was observed in the present contribution.

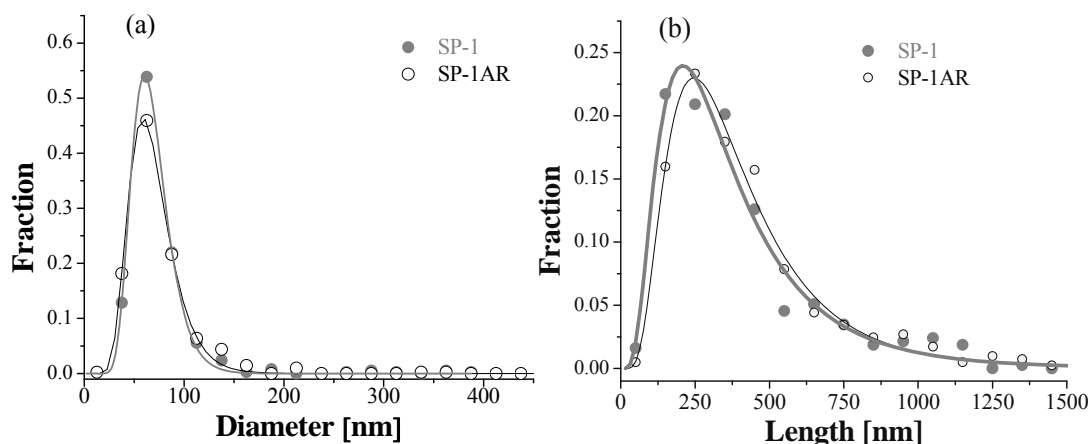


Figure 13. Shape analysis distribution of SP-1 before and after reaction: (a) diameter distribution and (b) length distribution.

The SP-1 catalyst, composed exclusively of M1 phase, and the MP-5 catalyst, composed of a mixture of phases including M1 and M2 phases, showed a propane conversion of ca. 20 % (**Figure 2a and 2d**). The selectivity to total oxidation products was rather similar for both catalysts, and comprised ca. 16 %. As expected, SP-1 showed higher selectivity to acrylic acid as compared with MP-5. Remarkably, the spectrum of the other partial oxidation products was different in both cases. Whereas no propylene was formed over SP-1, substantial amounts of propylene were detected in the final products obtained over

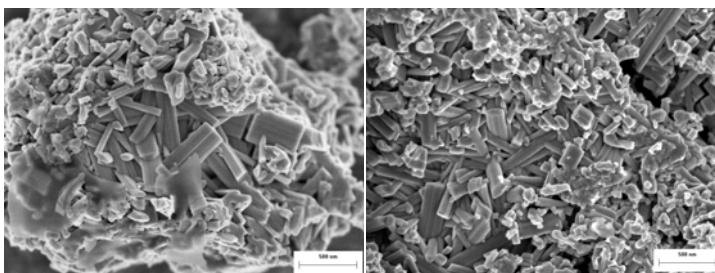
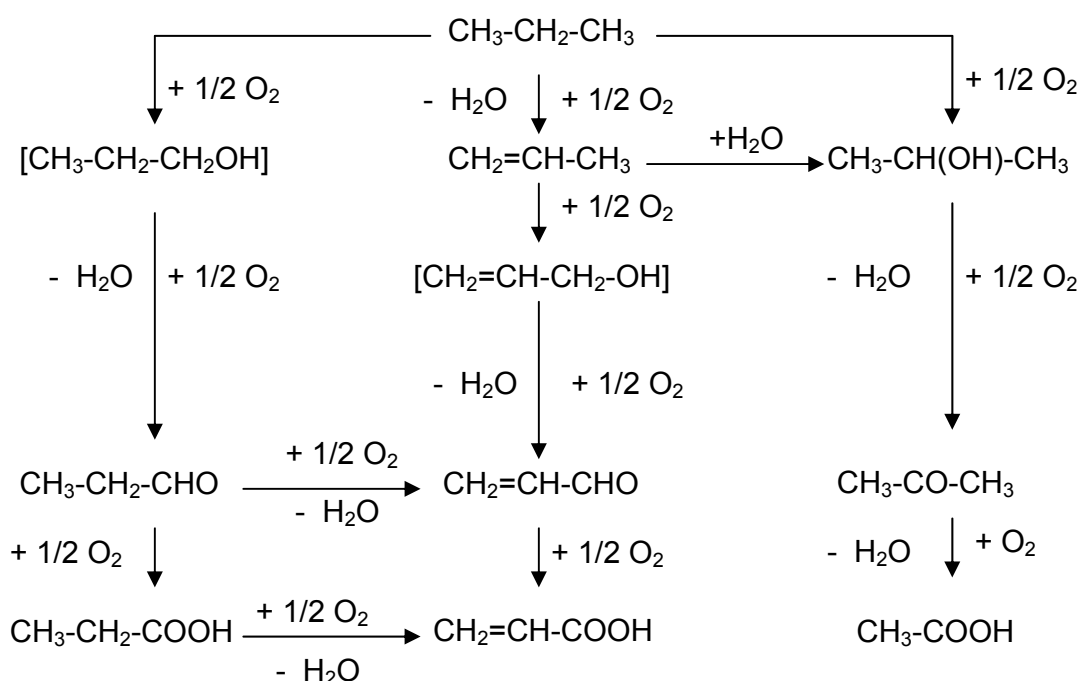


Figure 14. SEM images of SP-2 (a) before and (b) after reaction.

MP-5. These observations are inconsistent with the reported phase cooperation theory [7, 10, 11, 15, 16, 18-23], in which it is assumed that the M2 phase cooperates with the M1 phase by converting the propylene intermediate into acrylic acid. Moreover, acetic acid is one of the main products on MP-5, indicating that propylene formation may proceed via different reaction pathways (**Scheme 3**) on the multi-phase catalysts. In case of SP-1, only traces of acetic acid are detected.



Scheme 3. Pathways of the selective oxidation of propane.

The highest catalytic activities and formation rates of acrylic acid per unit surface area as well as per unit of catalytic mass have been achieved by materials composed exclusively of the M1 phase. On the other hand, the phase-pure materials differ slightly with respect to their intrinsic catalytic properties. Consequently, the differences in specific surface

areas of the M1 catalysts are not exclusively responsible for the different formation rates of acrylic acid.

The chemical composition of the bulk (**Table 2**) varies slightly and shows significant discrepancies with the composition of the M1 structural model reported in the literature [8] as well as the hydrothermally synthesized phase-pure catalysts reported by Ueda *et al.* [9]. Obviously, the M1 structure copes with a certain chemical flexibility. Changes in the chemical composition of the phase affect the nature of the active sites at the surface and, therefore, the catalytic properties. Consequently, catalysts with identical phase composition, such as phase-pure M1 materials, could exhibit different catalytic properties. This fact has to be taken into account when carrying out comparative studies in order to elucidate the role of the different structures. On the other hand, there is no correlation between the chemical composition of the bulk of the phase-pure M1 catalysts studied in the present work and the formation rate of acrylic acid.

The phase-pure materials show the typical needle-like morphology of this crystal structure. However, shape analysis based on the SEM projections shows that the dimensions of the needles, in particular the cross-sectional diameters, vary widely (Figure 15 of chapter 1). It has been suggested in the literature that the active centers of the catalysts are exclusively located on the surface of the basal *ab* plane (cross-section of the needles) [13-15], and that the sides of the needles are inactive in the selective oxidation of propane. However, such investigations were based on the assumption that mechanical treatment of the M1 materials exclusively increased the surface area of the exposed *ab* plane by means of breaking the needles perpendicularly to the needle length axis. Experimental evidence for corresponding changes in the morphology of the milled

catalysts has not been provided in the literature. In the present contribution, morphological analysis of the M1 phase catalysts has been presented as a suitable method to investigate the impact of the exposed *ab* plane on the catalytic performance. M1 materials that show identical bulk properties (structure and elemental composition) and are identically mechanically treated for the preparation of the sieve fraction, are appropriated candidates for those studies. It has to be mentioned that while the surface of the cross-section of the needles is flat, the sides of the needles are characterized by micro- and nano-step, which may increase the surface area of the needle, substantially. Differences in the morphology of the sides of the needles have not been considered in our simplified approach, assuming an ideal cylindrical shape of the crystals. Therefore, the contribution of the sides of the needles may have been underestimated. Investigation of a series of phase-pure M1 materials by applying the above-mentioned method is required in order to elucidate if a certain plane of this structure correlates with the catalytic properties of the material.

As revealed by HRTEM, the surface of the M1 crystals is covered by a structurally disordered layer, exhibiting no long-range order (**Figure 6 and 7**). The thickness of the terminating layer has been estimated to approximately 0.7 nm (**Figure 7 and 8**). Since the catalytic reaction takes place on the surface of M1, investigation of this surface layer is essential for understanding the functionality of these catalysts. *In-situ* XPS experiments show that the *surface* composition (information depth of ca. 0.5 nm) of the catalysts exhibit an increased content of tellurium at the expense of molybdenum as the catalyst is exposed to a gas mixture of propane and oxygen ($\text{C}_3\text{H}_8/\text{O}_2 = 0.5$ molar ratio) at a temperature of 623 K. The tellurium content at the *surface* increases even more as steam

is added to the feed. The latter reaction atmosphere is closer to the reaction conditions applied in the fixed bed reactor. On the other hand, the concentrations of vanadium and niobium remain rather constant under the different reaction conditions. An elemental composition on the *surface* that deviates from the bulk composition is confirmed by the XPS analyses of the quenched catalyst collected after the catalytic test in a fixed bed reactor at 1 bar. The surface dynamics of M1 are clearly reflected in these results. Tellurium may play an important role in the formation of acrylic acid. The higher tellurium content detected in the more active catalyst (SP-3) might explain the slight discrepancies in the catalytic properties of these phase-pure materials. However, the high Te content observed on the catalytic surface under the reaction conditions may also be explained by the formation of isolated tellurium particles, taking no part in the catalytic active centers. Further investigations to confirm the active involvement of the surface tellurium in the catalytic reaction are currently being carried out.

In conclusion, hydrothermally synthesized phase-pure M1 MoVTaNbO_x catalysts show the highest activity and the highest formation rate of acrylic acid in the selective oxidation of propane to acrylic acid as compared with MoVTaNbO_x catalysts composed by a mixture of phases. Therefore, no evidence of phase-cooperation is found in this contribution. Catalytic activity of phase-pure M1 materials depends mainly on the specific surface area, but also on the surface properties of the catalysts in question. In the presence of the reactant gas mixture, the surface of M1 is mainly composed of tellurium and molybdenum in a stoichiometric ratio that is not compatible with the M1 stoichiometry. Surface dynamics of these catalysts are confirmed by *in-situ* XPS experiments, resulting in tellurium enrichment at the *surface* as the catalyst is exposed to

reaction conditions (propane/oxygen) and even more distinctly as steam is presented to the atmosphere. Such results suggest a remarkable role of tellurium in the catalytic reaction. Tellurium is assumed [16] to be involved in hydrogen abstraction reactions from propane and from propylene.

The high stability detected for these single-phase catalysts under the real reaction conditions is of a great importance for their potential industrial application in the future.

In this contribution, it has also been described, a suitable method based on shape analysis of the M1 catalysts in order to elucidate the catalytic function of the *ab* plane of this structure.

5 Acknowledgments

The authors thank Dr. Olaf Timpe for helpful discussions, Edith Kitzelmann for conducting the XRD measurements, and Gisela Lorenz for carrying out the nitrogen adsorption measurements.

6 References

- [1] E. K. Novakova, V. C. Védrine, *Propane Selective Oxidation to Propene and Oxygenates on Metal Oxides in J. L. G. Fierro, Metal Oxides, Chemistry and Applications*, CRC Press (2006), 414.
- [2] G. Centi, F. Cavani, F. Cavani, F. Trifiro, *Selective Oxidation by Heterogeneous Catalysis*, Kluwer Academic/Plenum Publishers (2001), 363.
- [3] M. M. Lin, *Applied Catalysis A: General* 207 (2001), 1.
- [4] M. Tanimoto, H. Himeji-shi, I. Mihara, H. Aboshi-ku, T. Kawajiri, H. Himeji-shi, EP 0711745 B1 (1996); Nippon Shokubai.
- [5] A. Tenten, H. Hibst, F.-G. Martin, L. Marosi, V. Kohl, DE 4405514 A1 (1995); BASF.

- [6] T. Ushikubo, H. Nakamura, Y. Koyasu, S. Wajiki, US Patent 5 380 933 (1995); Mitsubishi Kasei Corporation.
- [7] T. Ushikubo, K. Oshima, A. Kayou, M. Hatano, *Studies in Surface Science and Catalysis* 112 (1997), 473.
- [8] P. DeSanto, D. J. Buttrey, R. K. Grasselli, C. G. Lugmair, A. F. Volpe, B. H. Toby, T. Vogt, *Zeitschrift für Kristallographie* 219 (2004), 152.
- [9] H. Murayama, D. Vitry, W. Ueda, G. Fuchs, M. Anne, J. L. Dubois, *Applied Catalysis A: General* 318 (2007), 137.
- [10] M. Baca, A. Pigamo, J. L. Dubois, J. M. M. Millet, *Topics in Catalysis* 23 (2003), 1-4, 39.
- [11] J. M. Oliver, J. M. López-Nieto, P. Botella, *Catalysis Today* 96 (2004), 241.
- [12] W. Ueda, D. Vitry, T. Katou, *Catalysis Today* 96 (2004), 235.
- [13] K. Oshihara, T. Hisano, W. Ueda, *Topics in Catalysis* 15 (2001), 153.
- [14] V. V. Guliants, R. Bhandari, R. S. Soman, O. Guerrero-Pérez, M. A. Bañares, *Applied Catalysis A: General* 274 (2004), 213.
- [15] R. K. Grasselli, D. J. Buttrey, P. DeSanto, Jr., J. D. Burrington, C. G. Lugmair, A. F. Volpe, Jr., T. Weingand, *Catalysis Today* 91–92 (2004), 251.
- [16] R. K. Grasselli, *Catalysis Today* 99 (2005), 23.
- [17] C. Hess, M. H. Looi, S. B. A. Hamid, R. Schlögl, *Chemical Communications* (2006), 451.
- [18] T. Ushikubo, *Catalysis Today* 57 (2000), 331.
- [19] R. K. Grasselli, J. D. Burrington, D. J. Buttrey, P. DeSanto Jr., C. G. Lugmair, A. F. Volpe Jr., T. Weingand, *Topics in Catalysis* 23 (2003), 1–4, 5.
- [20] J. Holmberg, R. K. Grasselli, A. Andersson, *Topics in Catalysis* 23 (2003), 1-4, 55.
- [21] J. Holmberg, R. K. Grasselli, A. Andersson, *Applied Catalysis A: General* 270 (2004), 121.
- [22] R. K. Grasselli, D. J. Buttrey, J. D. Burrington, A. Andersson, J. Holmberg, W. Ueda, J. Kubo, C. G. Lugmair, A. F. Volpe Jr., *Topics in Catalysis* 38 (2006), 1-3, 7.

- [23] E. García-González, J. M. López-Nieto, P. Botella, M. M. González-Calbet, *Chemistry of Materials* 14 (2002), 4416.
- [24] D. Vitry, Y. Morikawa, J. L. Dubois, W. Ueda, *Topics in Catalysis* 23 (2003), 1-4, 47.
- [25] J. B. Wagner, O. Timpe, F. A. Hamid, A. Trunschke, U. Wild, D. S. Su, R. K. Widi, S. B. A. Hamid, R. Schlögl, *Topics in Catalysis* 38 (2006), 51.
- [26] P. Beato, A. Blume, F. Girgsdies, R. E. Jentoft, R. Schlögl, O. Timpe, A. Trunschke, G. Weinberg, Q. Basher, F. A. Hamid, S. B. A. Hamid, E. Omar, L. Mohd Salim, *Applied Catalysis A: General* 307 (2006), 137.
- [27] *Preparation of phase-pure M1 MoVTenb oxide catalysts by hydrothermal synthesis – Influence of reaction parameters on structure and morphology.*
A. Celaya Sanfiz, T. W. Hansen, E. Rödel, O. Timpe, A. Trunschke, R. Schlögl, (accepted for publication in *Topics in Catalysis*).
- [28] W. Ueda, D. Vitry, T. Kato, N. Watanabe, Y. Endo, *Research on Chemical Intermediates* 32 (2006), 3–4, 217.
- [29] H. Bluhm, M. Hävecker, A. Knop-Gericke, E. Kleimenov, R. Schlögl, D. Teschner, V. I. Bukhtiyarov, D. F. Ogletree, M. Salmeron, *Journal of Physical Chemistry B* 108 (2004), 14340.
- [30] *How important is the (001) plane of M1 for selective oxidation of propane to acrylic acid.*
A. Celaya Sanfiz, F. Girgsdies, T. W. Hansen, A. Trunschke, R. Schlögl, A. Knoester, H. H. Brongersma, M. H. Looi, S. B. A. Hamid, (submitted in *Journal of Catalysis*).

CHAPTER 3- How important is the (001) plane of M1 for selective oxidation of propane to acrylic acid

Abstract

The role of the (001) crystallographic plane of the M1 phase of Mo-V-Te-Nb mixed oxide catalysts in selective oxidation of propane to acrylic acid has been addressed by investigating a phase-pure M1 material preferentially exposing this surface. A model catalyst has been prepared by complete silylation of M1 followed by breakage of the SiO₂ covered needles. Using this approach, the reactivity of the M1 (001) surface has been investigated by combining a micro-reactor study of propane oxidation with High-Sensitivity Low Energy Ion Scattering (HS-LEIS). Scanning electron microscopy (SEM) and transmission electron microscopy (TEM) have been used to study shape and microstructure of the model system and to verify the surface exposure of the model catalyst. The specific formation rate of acrylic acid on the model catalyst is similar to that on the phase-pure M1 reference material indicating that the (001) plane of the M1 crystal structure does not possess enhanced catalytic properties compared to the lateral surface of M1 needles in propane oxidation.

Keywords

Mo-V-Te-Nb oxide catalyst, M1, propane oxidation, propane ammoxidation, low-energy ion scattering, LEIS

1 Introduction

Selective oxidation of light alkanes requires multi-functional catalysts capable of simultaneous activation of C-H bonds, insertion of oxygen atoms, and prevention of CO_x formation by further oxidation of intermediates or desired reaction products, which are usually much more reactive than the inactive reactant. The necessary functional diversity is implemented in chemically and structurally complex MoVTaNbO_x catalysts, which show high activities and selectivities in partial (amm)oxidation of propane to acrylic acid and acrylonitrile, respectively [1, 2]. Usually, these catalysts consist of phase mixtures composed of the so-called “M1” and “M2” phases [3], as well as minor amounts of phases, like Mo₅O₁₄-type structures or binary Mo-V and Mo-Te oxides. Propane activation and high selectivities towards acrylic acid and acrylonitrile are generally attributed to the presence of the orthorhombic M1 phase [4-6]. The M1 structure (ICSD 55097) consists of corner-sharing MO₆ octahedrons, (M=Mo,V), which are assembled in the (001) plane forming characteristic hexagonal and heptagonal rings hosting Te-O units. Niobium is preferentially located in pentagonal bipyramidal environment [7-9]. However, due to a certain chemical flexibility of the phase, octahedral positions may also be occupied by Nb in M1 with higher Nb content [10]. A bronze like channel structure is established by stacking layers of the polyhedrons in the [001] direction resulting in a needle-like crystal morphology in which the (001) planes are arranged perpendicular to the length axis of the needle. It has been suggested that the (001) planes of the M1 phase contain the active and selective surface sites for selective oxidation reactions [11-14]. This claim has stimulated research on the structure and properties of the M1 surface by Low Energy Ion Scattering (LEIS) [15, 16]. One of the unique features of LEIS analysis

is that it gives the atomic composition of the outermost atoms of a surface. These outer atoms are precisely the atoms that largely control the catalytic properties of the solid. It has been shown before [17] that in cases where conventional surface analytic techniques, such as XPS, do not show correlation with the catalytic activity, the extreme surface sensitivity of LEIS gives a direct relationship between composition and catalysis. In a recent review [18], the underlying principles and quantification of LEIS are described. The general absence of matrix effects enables the use of simple reference samples for the quantification of the surface composition.

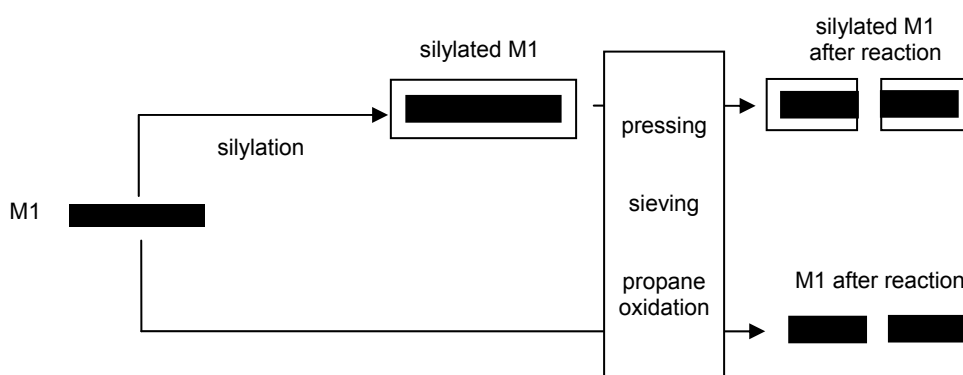
The present study addresses the origin of the positive effect of grinding on the catalytic activity of MoVTenNbO_x in the selective oxidation of propane to acrylic acid. Due to the needle-shape of the particles, the surface of (001) planes comprises only a minor fraction of the total surface area. Thus, increased activity after grinding of M1 needles has been attributed to the generation of additional (001) surface area [11, 12]. Even though an increased specific surface area is observed [12], the downside of the grinding process is the well-known effect of mechanical treatment on the nature and concentration of defects on the overall surface of transition metal oxides [19].

Therefore, a different strategy illustrated in **Scheme 1** has been pursued. A batch of crystalline, phase-pure M1 prepared by hydrothermal synthesis was divided into two parts. One part was fully coated with silica. The complete coverage of the mixed metal oxide surface by SiO₂ was verified by HS-LEIS. Both, the coated material and the non-coated reference M1, were pressed into pellets, crushed and sieved in order to prepare sieve fractions, which were then loaded into a micro-reactor and studied in the partial oxidation of propane to acrylic acid. The preparation of the sieve fraction represents a

gentle mechanical treatment that generates new M1 surface, which has been quantified by LEIS for the silica-coated catalyst [18] and by nitrogen adsorption for the reference material. Special attention has been paid to a comprehensive microstructural characterization of the model catalysts before and after the propane oxidation. Scanning electron microscopy (SEM) and transmission electron microscopy (TEM) revealed that complete coverage of M1 followed by breakage of the SiO₂-covered needles generates a model catalyst that predominantly exposes (001) planes (**Scheme 1**). In addition, LEIS was applied to compare the chemical composition of the newly formed M1 surface of the coated catalyst with that of the total surface of the M1 reference. Based on the results of the micro-reactor and LEIS study, the relevance of particular surface terminations will be discussed in view of the catalytic properties of phase-pure M1 catalysts in partial oxidation of propane to acrylic acid.

Scheme 1

Silylation and mechanical treatment of phase-pure M1



2 Experimental

2.1 Preparation of M1

A phase-pure M1 catalyst with nominal atomic ratio Mo/V/Te/Nb = 1/0.3/0.23/0.13 has been prepared starting from 18.71 g MoO₃ (Fluka) suspended in 300 ml bidistilled water.

After adding 19.90 g oxalic acid at 363 K a light yellowish solution has been obtained. The mixture was stirred for 25 minutes and cooled down to 313 K. Afterwards, 6.86 g of telluric acid (Sigma-Aldrich) dissolved in 30 ml bidistilled water at 313 K was added to the molybdenum oxalate solution. A vanadium solution was synthesized by carefully mixing 7.05 g oxalic acid and 3.55 g V_2O_5 (Riedel-de-Haën) in 30 ml bidistilled water at 338 K. The resulting blue solution was cooled down to 313 K and added to the binary MoTe solution. Finally, a solution of 7.35 g ammonium niobium oxalate (Sigma-Aldrich) in 30 ml bidistilled water was added at 313 K to the previous mixture. The clear quaternary solution was stirred for 10 min and spray-dried in a Büchi B-191 spray-dryer at an inlet temperature of 423 K. The delivery rate of the pump and the aspirator were tuned to an outlet temperature of 383 K. The spray-dried material was calcined in flowing air at 548 K (heating rate 5 K/min) for one hour. The calcined mixed oxide was then heated for two hours at 773 K (heating rate 5 K/min) and 20 MPa in the presence of steam. The resulting solid was finally crystallized to M1 in flowing argon at 873 K (heating rate 15 K/min) for another two hours (catalyst ID 3030). The atomic ratio of the metals in the final catalyst, Mo/V/Te/Nb = 1/0.34/0.08/0.14, as determined by EDX, was close to the nominal ratio, with the exception of the reduced tellurium content due to evaporation of elemental Te during thermal activation of the catalyst

2.2 Silylation of M1

Silylation of M1 has been performed by addition of 5.8 g $HSi(OEt)_3$ (Sigma-Aldrich) to a suspension of 0.5 g phase-pure M1 (catalyst 3030) in 100 ml toluol. The mixture was kept for 16 hours at 384 K under reflux. Cross-linking of anchored silanol groups has been achieved by treating the resulting solid in a mixture of 90 ml ethanol, 10 ml of

bidistilled water and 1 ml concentrated sulphuric acid for four hours under reflux. The two-step procedure has been repeated three times in order to assure complete silylation of the entire M1 surface (catalyst ID 3159).

2.3 Activity measurements

For testing of the catalysts in selective oxidation of propane to acrylic acid, 0.5 g of each material was pelletized (8 ton on a round, 3-cm-diameter surface) and sieved to 200–400 μm . This shape-forming procedure, referred to as mechanical treatment, causes partial disruption of the needles, changing the size distribution of the primary particles in the original M1 and making catalytic testing of completely silylated M1 impossible. But pure silica (Aerosil 300) was shown to be inactive in propane oxidation under the reaction conditions applied. The sieve fractions of the mechanically treated M1 and silylated M1 were loaded into quartz reactors with a diameter of 4 mm. The feed was composed of propane/oxygen/nitrogen/steam in a molar ratio of 0.85/1.9/15.2/12. The reaction was performed at atmospheric pressure, a GHSV of 4800 h^{-1} , and a reaction temperature of 673 K. The products were analyzed by gas chromatography. A molecular sieve column and a Porapak column coupled with a thermal conductivity detector were used to analyze O_2 , N_2 , CO , CO_2 , and hydrocarbons (C1–C3). The oxygenated products were analyzed with a HP-FFAP column coupled with a flame ionization detector. The detection limit of the individual products depended on the detector used but was generally $>0.2\text{ vol.-%}$. A mass balance of $100 \pm 10\%$ was calculated.

2.4 Catalysts characterization

X-ray diffraction

The phase-purity of the materials was verified by X-ray diffraction (XRD). The measurements were performed with a STOE STADI-P transmission diffractometer equipped with a focusing primary Ge (111) monochromator and a position sensitive detector, using Cu-K α_1 radiation. For data analysis, the program Topas (v.2.1, Bruker AXS) was used to fit the diffraction pattern of the activated materials.

Electron microscopy

The microstructure of the catalysts was investigated by TEM using a Philips CM 200 FEG transmission electron microscope operated at 200 kV, equipped with a Gatan CCD camera for image acquisition and an EDAX Genesis EDX system. Morphology studies and shape analysis were performed by SEM, using a Hitachi S-5200 with a PGT Spirit EDX system and a Hitachi S-4800 with an EDAX Genesis EDX detector. EDX studies in the SEMs were carried out with an accelerating voltage of 10 kV, with images acquired at 2 kV to optimize surface resolution. For TEM, the specimens were prepared by dry dispersing the catalyst powder on a standard copper grid coated with holey carbon film. For SEM investigations, the samples were deposited on carbon tape. The shape of the M1 needles was analyzed by measuring the length and diameter of more than 200 needles on SEM images. Based on the average length and diameter of the needles, the total surface area and the surface area of the (001) plane were calculated for an average needle for each catalyst (Table 1). These calculations were done under the assumptions that the material was 100% crystalline and each crystal was cylindrically shaped. Furthermore, the cylinder was assumed to have a circular basal plane. A SEM-derived specific surface area was calculated using the surface area of the average needle and the crystallographic density of M1 (4.4 g/cm³ [8]).

Nitrogen adsorption

The specific surface areas of the catalysts were measured using an AUTOSORB-1-C physisorption/chemisorption analyzer (Quantachrome). Eleven points in the linear range of the nitrogen adsorption isotherm measured at 77 K have been used to calculate the BET surface area. Prior to adsorption, the samples have been degassed at 353 K for 2 hours.

High-Sensitivity LEIS

The Calipso LEIS uses a double toroidal analyzer, which combines a large acceptance angle with parallel energy analysis of the backscattered ions. This gives orders of magnitude higher sensitivity (HS-LEIS) than that of conventional LEIS equipment [20]. The required ion dose for analysis is so low that HS-LEIS analysis is essentially non-destructive ("static").

The extreme surface sensitivity of LEIS requires that organic contaminations due to transport and storage as well as carbonaceous deposits from the catalytic reactions are removed from the catalysts before analysis. This was done with an oxygen atom source (Oxford Applied Research, type MPD 21) which produces O-atoms of thermal energy. In contrast to molecular oxygen and ozone, the chemical energy of these O-atoms enables the complete removal of organic contaminations at room temperature without sputtering the surface. All samples were cleaned in this way (200 W, 5 min) before analysis. Prolonged treatment had no influence on the LEIS spectra, thus confirming the cleanliness of the samples.

Calibration of the LEIS signals

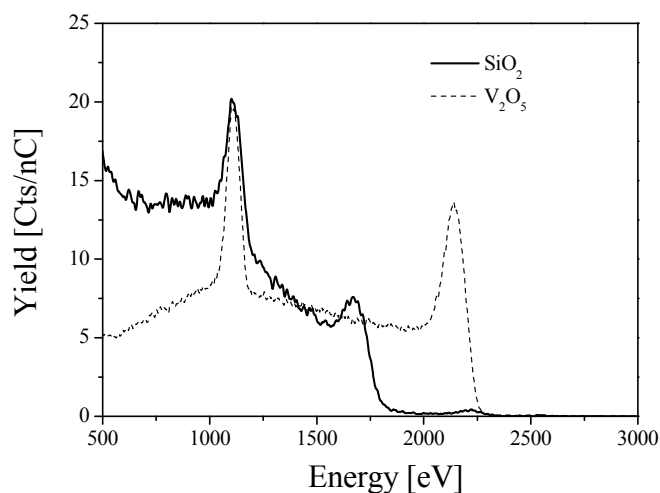


Figure 1. 3 keV He^+ scattering.
References SiO_2 and V_2O_5 .

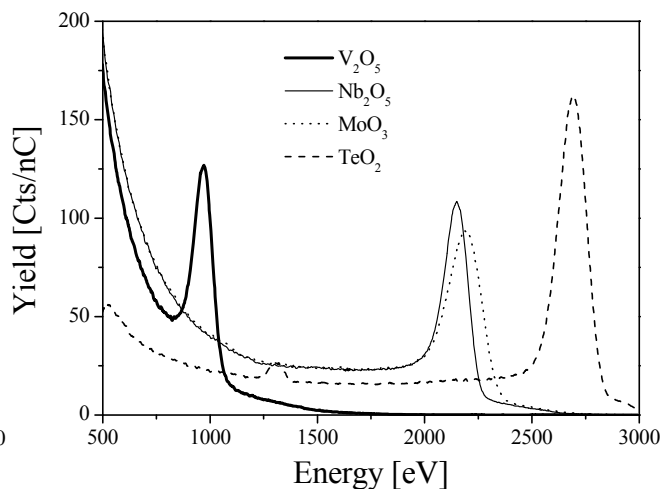


Figure 2. 5 keV Ne^+ scattering.
References V_2O_5 , Nb_2O_5 , MoO_3 and TeO_2 .

It has been shown previously that roughness has a very small effect on the LEIS signals [21]. Thus, the precise dispersion is not of great importance for a good reference for calibrating the LEIS signals of the catalysts. Thus, high-purity powder samples of SiO_2 , V_2O_5 , Nb_2O_5 , MoO_3 , and TeO_2 were used as references to quantify the surface concentrations of Si, V, Nb, Mo, and Te. Because the surfaces were cleaned with O atoms, the cations in the outer surface were in their highest oxidation state (e.g., TeO_3 for Te). The LEIS spectra are given in **Figures 1** and **2**. The lighter elements (Si, V) were quantified with 3 keV $^4\text{He}^+$ ions; the heavier elements (V, Nb, Mo and Te), with 5 keV $^{20}\text{Ne}^+$ ions. As can be seen in **Figures 1** and **2**, the SiO_2 surface was contaminated with a trace of iron oxide, whereas the TeO_2 contained some cobalt or nickel oxide (mass 59). Even with the heavier Ne ions, there was an overlap of the Nb and Mo peaks. The elements are neighbors in the periodic table, and their isotopes (Nb: 93; Mo: 92–100) overlap. For the catalysts, the relative concentrations of Nb and Mo were determined by

curve fitting. The large width of the Te peak originates from isotopic broadening (atomic mass 122–130). Because these masses are very different from those of the other elements, Te can be readily quantified. V can be analyzed using both He and Ne ions, and the two analyses give very similar results. The values given for V are the average of the two measurements. LEIS calibration gives the fractions of the surface that are composed of the various oxides. To obtain atomic concentrations, these fractions must be corrected for the surface densities of the cations in the references. These surface densities have been estimated as $(\rho \cdot N_A v / M)^{2/3}$, where ρ is the bulk density, $N_A v$ is Avogadro's number, and M is the molar mass. It has been shown previously [22] that this estimate agrees closely with the estimate from the surface unit-cell taking the close-packed surface plane, which is dominant on powders. For V_2O_5 , Nb_2O_5 , MoO_3 , and TeO_3 these densities are 9.96, 9.36, 7.28, and $7.68 (\times 10^{14})$ metal atoms/cm², respectively.

3 Results

3.1 Silylation of M1

The surface of a $MoVTenbO_x$ mixed oxide composed mainly of the M1 phase has been covered with a layer of silica by silylation using $HSi(OEt)_3$. The silylation was optimized using LEIS. **Figure 3 and Figure 4** show the LEIS spectra of the catalyst before and after silylation according to the process described in **Section 2.2**. The 3 keV He^+ spectrum before silylation shows the peaks for O, V and a combined peak for Nb, Mo and Te. In addition, some Na contamination is observed. The 5 keV Ne^+ spectrum gives a better mass resolution for the heavier elements. It shows the peaks for V, Te and a broad peak due to Nb and Mo. After silylation, only the peaks for O and Si (He spectrum) are

present. No peaks are observed in the Ne spectrum. This confirms the successful complete silylation of the catalyst.

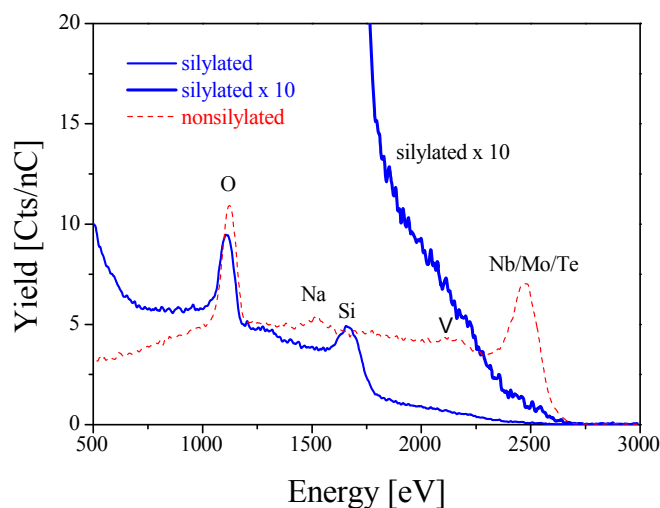


Figure 3. 3 keV He⁺ scattering. Non-silylated, silylated and silylated x 10.

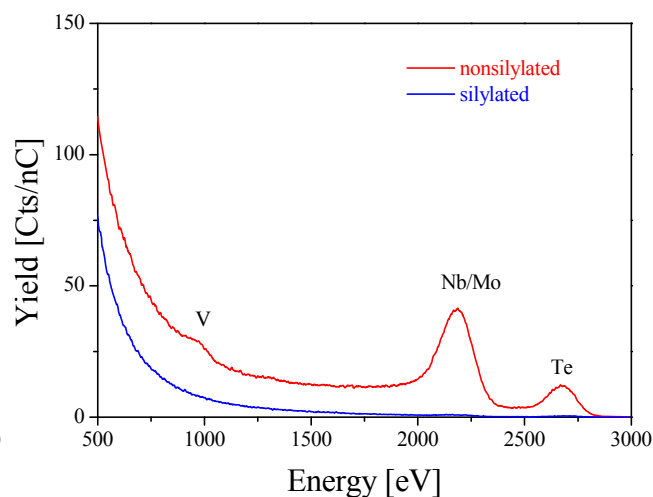


Figure 4. 5 keV Ne⁺ scattering. Non-silylated and silylated.

In addition to the peaks in the He spectrum there is a background extending to higher energies. This background is due to ions that were backscattered by Nb, Mo/Te in deeper layers. The most likely process being that the ions were neutralized at the first interaction with the surface, lost some energy along the ingoing (straggling) trajectory, backscattered in a hard binary collision with a Nb, Mo, or Te atom, and lost again some energy on the straggling way back to the surface. Since in LEIS only backscattered ions are detected, it is necessary that the backscattered He atoms are reionized in an interaction with a surface atom, just before leaving the surface. For 3 keV He⁺ ions scattered by this type of oxides the straggling energy loss contributes about 160 eV for backscattering from a depth of 1 nm. The shape of the 10x magnified background thus gives information on the thickness distribution of the silica coating. It shows that a small fraction of the coating is only just

covered (1-2 atoms thick), while the maximum thickness is about 2 nm. Consistently, TEM (see below) shows that the silica layer is not homogeneous and its thickness varies.

3.2 Phase composition of the Mo-V-Te-Nb oxides

In regard to the bulk structure, a material of high phase purity has been exposed to the silylating agent (**Figure 5a**), as it is evident from comparing the measured XRD patterns with the patterns calculated under the assumption that the solid is composed exclusively of M1 [8] (dotted line, **Figure 5b**). Within the method's range of accuracy, the material is phase-pure. The phase composition of the mixed oxide remained unchanged after catalytic reaction (**Figure 5c**) as well as after the silylation procedure (**Figure 5d, and e**). The materials are highly crystalline, which is also confirmed by TEM.

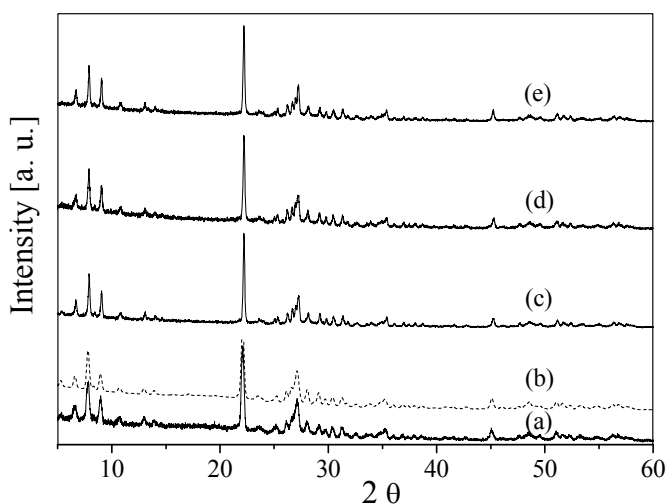


Figure 5. XRD patterns of (a) as synthesized M1, and (b) calculated patterns assuming phase-pure M1 [8]; XRD patterns of (c) M1 after propane oxidation, and of silylated M1 (d) before, and (e) after propane oxidation.

3.3 Microstructure of the model catalysts

The typical needle-shape morphology of the original phase-pure M1 material is observed in the SEM image shown in **Figure 6a**. Only very few particles are found that clearly differ in morphology indicating the presence of traces of other phases not detectable by XRD, or minor amounts of amorphous fractions. The needle-shape morphology is maintained after catalytic test (**Figure 6b**) and after silylation (**Figure 6c**). In the latter material, some spherical particles are observed that have been assigned to pure SiO₂ by EDX analysis. The needle-like shape of the silylated M1 particles (**Figure 6c**) is also not

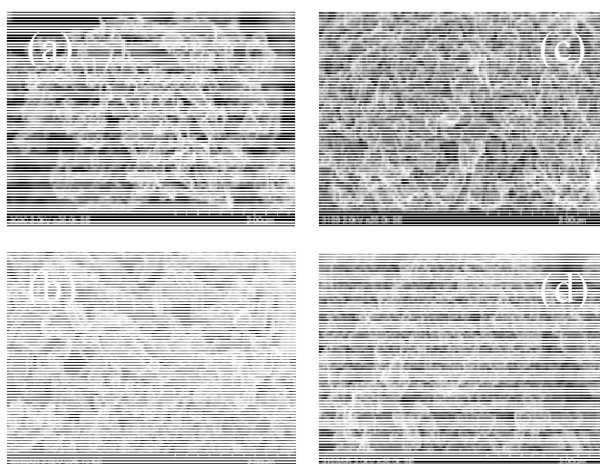


Figure 6. SEM images of phase-pure M1 (a) before and (b) after propane oxidation; SEM images of silylated M1 (c) before and (d) after propane oxidation.

substantially affected by propane oxidation (**Figure 6d**).

Shape analysis of the original M1 catalyst revealed a broad distribution of the needle length with a maximum between 100 and 400 nm (**Figure 7a**). The abundance of shorter needles, especially those with length shorter than 400 nm, clearly increases after propane oxidation (**Figure 7b**), which is attributed to breakage of the needles due to the

mechanical manipulation during preparation of the sieve fraction before the catalytic test. A similar length distribution has been observed with the silylated catalyst after the catalytic reaction (**Figure 7c**), indicating a comparable impact of mechanical treatment

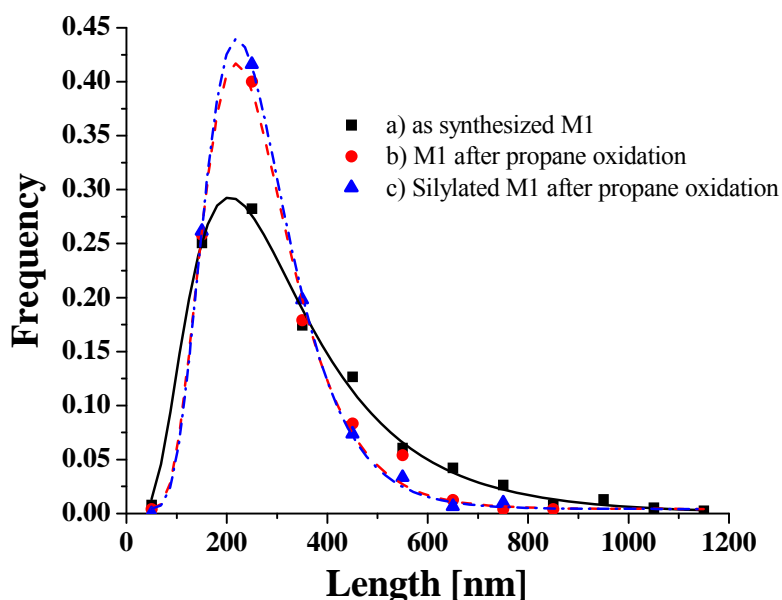


Figure 7. Distribution of the needle length (a) in as synthesized phase-pure M1, (b) in M1 after propane oxidation, and (c) in silylated M1 after propane oxidation.

for silylated and non-silylated M1.

Table 1 summarizes mean needle length, mean needle diameter and mean diameter/length ratio of the needles obtained by shape analysis of about 300 needles for the original M1 material, the M1 catalyst after propane oxidation and the silylated M1 after the catalytic testing. As the M1 needles are naturally crystals with a preferred growth direction perpendicular to the $\{001\}$ planes, a preferential breaking perpendicular to the length axis would be expected during mechanical treatment. This preferential breaking is reflected in a slight increase of the mean diameter/length ratio from 0.56 for the original M1 catalyst before propane oxidation to 0.59 and 0.61 for the nonsilylated

and the silylated M1, respectively, after propane oxidation. Assuming that all needles have cylindrical geometry with circular basal planes and mean geometric parameters (diameter, length) as given in **Table 1**, the total surface area and the surface area of the (001) planes of an average needle have been calculated for the three model catalysts (**Table 1**). Taking into account a unit cell density of M1 of 4.4 g/cm^3 [8], specific surface areas can be calculated that agree well with the BET surface areas measured (**Table 1**), confirming high crystallinity of the materials.

If each needle was disrupted once, an increase in surface area of about 20% is expected from the cylindrical geometry. The actual increase in BET surface area of the nonsilylated M1 before and after propane oxidation of 13% agrees well with the increase in specific surface area of 14% calculated based on the shape analysis, confirming the reliability of the method. The BET surface area of the silylated M1 was not measured since falsification due to the presence of silica particles was expected. However, considering the similar size distribution of nonsilylated and silylated needles after the catalytic testing (**Figure 7**), an increase in surface area of 13% could be expected for the silylated catalyst as well.

In summary, combined shape and BET surface area analysis clearly indicate a preferential disruption of the M1 needles perpendicular to the [001] direction by mechanical treatment before catalytic testing. Comparing nonsilylated and silylated M1 needles, the similar impact of the mechanical treatment on particle morphology provides further evidence for the applicability of the present approach.

Table 1

Results of particle shape analysis based on SEM images and BET surface areas measured by nitrogen adsorption

Catalyst	Number of particles	Mean length (nm)	Mean diameter (nm)	Mean aspect ratio ³	BET surface area (m ² /g)	Calculated ³ total surface area of one needle (nm ²)	Calculated ³ surface area of the (001) plane of one needle (nm ²)	Calculated ³ specific surface area (m ² /g)
M1 ¹	379	336±189	184±99	0.56	6.7	2.47 10 ⁵	0.53 10 ⁵	6.3
M1 ²	241	277±119	164±85	0.59	7.6	1.85 10 ⁵	0.42 10 ⁵	7.2
silyl. M1 ²	298	275±114	167±71	0.61	n. d.	1.88 10 ⁵	0.44 10 ⁵	7.1

¹ M1 as synthesized² catalyst after propane oxidation³ calculation under consideration of mean diameter, mean length and under assumption of cylindrical geometry with circular basal plane**Table 2**

Catalytic properties of M1 and silylated M1 in propane oxidation to acrylic acid (AA) after 32 h time on stream at 673 K

Catalyst	X _{C₃H₈} [%]	S _{AA} [%]	Y _{AA} [%]	Activity [mmol _{C₃H₈} /h·g _{cat}]	Activity [mmol _{C₃H₈} /h·m ² _{exp.surf.}]	Formation rate AA [mmol _{AA} /h·g _{cat}]	Formation rate AA [mmol _{AA} /h·m ² _{exp.surf.}]
M1	49	73	36	2.94	0.39	2.15	0.28
Silylated M1	9	100	9	0.54	0.24	0.54	0.24

Provided that no silica is removed from the sides of the needles, the new surface area formed by mechanical treatment of completely silylated M1 is mainly composed of (001) planes (**scheme 1**). Needles that exclusively expose the (001) plane, have been detected by high-resolution transmission electron microscopy in the silylated M1 catalyst after the catalytic test reaction (**Figure 8a**). The image in **Figure 8a** shows one needle with the sides covered by silica and with the cross-section plane free of SiO_2 confirming that the needles can break perpendicular to the length axis. Furthermore, needles completely covered by a layer of silica are also observed (**Figure 8b**), indicating that not every

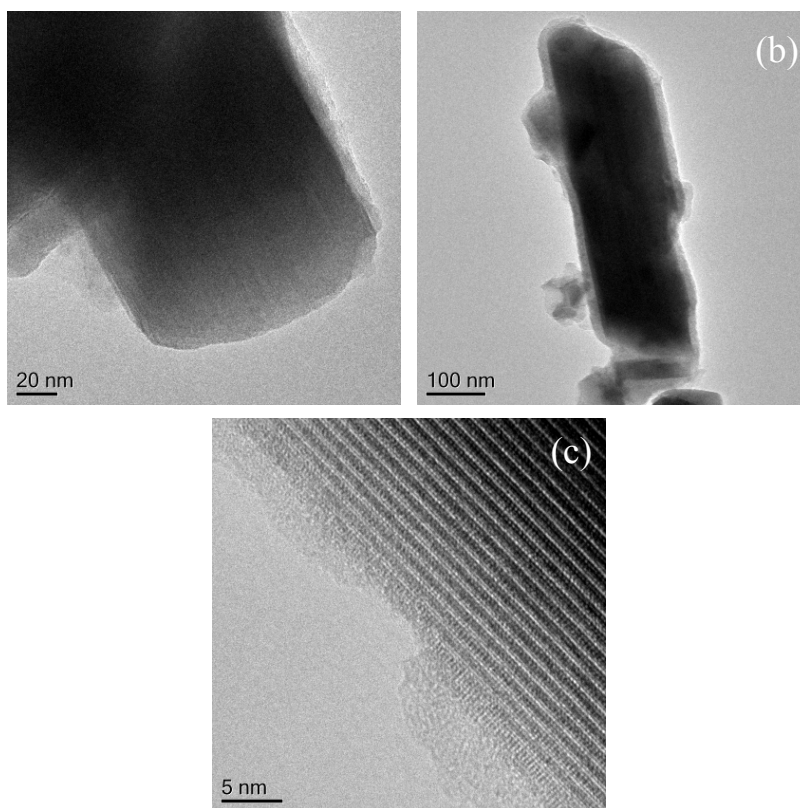


Figure 8. HRTEM images of (a) a silylated M1 needle disrupted along the (001) plane, of (b) a completely silylated M1 needle and of (c) a silylated M1 needle with silica scratched from the sides.

needle is broken. This is in agreement with the results of shape analysis and nitrogen adsorption. The possibility of partial removal of silica from the sides of the needles cannot be excluded, as evidenced by the TEM image shown in **Figure 8c**.

3.4 Catalytic properties of the model catalysts in propane oxidation

Pure silica shows no catalytic activity in propane oxidation under the reaction conditions applied. Thus, completely silylated M1 is expected to be inactive. But, experimental verification of this statement for a completely silylated model catalyst is impossible. Mechanical manipulation of the catalyst by pressing and sieving is required to prepare a sieve fraction before catalytic testing. This causes partial damage of aggregates and even of the primary particles, resulting in exposure of a new MoVTenbO_x surface in both the silylated as well as in case of the nonsilylated reference catalysts (**Scheme 1**).

Table 2 compares the catalytic performance of the two mechanically treated catalysts. Propane oxidation was performed in parallel reactors applying the same temperature, space velocity, and feed composition. Under steady-state conditions, the conversion of propane is fivefold greater over the reference M1 than over the silylated model catalyst. Whereas only acrylic acid is formed over silylated M1, the selectivity is lower for the reference material producing 12% CO₂ and 15% CO as byproducts. These differences in selectivity most likely are related to the different propane conversion levels. The carbon oxides may be formed in consecutive reactions, thus lowering the selectivity to acrylic acid over the reference M1. Table 2 gives average rates. Due to the high conversion of the nonsilylated reference catalyst, the average consumption rate of propane is underestimated for this catalyst. Nevertheless, it is fivefold higher than that of the silylated catalyst. The greater MoVTenbO_x surface area that is exposed to the reactants

in case of the nonsilylated reference catalyst is a possible explanation for this finding. The surface area of the reference M1 was measured by nitrogen adsorption (**Table 1**). LEIS was used to determine the accessible MoVTenbO_x surface area of the silylated catalyst, as described in the following section.

3.5 LEIS after catalysis

To properly compare between the catalysts, the silylated and nonsilylated samples were both investigated with LEIS after the same mechanical treatment (pelletizing, crushing, sieving) and catalytic testing (see **Scheme 1**). **Figures 9 and 10** show the He and Ne spectra after background subtraction. Due to partial disruption of the needles, significant signals can be seen for V, Nb, Mo, and Te in the silylated sample. Again, some Co/Ni contamination is present. The surface fractions of the elements in **Figures 9 and 10** can be quantified using the reference spectra in **Figures 1 and 2**. It is found that the sum of the surface fractions of V₂O₅, Nb₂O₅, MoO₃ and TeO₃ in the treated silylated sample amounts to 30% of that in treated nonsilylated sample. The other part of M1 (70%)

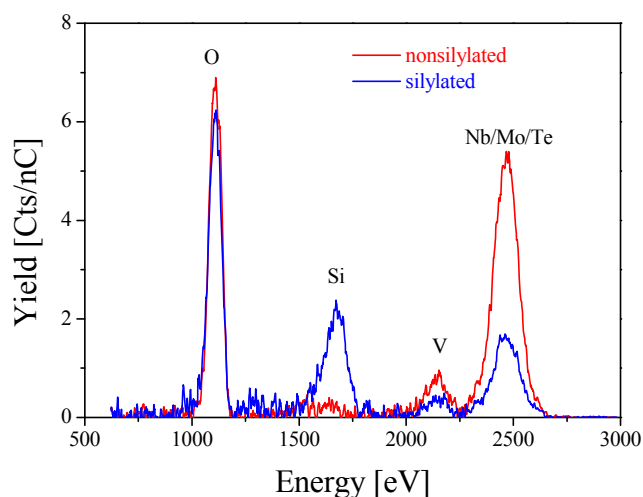


Figure 9. Background-subtracted 3 keV $^4\text{He}^+$ spectra from catalytically tested samples.

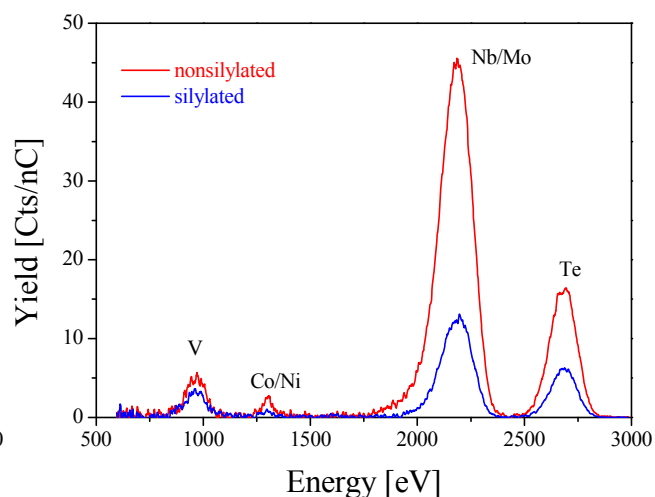


Figure 10. Background-subtracted 5 keV $^{20}\text{Ne}^+$ spectra from catalytically tested samples

remains covered by SiO₂. The 30% thus represents the new surface generated by the mechanical treatment.

Table 3

Metal content of the bulk (EDX) and topmost layer (LEIS) in at.-%. The numbers in parenthesis represent molar ratios of the metals normalized to molybdenum

Catalyst	Method	Mo	V	Te	Nb
M1¹	EDX	64 (1)	22 (0.34)	5 (0.08)	9 (0.14)
	LEIS				
M1²	EDX	64 (1)	20 (0.31)	6 (0.09)	10 (0.16)
	LEIS	65 (1)	12 (0.18)	12 (0.18)	11 (0.17)
silylated M1¹	EDX	63 (1)	22 (0.35)	6 (0.09)	9 (0.14)
	LEIS	0	0	0	0
silylated M1²	EDX	62 (1)	21 (0.34)	6 (0.09)	11 (0.18)
	LEIS	55 (1)	20 (0.37)	15 (0.27)	10 (0.17)

¹ as synthesized

² catalyst after propane oxidation

To obtain the atomic surface concentrations, the surface fractions of the oxides must be corrected for the differing metal atoms/cm² in these oxides. **Table 3** gives the atomic compositions (in parentheses normalized to Mo) for the treated nonsilylated sample and the new surface of the silylated sample, along with the results of the bulk analyses by EDX for comparison. In agreement with earlier studies [15], the chemical composition of the outermost surface layer differs significantly from that of the bulk. The LEIS measurement of the M1 reference provides important information, including the basal plane and the lateral surface, showing an enrichment of tellurium at the expense of vanadium. The situation on the freshly formed surface of the silylated model catalyst, which is dominated by the (001) plane, is different, with an increase of tellurium at the expense of molybdenum. No depth profile and no differences between the catalysts with respect to the Nb concentration are noted. **Figure 11** also illustrates the clear differences

in the surface compositions, with the Ne spectra normalized on the maximum of the Nb/Mo peak.

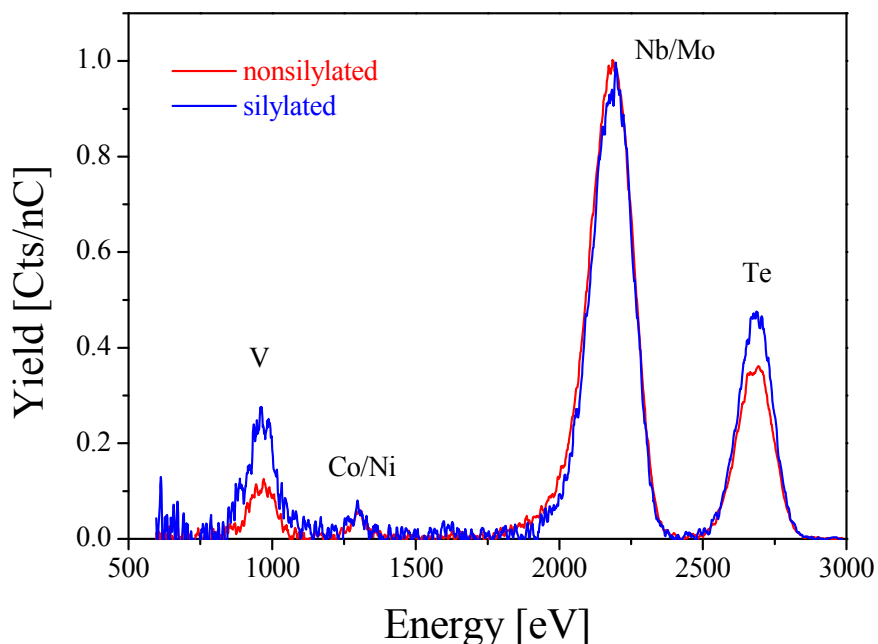


Figure 11. Normalised 5 keV $^{20}\text{Ne}^+$ spectra (Mo=1.00) from catalytically tested sample (after subtraction of background).

4 Discussion

It has been well documented that the M1 phase occurring in MoVTeNb mixed oxide catalysts possesses a key function in selective oxidation and ammoxidation of propane [6, 14, 23]. The crystal structure hosts four different metals, three of them with variable oxidation state, meeting the requirements for catalyzing redox reactions by exposing or bearing structural arrangements at the surface that easily meet the demands of propane activation and the transfer of 8 electrons in its selective oxidation to acrylic acid or in its ammoxidation to acrylonitrile, respectively. Surface and sub-surface reduction and reoxidation of M1 crystals without structural collapse seem to be possible [24]. The

occupancy of the 13 metal sites in the unit cell of the crystal structure is variable [9, 10, 14]. Accordingly, the catalytic properties may be controlled by synthesis or post-treatment procedures. Crystallinity seems to be required to obtain catalytic activity for selective (amm)oxidation of propane [6, 25, 26]. The possible role of defects remains an open question [24, 27]. Typically, nanocrystalline M1, composed of fine needles of a few hundred nanometers in length, exhibits excellent catalytic behavior.

The phase-pure M1 synthesized in the present study exhibits the corresponding morphology and has very small amounts of impurity phases or amorphous fractions, as evidenced by XRD (**Figure 5**) and electron microscopy (**Figure 6a**). Compared with published M1 stoichiometries, (e.g., $\text{Mo}_1\text{V}_{0.15}\text{Te}_{0.12}\text{Nb}_{0.13}\text{O}_x$ [8] or $\text{Mo}_1\text{V}_{0.23}\text{Te}_{0.11}\text{Nb}_{0.14}\text{O}_x$ [9]), the present material is characterized by increased V content and a reduced Te content (**Table 3**), which might be the reason for its exceptional catalytic behavior (**Table 2**). The average formation rate of acrylic acid measured in the stationary state after 32 hours on stream is $2.15 \text{ mmol/h}\cdot\text{g}_{\text{cat}}$, which exceeds results reported for M1 in the literature [28]. Due to its phase purity and catalytic activity the present material was chosen to prepare a model catalyst preferentially exposing the (001) plane. Based on grinding experiments, and under the assumption that the structural characteristics and the chemical composition of the surface do not differ from the bulk even under reaction conditions, it was previously concluded that the catalytically active sites in propane oxidation [11, 12] or ammoxidation [14, 26] are located on terminating (001) planes. This assumption is not consistent with room temperature LEIS measurements that give an indication of gradients in elemental composition between surface and bulk of M1 [29]. Surface texturing of catalyst particles also has been revealed by high-resolution TEM on

the surface of high-performing MoVTeNbO_x catalysts that have been leached with solvents [27]. In any case, a well-defined and rigid arrangement of structural units may be rather unlikely at reaction temperature and in the presence of steam in the feed.

Exploring this question by in-situ spectroscopic methods is quite challenging, however. Thus, in the present study we used propane oxidation itself as a probe reaction to ascertain the specific catalytic activity of the (001) plane compared with the integral activity of the entire M1 surface. For this purpose, the M1 crystals were covered completely by a thin layer of silica. HS-LEIS confirms coverage of the whole mixed oxide surface (**Figure 4**). The thickness of the layer ranges from a few monolayers to maximum 20 nm, as verified by LEIS and TEM. Neither the particle size distribution of the original M1 (**Table 1**) nor its chemical composition (**Table 3**) is affected by the silylation procedure. But the powders were pelletized, crushed, and sieved before being introduced into the catalytic test reactor. Such a gentle mechanical treatment leads to partial disruption of needles and formation of fresh MoVTeNbO_x surface. For the silylated M1, the newly emerging MoVTeNb oxide surface was verified by HS-LEIS (**Figures 9 and 10**). For the pure, nonsilylated M1, these morphological changes should be reflected in an increased specific surface area as measured by nitrogen adsorption. Under the assumption that the mechanical treatment leads exclusively to a breakage of needles perpendicular to the [001] direction, the difference corresponds to the surface of newly formed (001) planes. In the present experiment, the difference in the specific surface area is 13.4% (**Table 1**). A quite similar result (14.3%) is obtained if the mean particle size determined based on the shape analysis by SEM and the bulk density of M1 (4.4 g/cm³ [8]) are used to calculate the increase in surface area of pure, nonsilylated M1

(**Table 1**), satisfactorily confirming the reliability of the shape analysis and demonstrating that the mechanical treatment applied is associated mainly with breakage of needles and not with other damage. The relevance of shape analysis is important, because in the silylated catalyst, BET surface area measurements cannot be relied on for calculation due to an expected increase in surface area caused by the possibly not smooth SiO_2 layer and the occasional formation of pure silica particles.

Both the original M1 needles and the silylated needles have a low probability of breaking (**Table 1**, **Figure 7**), and long needles break more frequently than short needles (**Figure 7**). **Figure 7** confirms that nonsilylated and silylated needles break in a similar way, because the two materials have essentially the same particle size distribution after the catalytic test. For the silylated catalyst, the increase in surface area (i.e., the yield in newly formed basal plane surface area) corresponds to 12.7% when the mean particle size determined by shape analysis is used for the calculation (**Table 1**).

In summary, based on shape analysis and/or nitrogen adsorption before and after catalytic test, the breakage of the M1 needles benefits in newly formed (001) surface area of approximately 15% both for original and silylated M1.

As an independent method, LEIS analysis was applied to determine the freshly formed MoVTaNbO_x surface of the silylated catalyst. This fraction corresponds to 30% of the surface of the original M1. This value is twice as high as the increase calculated from shape analysis, implying that more than silica-free (001) planes were generated. HRTEM (**Figure 8c**) shows that some silica was scratched from the sides of the needles as well. Assuming that the approximate 15% increase in surface area calculated from shape analysis (**Table 1**) corresponds exclusively to the newly formed silica-free (001) planes,

the ratio of the basal plane area versus other MoVTeNbO_x surface area (i.e., lateral surface area) is about 1 in the silylated M1. In the original M1, the entire surface of the needles is exposed to the gas phase during propane oxidation and, thus the ratio of (001) surface area to lateral surface area corresponds to 0.25 (**Table 1**). Consequently, even though other surface planes also are to some extent exposed to the reactants in the silylated M1 during propane oxidation, we can conclude that the silylated, mechanically treated M1 catalyst represents a suitable model system for studying the catalytic properties of the (001) plane, since half of the exposed MoVTeNbO_x surface is composed of (001) planes.

Table 2 compares the catalytic performance of M1 and silylated M1. As expected, the conversion of silylated M1 is much lower than that of M1, because less MoVTeNbO_x surface is accessible in the former catalyst. Based on the information obtained from the HS-LEIS study indicating that actually 30% more MoVTeNbO_x surface is available in the silylated catalyst, consumption rates of propane normalized to the area of exposed MoVTeNbO_x surface were calculated considering 7.6 m²/g MoVTeNbO_x surface for M1 (BET surface area given in **Table 1**) and a 2.3 m²/g MoVTeNbO_x surface for silylated M1 (0.30 x 7.6 m²/g). The rates given are quite similar for both catalysts, meaning that the intrinsic catalytic properties of the entire M1 surface are similar to the catalytic behavior of a surface composed of 50% (001) planes. This finding casts some doubt on the uniqueness of the basal plane of M1.

The result is especially surprising since the chemical composition of the newly formed M1 surface of the silylated catalyst (which can be regarded at least partially, as the inner surface of M1) has a different chemical composition than the average surface

composition of M1, as shown by the LEIS experiment. **Table 3** compares the bulk composition measured by EDX and the surface composition measured by HS-LEIS. Whereas the EDX bulk compositions of the samples are almost the same, confirming that the silylation procedure does not affect the bulk composition, the HS-LEIS surface composition of the newly-generated surface shows relatively large differences, specifically an increased concentration of tellurium at the expense of molybdenum. But, prior to the present LEIS measurements, a mild pre-treatment with oxygen atoms at room temperature was necessary to eliminate environmental contamination from the reaction, transport, and storage. This procedure, which converts all the surface metal ions into their highest oxidation states, may be connected with structural changes. Although the local structure is affected, it is unclear whether the elemental composition changes. However, the surface reconstruction holds for the entire surface of M1, thus justifying a comparison of the basal plane with the total surface in terms of elemental composition.

In any case, these uncertainties do not affect the findings that the intrinsic catalytic properties of the basal plane of M1 in the selective oxidation of propane to acrylic acid do not differ much from those of the lateral surface of the M1 needles. If we accept this result, then the question arises as to why increased catalytic activity and improved selectivity to acrylic acid were observed in previous studies after grinding of M1 [11, 12]. The details of the grinding procedure were not given in those reports; however, most likely, the mechanical treatment was less gentle than that in the present study and probably generated a more defect-rich material along with extra basal planes. Another possible explanation could be that contaminations, such as residues from the preparation procedure, which are common on catalyst surfaces, were removed by extended grinding.

Breaking the needles and scratching deposited impurities away from the sides of the needles would expose fresh, uncontaminated, thus active MoVTaNb oxide surface.

5 Conclusions

The model studies presented here suggest that a distinguished lattice plane of the M1 crystal structure, the (001) plane, is not solely responsible for its outstanding catalytic activity and selectivity in the partial oxidation of propane to acrylic acid. The chemical and structural natures of the active ensembles on the catalyst surface remain unknown. The unique crystal structure of the M1 phase certainly plays an essential role in the selective (amm)oxidation of propane, because amorphous material or MoVTaNb oxide comprising different phases cannot compare with phase-pure crystalline M1. All experimental experience to date suggests that this may differ from the situation for related mixed oxides, such as nanostructured MoVW oxides, which have been reported to be active in propylene oxidation in a semicrystalline state [30]. Similar intrinsic reactivity irrespective of the terminating lattice plane implies that related active ensembles of metal-oxo clusters are exposed to the reactants on the entire surface of the M1 needles. The lateral surface of the needles accounts for the main part of the surface area of M1 (80%). The stepped morphology of the latter surface may generate similar metal-oxo arrangements as on the surface of the basal plane of the needles. HR-TEM studies together with targeted synthesis of M1 showing different microstructure are currently in progress to verify this assumption.

6 Acknowledgments

The authors thank Dr. Olaf Timpe for helpful discussions, Dr. Frank Girgsdies for performing phase analysis of the catalysts, Edith Kitzelmann for conducting the XRD measurements, and Kilian Klaeden, and Gisela Lorenz for carrying out the nitrogen adsorption measurements.

7 References

- [1] T. Ushikubo, H. Nakamura, Y. Koyasu, S. Wajiki, US Patent 5 380 933 (1995); Mitsubishi Kasei Corporation.
- [2] M. Hatano, A. Kayo, US Patent 5 049 692 (1991); Mitsubishi Kasei Corporation.
- [3] T. Ushikubo, K. Oshima, A. Kayo, M. Hatano, *Studies in Surface Science and Catalysis* 112 (1997), 473.
- [4] M. Baca, A. Pigamo, J. L. Dubois, J. M. M. Millet, *Topics in Catalysis* 23 (2003), 39.
- [5] J. M. Oliver, J. M. López-Nieto, P. Botella, *Catalysis Today* 96 (2004), 241.
- [6] W. Ueda, D. Vitry, T. Katou, *Catalysis Today* 96 (2004), 235.
- [7] H. Tsuji, K. Oshima, Y. Koyasu, *Chemistry of Materials* 15 (2003), 2112.
- [8] P. DeSanto Jr., D. J. Buttrey, R. K. Grasselli, C. G. Lugmair, A. F. Volpe Jr., B. H. Toby, T. Vogt, *Zeitschrift für Kristallographie* 219 (2004), 152.
- [9] H. Murayama, D. Vitry, W. Ueda, G. Fuchs, M. Anne, J. L. Dubois, *Applied Catalysis A: General* 318 (2007), 137.
- [10] *Preparation of phase-pure M1 MoVTaNb oxide catalysts by hydrothermal synthesis – Influence of reaction parameters on structure and morphology.*
A. Celaya Sanfíz, T. W. Hansen, E. Rödel, O. Timpe, A. Trunschke, R. Schlögl,
(accepted for publication in *Topics in Catalysis*).
- [11] W. Ueda, K. Oshihara, *Applied Catalysis A: General* 200 (2000), 135.
- [12] K. Oshihara, T. Hisano, W. Ueda, *Topics in Catalysis* 15 (2001), 153.
- [13] V. V. Guliants, R. Bhandari, R. S. Soman, O. Guerrero-Pérez, M. A. Bañares, *Applied Catalysis A: General* 274 (2004), 213.

- [14] R. K. Grasselli, D. J. Buttrey, P. DeSanto, Jr., J. D. Burrington, C. G. Lugmair, A. F. Volpe, Jr., T. Weingand, *Catalysis Today* 91–92 (2004), 251.
- [15] V. V. Guliants, R. Bhandari, B. Swaminathan, V. K. Vasudevan, H. H. Brongersma, A. Knoester, A. M. Gaffney, S. Han, *Journal of Physical Chemistry B* 109 (2005), 24046.
- [16] V. V. Guliants, R. Bhandari, A. R. Hughett, S. Bhatt, B. D. Schuler, H. H. Brongersma, A. Knoester, A. M. Gaffney, S. Hann, *Journal of Physical Chemistry B* 110 (2006), 6129.
- [17] J.-P. Jacobs, A. Maltha, J. G. H. Reintjes, J. Drimal, V. Ponc, H. H. Brongersma, *Journal of Catalysis* 147 (1994), 294.
- [18] H. H. Brongersma, M. Draxler, M. de Ridder, P. Bauer, *Surface Science Reports* 62 (2007), 63.
- [19] G. Mestl, N. F. D. Verbruggen, H. Knözinger, *Langmuir* 11 (1995), 3034.
- [20] G. J. A. Hellings, H. Ottevanger, S. W. Boelens, C. L. C. M. Knibbeler, H. H. Brongersma, *Surface Science* 162 (1985), 913.
- [21] W. P. A. Jansen, A. Knoester, A. J. H. Maas, P. Schmitt, A. Kytöki, A. W. Denier van der Gon, H. H. Brongersma, *Surface Interface Analysis* 36 (2004), 1469.
- [22] L. C. A. Van den Oetelaar, H. E. Van Benthem, J. H. J. M. Helwegen, P. J. A. Stapel, H. H. Brongersma, *Surface Interface Analysis* 26 (1998), 537.
- [23] M. Baca, A. Pigamo, J. L. Dubois, J. M. M. Millet, *Topics in Catalysis* 23 (2003), 39.
- [24] R. K. Grasselli, D. J. Buttrey, J. D. Burrington, A. Andersson, J. Holmberg, W. Ueda, J. Kubo, C. G. Lugmair, A. F. Volpe Jr, *Topics in Catalysis* 38 (2006), 7.
- [25] R. K. Grasselli, *Catalysis Today* 99 (2005), 23.
- [26] R. K. Grasselli, J. D. Burrington, D. J. Buttrey, P. DeSanto, C. G. Lugmair, A. F. Volpe Jr., T. Weingand, *Topics in Catalysis* 23 (2003), 5.
- [27] J. B. Wagner, O. Timpe, F. A. Hamid, A. Trunschke, U. Wild, D. S. Su, R. K. Widi, S. B. A. Hamid, R. Schlögl, *Topics in Catalysis* 38 (2006), 51.
- [28] D. Vitry, Y. Moriwaka, J. L. Dubois, W. Ueda, *Applied Catalysis A: General* 251 (2003), 411.

- [29] V. V. Guliants, R. Bhandari, H. H. Brongersma, A. Knoester, A. M. Gaffney, S. Han, *Journal of Physical Chemistry B* 109 (2005), 10234.
- [30] H. Hibst, F. Rosowski, G. Cox, *Catalysis Today* 117 (2006), 23

CHAPTER 4- New synthesis routes of MMO catalysts by dilution of Mo-V-X-Nb (X=Te, Bi, and P) mixed oxides with SiO₂, Cr₂O₃ or ZrO₂ for the oxidation of propane to acrylic acid.

Abstract

Metal substitution and/or dilution of the up-to-date most active catalyst MoVTenbO_x in the selective oxidation of propane to acrylic acid was investigated in an exploratory study. The structural consequences of (i) substituting the “in-channel” element (Te vs. P or Bi), and (ii) diluting the multimetal oxide (MMO) by using SiO₂ (Aerosil 300), ZrO₂, and Cr₂O₃ as diluents, were studied applying a parallel screening approach. Hydrothermal synthesis was used for preparation of the MMO catalysts.

The hydrothermal synthesis of the undiluted Mo-V-X-Nb (X=Te, P, Bi) materials resulted in the formation of crystalline catalysts composed of various phases. The catalytically relevant M1 phase was only obtained in case of the Mo-V-Te-Nb oxide. Cr₂O₃ as diluent did not interfere in phase formation, while SiO₂ prevented the formation of the M1 phase in the diluted Mo-V-Te-Nb oxide. ZrO₂ reacted with molybdenum oxide under formation of a more stable zirconium molybdate.

The undiluted Mo-V-Te-Nb oxide catalyst, mainly composed of the M1 phase, showed the highest activity and the highest formation rate of acrylic acid normalized to the specific surface area of the catalyst. Unexpectedly, all materials showed substantial catalytic performance, irrespective of their chemical and phase composition. These results underline on one side the exceptional role of the M1 phase but also prove that this phase is not essential for the selective oxidation of propane to acrylic acid. Moreover, the observations presented in this work support the hypothesis that the active sites on the surface of crystalline M1 can be associated with high-energy sites created from the bulk under reaction conditions.

Keywords: multi-metal oxide catalysts, Mo-V-Te-Nb oxide, tellurium, phosphor, bismuth, SiO₂, ZrO₂, Cr₂O₃, propane oxidation, M1 phase, BiVO₄

1 Introduction

Catalysts for alkane oxidation are usually complex multimetal oxides (MMO) containing molybdenum and vanadium oxide as essential constituents [1-3]. Particularly for selective oxidation of propane to acrylic acid, mixed oxides of molybdenum, vanadium, niobium, and tellurium have been identified in extensive compositional searches as the most promising catalysts [3], reaching yields of acrylic acid of about 50 %. Currently, acrylic acid is industrially produced in a two-step oxidation process starting from propene [4-5] over promoted bismuth molybdate and Mo-V mixed oxide catalysts achieving yields up to 86 %. Despite the lower price of propane compared to propene, the yield of acrylic acid in the direct oxidation of propane is still below the profitability threshold at actual commercial conditions. Thus, further improvement of catalysts for selective activation of alkanes is desired.

MoVTaNbO_x catalysts mainly consist of two orthorhombic phases called “M1” and “M2” [6]. The structural and chemical complexity of M1 seems to cope with the challenging task of propane activation [7, 8], while M2 is regarded to be active and selective in oxidation of propene to acrylic acid [7, 9]. The M2 phase is richer in tellurium than M1. It was postulated that Te is an active element in propene conversion [8], but its beneficial effect found empirically may also be related to the generation of Te-free active sites. Specifically, tellurium seems to play a critical role with respect to phase formation. It was assumed that Te acts structure-directing and structure-stabilizing regarding the M1 phase. However, Ueda and co-workers showed that a Mo-V oxide with a related orthorhombic structure may also be obtained by crystallization in inert atmosphere at 773 K in absence of tellurium [10], proposing that NH₄⁺ serves as

structure-directing component [11]. A structure stabilizing role has been attributed to Te based on the observation that the precursor material of the ternary Mo-V-Te oxide treated at 873 K crystallizes in the desired orthorhombic structure, whereas the binary Mo-V system decomposes into other phases at such high temperatures [10-12]. Orthorhombic MoVO_x and MoVTeO_x systems show similar activity in the partial oxidation of propane to acrylic acid. However, the tellurium containing catalyst is significantly more selective to acrylic acid [11-12]. Therefore, tellurium seems to play an essential role in view of the specific catalytic properties of these catalysts. However, the concentration of tellurium on the surface under operating conditions is poorly defined. Another disadvantage consists in the volatility of elemental tellurium at temperatures higher than 723 K that causes substantial Te loss during thermal activation of the catalyst and contamination of reactors and exhaust systems. The substitution of this element is, therefore, not only of interest for a deeper understanding of the role of tellurium in catalysis, but also for the prevention of tellurium contamination during catalyst preparation and operation.

Recently, tellurium has been substituted by a number of metals in hydrothermally synthesized Mo-V-X ternary oxides with either $X=\text{Al, Fe, Cr, Ti}$ [13], or $X=\text{Al, Ga, Bi, Sb, Te}$ [14] and Mo-V-X-Nb quaternary oxides with ($X=\text{Te, Sb}$) [15]. The orthorhombic M1 structure was achieved only through substitution of Te by Sb in the ternary as well as in the quaternary system [14, 15]. However, none of the substituted catalysts reached the efficiency of tellurium-containing materials. Tellurium was also partly replaced by cesium in the M2 structure. The maximum tellurium substitution was 30 % [9]. With such a catalyst, improved activity for the ammoxidation of propene to acrylonitrile was observed.

Dilution of the active metal oxides could also be an option for improving the productivity of multi-metal oxide catalysts. Thus, dispersion of M1 crystallites on a support resulting in an increased number of active sites exposed to the gas phase might be achieved. However, enhanced dispersion of the active phase does not always compensate the dilution in terms of activity per unit surface area [16]. Furthermore, dilution of the catalyst is also highly interesting for preventing the occurrence of “hot spots” under reaction conditions resulting in sintering and phase transformations, such as the formation of the detrimental but stable α -MoO₃. Dispersion of the active MMO crystals by dilution impedes the growth of crystallites increasing in this way the resistance of the catalyst under reaction conditions. Silica, alumina, titania, zirconia, and niobium oxide have been studied as diluents or supports for multimetal oxides in selective oxidation reactions [16-18]. MCM41 was used to prepare highly dispersed Mo-V-Te oxide catalysts for direct oxidation of propane to acrolein [19]. In all these cases, the MMO were prepared by precipitation and evaporation.

Hydrothermal synthesis is an approved preparation method for crystalline Mo-V-Te-Nb mixed oxides. In the present exploratory study, hydrothermal synthesis was applied to substitute tellurium with phosphor or bismuth both in presence and in absence of silica, zirconia, or chromia as diluents. The consequences on phase formation and catalytic properties are studied. Based on the extended parameter field, the function of crystallinity in selective oxidation of propane to acrylic acid is discussed. Although Mo-V-Te-Nb oxide containing the M1 phase was still proven to be excellent, alternative compositions with great potential for optimization are disclosed.

2 Experimental

2.1 Catalysis preparation

Diluted and undiluted Mo-V-X-Nb (X=Te, Bi, P) mixed metal oxides were prepared by hydrothermal synthesis in a high-throughput (HT) autoclave system. The HT autoclave system is composed of 12 parallel reactors with volume of 140 ml each. The hydrothermal synthesis was carried out at 448 K applying reaction times between 10 minutes and 24 hours. SiO₂ (Aerosil 300, Degussa), Cr₂O₃ (Merck) and ZrO₂ (MEL Chemicals) were used as diluents. MoO₃ was purchased from Merck and all other chemicals were purchased from Aldrich and used without further purification.

a) Mo-V-X-Nb-O (X=Te and Bi) mixed oxides

Initially, 2.59 g of molybdenum trioxide (MoO₃) were dispersed in 45 ml bidistilled water at 353 K. Afterwards, 0.95 g of telluric acid (Te(OH)₆) or 1.65 g of bismuth nitrate (Bi(NO₃)₃), respectively, were added to this slurry. Separately, 0.5 g of vanadium pentoxide (V₂O₅) was dispersed in 22.5 ml bidistilled water at 353 K. The latter slurry was added to the first mixture and stirred for 5 minutes. Finally, 0.94 g of ammonium niobium oxalate ((NH₄)[NbO(C₂O₄)₂(H₂O)₂].3H₂O) was dissolved in 22.5 ml bidistilled water at 353 K and added to the previous mixture. The resulting molar ratio of the active metal oxides corresponds to the stoichiometry Mo₁V_{0.3}X_{0.23}Nb_{0.125}, X=Te, Bi. The slurry was then stirred for 10 minutes at 353 K and the diluent was added. The amount of diluent comprised 50 wt.-%, based on mass of the stoichiometric oxides.

b) Mo-V-P-Nb-O mixed oxide

12-Molybdophosphoric acid, H₃(PMo₁₂O₄₀)·nH₂O, was synthesized by dissolving 103.64 g MoO₃ using 4 ml phosphoric acid (85 %, ρ = 1.7 kg/l) in bidistilled H₂O and filling up

with bidistilled H₂O to a total volume of 1 l. Thereafter, 38.8 ml of the synthesized molybdophosphoric acid solution and another 0.35 ml H₃PO₄ were mixed and further diluted with bidistilled water to a total volume of approximately 45 ml. Then, the solution was heated to 353 K. Separately, 0.5 g vanadium oxide (V₂O₅) was dispersed in 22.5 ml bidistilled water at 353 K. The latter mixture was added to the first solution and stirred for 5 minutes. Finally, 0.94 g of ammonium niobium oxalate ((NH₄)[NbO(C₂O₄)₂(H₂O)₂]·3H₂O) was dissolved in 22.5 ml bidistilled water at 353 K and added to the previous mixture. The resulting molar ratio of the active metal oxides corresponds to the stoichiometry of Mo₁V_{0.3}P_{0.27}Nb_{0.125}. The slurry was stirred for 10 minutes at 353 K and then the diluent was added in a mass ratio of 1:1 with respect to the weight of the mixture of the stoichiometric oxides.

Subsequently, the slurries were introduced into the autoclaves. Residual air was replaced by bubbling nitrogen for 5 minutes through the suspension. After hydrothermal synthesis, the resulting gel was filtered, washed and dried at 353 K for 16 hours, resulting in the precursor materials. An identical synthesis procedure was followed to prepare reference Mo-V-X-Nb (X=Te, P, Bi) mixed oxide catalysts without diluent. Starting from the precursors, the final catalysts were obtained by heat treatment in inert gas with a flow of 50 ml/min for 2 h at 873 K (undiluted precursors) or 923 K (diluted precursors), heating rate 15 K/min, with preceding calcination in air for 1 h at 548 K (undiluted precursors) or 598 K (diluted precursors), heating rate 10 K/min. Sample denomination and preparation parameters are summarized in **Table 1**.

Table 1

Characteristics of MoVXNbO – Y mixed oxides (X=Te, Bi, P; Y=Aerosil 300 (A), ZrO₂ (Z), Cr₂O₃ (Cr))

Notation	ID (precursor /catalyst)	X	Y	Hydrothermal synthesis time [h]	Phases composition (XRD)	
					Precursor	Catalyst
TeA-1/6	992/1151	Te	Aerosil 300	1/6	α -MoO ₃ V ₂ O ₅ SiO ₂	
TeA-1/2	988/1143	Te	Aerosil 300	1/2	α -MoO ₃ SiO ₂	
TeA-2	986/1139	Te	Aerosil 300	2	α -MoO ₃ SiO ₂	
TeA-24	1034/1183	Te	Aerosil 300	24	peak at 22° traces of α -MoO ₃ SiO ₂	Mo _{5-x} (V/Nb) _x O ₁₄
PA-1/6	954/1128	P	Aerosil 300	1/6	unknown phase SiO ₂	
PA-1/2	988/1143	P	Aerosil 300	1/2	unknown phase SiO ₂	
PA-2	987/1141	P	Aerosil 300	2	unknown phase SiO ₂	
PA-24	1040/1135	P	Aerosil 300	24	unknown phase SiO ₂	MoOPO ₄ (weak peaks) amorphous
TeZ-1/6	1013/1167	Te	ZrO ₂	1/6	α -MoO ₃ ZrO ₂	
TeZ-1/2	1011/1163	Te	ZrO ₂	1/2	α -MoO ₃ ZrO ₂	
TeZ-2	1007/1155	Te	ZrO ₂	2	peak at 22° α -MoO ₃ (traces) ZrO ₂	
TeZ-24	990/1147	Te	ZrO ₂	24	peak at 22° ZrO ₂	m-ZrO ₂ α -Zr(MoO ₄) ₂ , peak at 22°
BiCr-24	1049/1201	Bi	Cr ₂ O ₃	24	M1 Bi _{0.82} (V _{0.45} Mo _{0.55}) Cr ₂ O ₃	Cr ₂ O ₃ Mo _{5-x} (V/Nb) _x O ₁₄ Bi _{0.82} (V _{0.45} Mo _{0.55}) extra peaks: 26-28°
Te-24	1048/1112	Te	-	24	α -MoO ₃ peak at 22° small extra peaks	M1 α -MoO ₃ Mo _{5-x} (V/Nb) _x O ₁₄
P-24	1052/1118	P	-	24	unknown phase	MoOPO ₄ ~ VOMoO ₄ (traces)
Bi-24	1050/1114	Bi	-	24	peak at 22° Bi _{0.82} (V _{0.45} Mo _{0.55})	Bi _{0.82} (V _{0.45} Mo _{0.55}) Mo _{5-x} (V/Nb) _x O ₁₄ extra peaks: 26-28°

2.2 Activity measurements

Selective oxidation of propane to acrylic acid was carried out in a setup with twelve parallel fixed bed quartz reactors (i.d., 4 mm; length, 225 mm), working at atmospheric pressure. Catalyst samples (sieve fraction: 0.24 to 0.45 mm particle size) were introduced into each reactor tube. The feed flow rate was fixed at a gas hourly space velocity (GHSV) of 1200 h^{-1} (at STP) with standard catalytic bed volume of 0.5 ml. In the feed, a propane/oxygen/nitrogen/steam ratio of 0.85-1/1.9-6.7/15.2-18/9-12 vol.-% was applied. The reaction was carried out at 673 K. The products were analyzed by gas chromatography. Inorganic gases and $\text{C}_1\text{-C}_3$ hydrocarbons were analyzed with a TCD detector using a molecular sieve column and a Porapak Q column, respectively, for separation. Oxygenated products were detected applying a HP-FFAP column and a flame ionization detector.

2.3 Catalyst characterization

XRD measurements were performed with a STOE STADI-P transmission diffractometer equipped with a focusing primary Ge (111) monochromator and a position sensitive detector, using $\text{Cu-K}\alpha_1$ radiation ($\lambda = 1.54 \text{ \AA}$). For data analysis, the program TOPAS (v.2.1, Bruker AXS) was used to fit the diffraction patterns of the activated materials. Specific surface areas of the catalysts were measured with an AUTOSORB-1-C physisorption/chemisorption analyzer applying the BET method. All the samples were degassed in vacuum at 353 K for 2 hours prior to analysis.

3 Results

3.1 Bulk structure of precursors and catalysts

The phase composition of the as-synthesized materials (precursors) and activated materials (catalysts) was analyzed by X-ray diffraction. For reference, the XRD patterns of the oxides used as diluents are shown in **Figure 1**. Chromia with a corundum structure (ICSD 250078) and monoclinic zirconia (ICSD 89426) are more or less crystalline, whereas the silica is a X-ray amorphous powder.

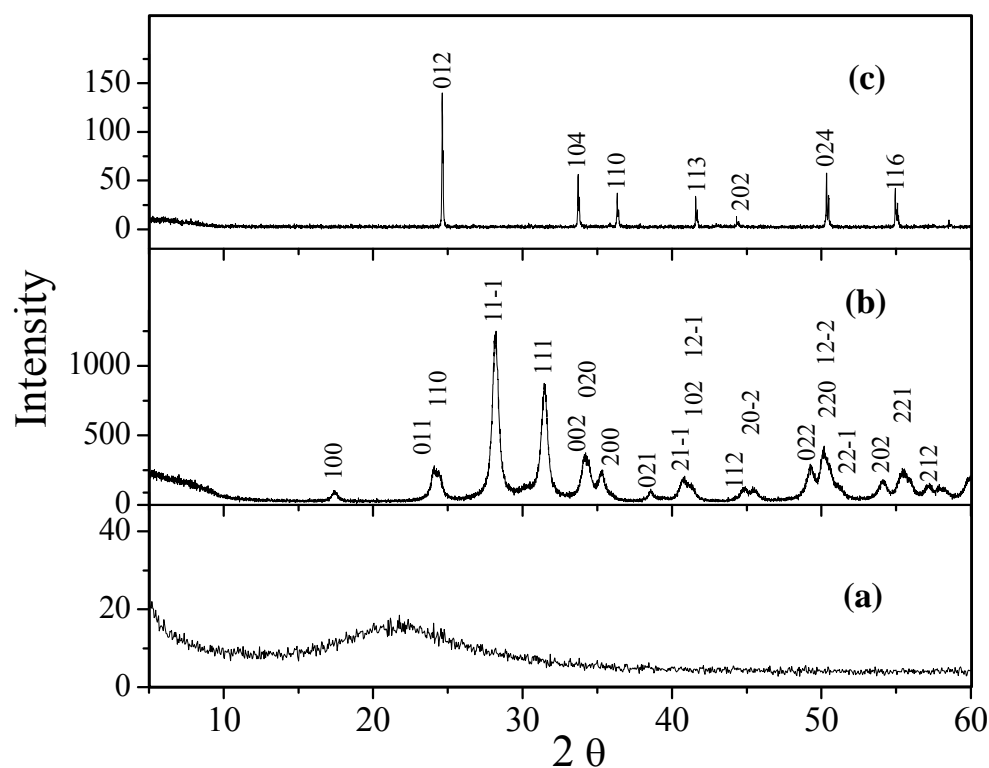


Figure 1. XRD patterns of the diluents: (a) SiO_2 (Aerosil 300), (b) ZrO_2 and (c) Cr_2O_3 .

a) *Mo-V-Te-Nb oxides diluted with SiO_2*

The X-ray diffractograms of Mo-V-Te-Nb oxide precursors diluted with silica, hydrothermally synthesized for 1/6, 1/2, 2 and 24 hours, are shown in **Figure 2**. As expected, after a short synthesis time of 1/6 h, no complete reaction of the educts was

achieved. The corresponding XRD patterns show sharp peaks due to α - MoO_3 (ICSD 35076) and to V_2O_5 (ICSD 60767) (**Figure 2a**). The broad halo between 15 and $30^\circ 2\theta$ is characteristic for SiO_2 (**Figure 1a**). The reflections of the α - MoO_3 structure are still present in the diffractograms of the precursors obtained after synthesis times of $1/2$ and 2 h (**Figure 2b and 2c**). However, the latter diffractogram shows a preferred orientation of

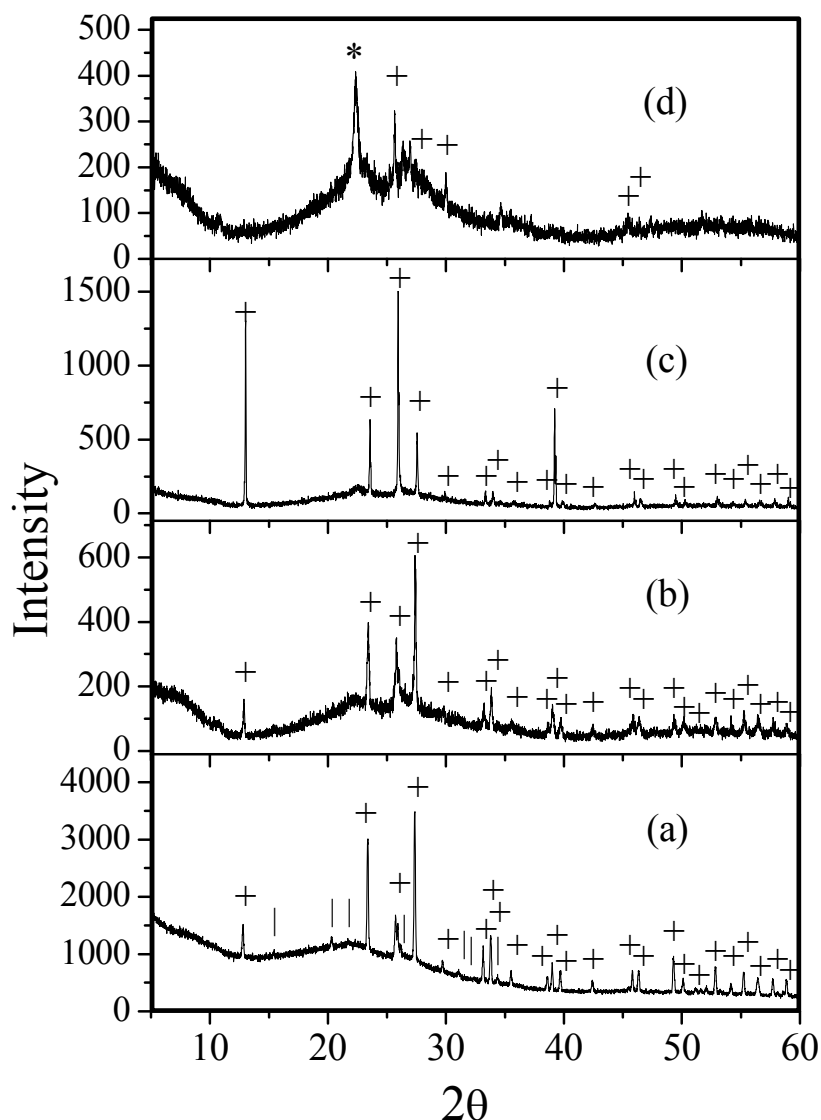


Figure 2. XRD patterns of MoVTaNb/SiO_2 precursor materials prepared with a synthesis time of (a) $1/6$ h, (b) $1/2$ h, (c) 2 h and (d) 24 h. Diffraction peaks are marked as follows: α - MoO_3 (+), V_2O_5 (l), peak $22^\circ 2\theta \rightarrow d = 4 \text{ \AA}$ (*).

the α -MoO₃ crystals in [010] direction. The XRD fingerprint of the as-synthesized oxide changes after a hydrothermal synthesis time of 24 hours. The sharp peaks of the α -MoO₃ structure disappear. However, residual α -MoO₃ cannot be ruled out considering the presence of weak peaks observable between 25° and 30° 2 θ . Additionally, a sharp peak appears at 22° 2 θ (**Figure 2d**). Basically, the diffraction patterns shown in **Figure 2d** resemble the patterns of crystalline M1. In fact, simulated broadening of all peaks in the calculated diffractogram of M1 (ICSD 55097) [20] except from the sharp peak at $2\theta = 22.2^\circ$ results in a patterns that is in good agreement with **Figure 2d**. Shear structures, which are characterized by a high order of corner-sharing MO₆ octahedra in the crystallographic *c* direction, which is the growth direction of the needle-like M1 crystals, and without long-range order in the *ab* plane were also reported in the literature for mixed metal oxides that are able to form oxidic bronze-like structures [21]. An example is semi-crystalline (Mo,V,W)₅O₁₄ that crystallizes during heat treatment at 693 K in He into a Mo₅O₁₄-type structure (ICSD 27202) [22-24] For crystalline orthorhombic M2 (ICSD 55098) [20], the most intense reflection is also the peak at $2\theta = 22.2^\circ$ that represents again long-range order of corner-sharing MO₆ (M=Mo, V, Nb) units in the crystallographic *c* direction corresponding to a distance between the {001} lattice planes of $d = 4 \text{ \AA}$.

Thermal treatment of the precursor TeA-24 at 873 K in Ar results in crystallization of the Mo_{5-x}(V,Nb)_xO₁₄ structure [24] (**Figure 3a**) as evident by the presence of the characteristic peaks of this phase (**Table 2**). Crystalline α -MoO₃ is identified as the second phase in this catalyst (**Figure 3a**). The M1 phase was identified as the main constituent of the reference, Te-24, prepared in absence of the diluent (**Figure 3b**). The

XRD patterns of the orthorhombic M1 phase show characteristic peaks at 6.6° , 7.9° , 9.0° , 22.2° , 27.3° and 45.3° 2θ , with the peak located at 22.2° 2θ being the most intense line. In addition to M1, α - MoO_3 and $\text{Mo}_{5-x}(\text{V},\text{Nb})_x\text{O}_{14}$ -type phases are also present. It should be mentioned that phase-pure M1 has been prepared successfully by hydrothermal synthesis over 48 h starting from ammonium heptamolybdate and vanadyl sulfate [25]. Therefore, it may be assumed that the short hydrothermal synthesis time (24 h) applied in the present work may be responsible for the incomplete formation of M1.

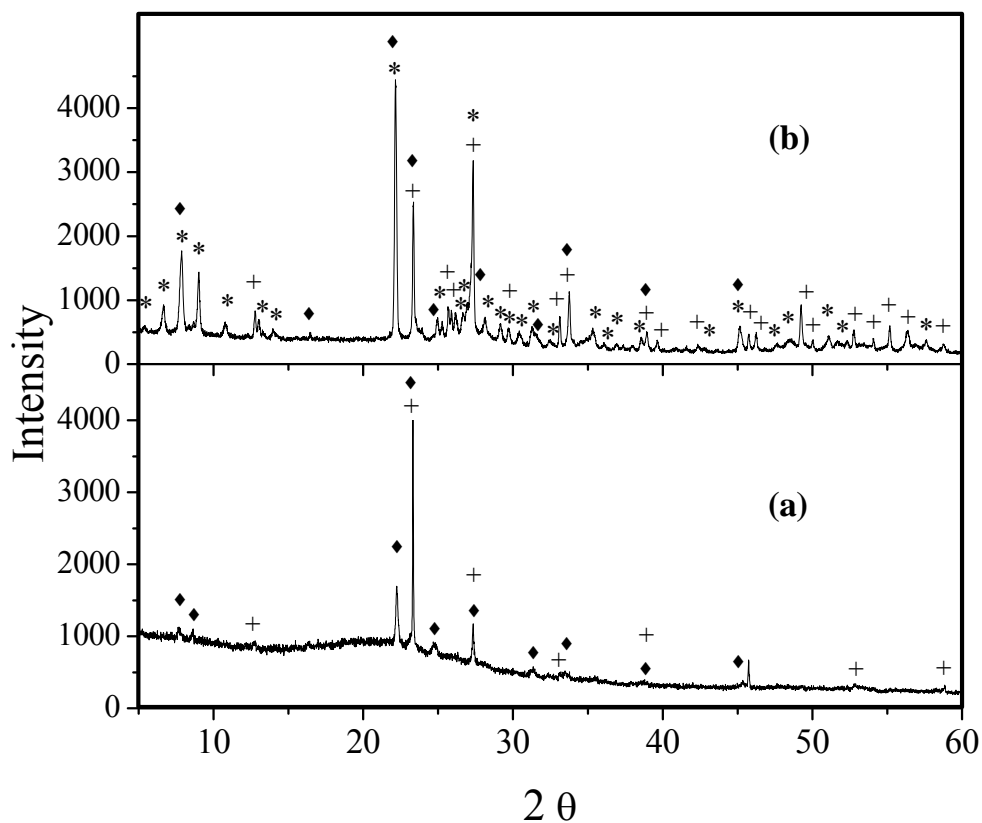


Figure 3. XRD patterns of activated MoVTenb oxide catalysts; (a) diluted with SiO_2 and (b) in absence of diluent. Diffraction peaks are marked as follows: MoO_3 (+), M1 (*), M_5O_{14} (M=Mo, V or/and Nb) (♦).

Table 2

XRD peaks due to the $\text{Mo}_{5-x}(\text{V},\text{Nb})_x\text{O}_{14}$ phase present in the activated TeA-24 catalyst

XRD peaks [2 θ]	Indexing
7.7°	200
8.6°	210
22.5°	530
23.2°	600
24.8°	540
27.3°	710, 550
31.3°	810, 740
33.8°	541
39.0°	811
45.0°	970, 1130

In summary, the presence of SiO_2 in the hydrothermal preparation of Mo-V-Te-Nb mixed oxide catalysts suppresses the formation of the M1-phase. By applying other preparation methods such as evaporation [16] or precipitation [17], the M1-phase was reported to be successfully obtained despite dilution with SiO_2 . It is thus rather the choice of synthesis parameters and not a property of the diluent that prevented successful preparation of diluted M1 in phase-pure quality.

b) Mo-V- Te- Nb oxide diluted with ZrO_2

By applying zirconia instead of Aerosil 300 as diluent, the XRD patterns of the Te-system precursors (**Figure 4**) show the characteristic reflection patterns of monoclinic zirconia (ICSD 89426), **Figure 1b**. In the XRD patterns of the precursors prepared using short hydrothermal synthesis times of 1/6 and 1/2 hours (**Figure 4a, 4b**), peaks belonging to non-converted MoO_3 and a few peaks belonging to V_2O_5 are observed. Moreover, both diffractograms show a preferred orientation of the α - MoO_3 crystals in [010] direction.

Traces MoO_3 are also detected in the precursor synthesized for 2 hours (**Figure 4c**). In this diffractogram, an additional weak peak emerges at 22° 2 θ . As mentioned above, this

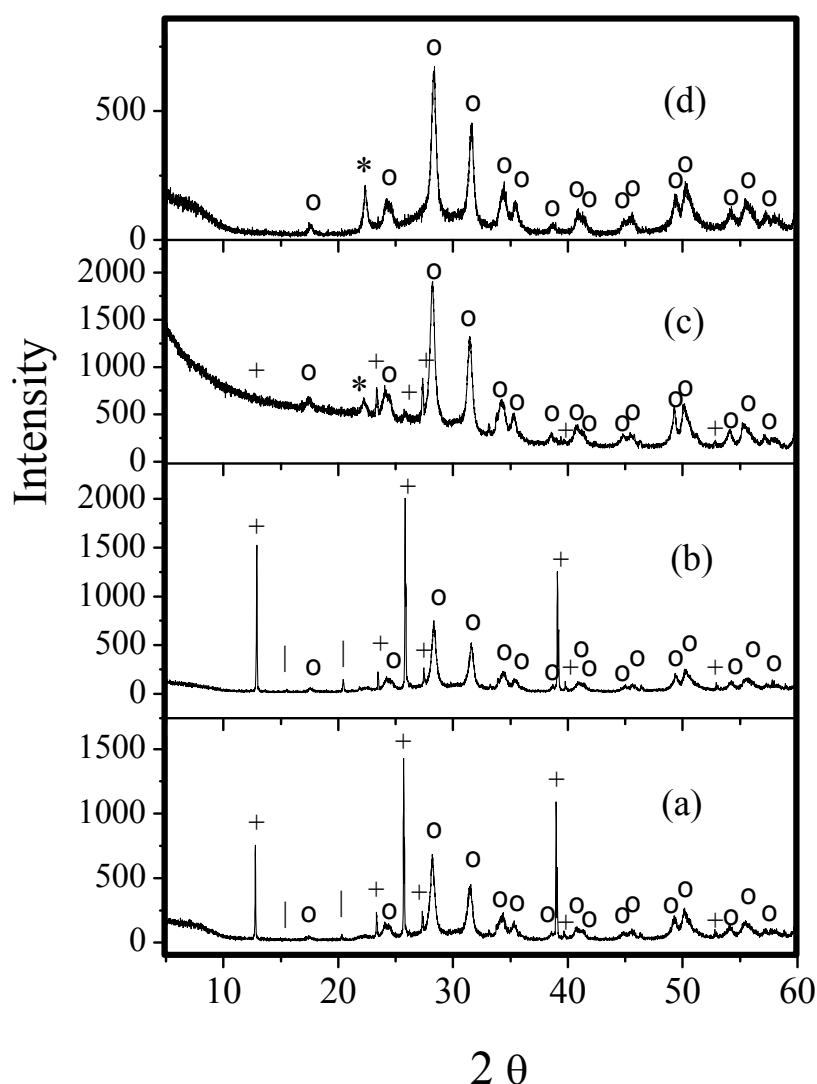


Figure 4. XRD patterns of MoVTenb/ZrO₂ precursor materials prepared with a synthesis time of (a) 1/6 h, (b) 1/2 h, (c) 2h and (d) 24h. Diffraction peaks are marked as follows: α -MoO₃ (+), peak 22° 2 θ \rightarrow d = 4 Å (*), *m*-ZrO₂ (o).

peak could be assigned to the (001) reflection of M1, M2 or Mo₅O₁₄-type phases or to a semi-crystalline oxidic bronze structure (structural analogue in the family of the shear structures). For the material, hydrothermally synthesized for 24 hours, similar XRD patterns were obtained. However, this pattern did no longer show any evidence of the α -MoO₃ phase (**Figure 4d**). Additionally, it is observed that the color of the as-synthesized

materials gets darker by increasing the synthesis time in the autoclave, which could be due to a decrease in either particle size or the band gap.

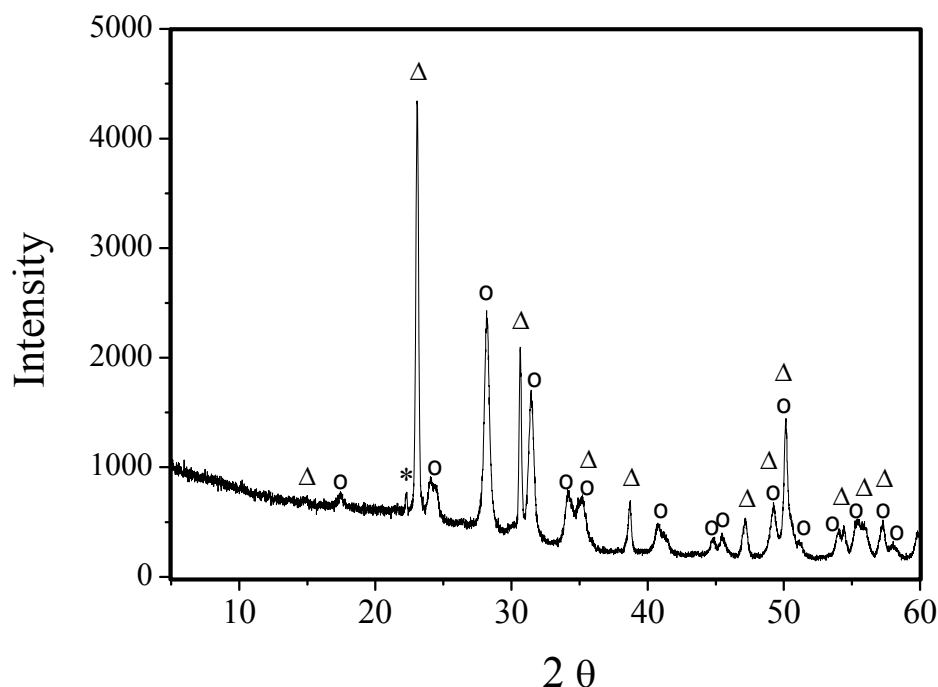


Figure 5. XRD patterns of activated MoVTenb oxide catalyst diluted with ZrO_2 . Diffraction peaks are marked as follows: $m\text{-ZrO}_2$ (o), $\alpha\text{-Zr}(\text{MoO}_4)_2$ (Δ), peak $22^\circ 2\theta \rightarrow d = 4 \text{ \AA}$ (*).

The TeZ-24 precursor was activated in Ar at 873 K generating the phase $\alpha\text{-Zr}(\text{MoO}_4)_2$ (ICSD 59144) (**Figure 5**). Evidently, zirconia does not represent an inert diluent under the present preparation conditions. It reacts with molybdenum at high temperature, in accordance with previously published results [26]. For zirconia supported MoO_3 , it has been reported that at a high surface density of molybdenum ($> 5 \text{ Mo/nm}^2$), $\alpha\text{-Zr}(\text{MoO}_4)_2$ is formed above 773 K in air [26]. The reflections of monoclinic zirconia and the additional peak at $22^\circ 2\theta$ remain in the diffractogram after the heat treatment step.

However, lower intensity of the peak at $22^\circ 2\theta$ is observed as compared with that of the corresponding precursor material (TeZ-24) (**Figure 4d**).

c) Mo-V- P- Nb oxide diluted with SiO_2

The precursors diluted with SiO_2 and synthesized for 1/6 and 1/2 hours (**Figure 6a and 6b**) are XRD amorphous displaying a broad halo between 15° and $30^\circ 2\theta$ and a weak

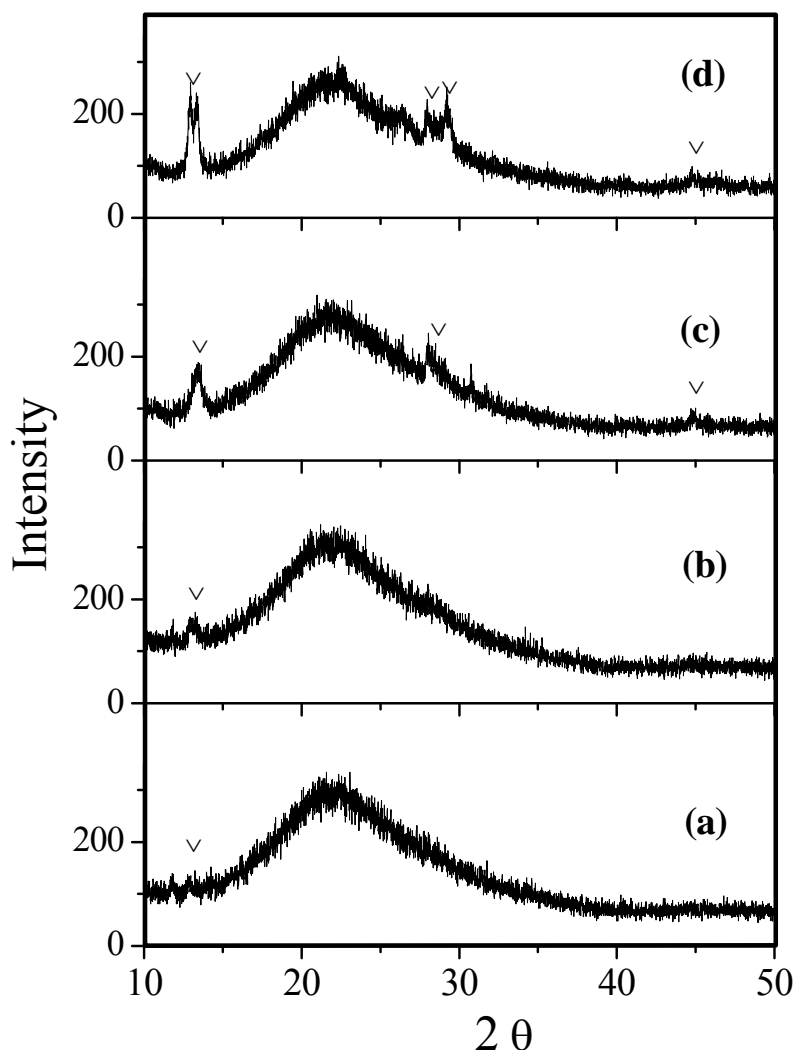


Figure 6. XRD patterns of MoVPNb/ SiO_2 precursor materials prepared with a synthesis time of (a) 1/6 h, (b) 1/2 h, (c) 2 h, and (d) 24 h. Diffraction peaks are marked as follows: unknown phase (v).

peak at about $13^\circ 2\theta$. After hydrothermal synthesis for 2 and 24 hours, the XRD patterns (**Figure 6c and 6d**) of the corresponding precursor show the peak at about 13° , whose intensity increases with increasing synthesis time, and two additional reflections around 28° and $45^\circ 2\theta$. None of these reflections could be assigned to a specific phase. After thermal treatment of the precursor PA-24 in Ar, no phase crystallization is achieved (**Figure 7a**). Only a few weak peaks at about 25.5° , 28.8° and $29.4^\circ 2\theta$, possibly belonging to the MoOPO_4 (ICSD 24894) structure, are observed. The bulk structure of the reference, P-24, prepared in absence of the diluent contains the crystalline MoOPO_4

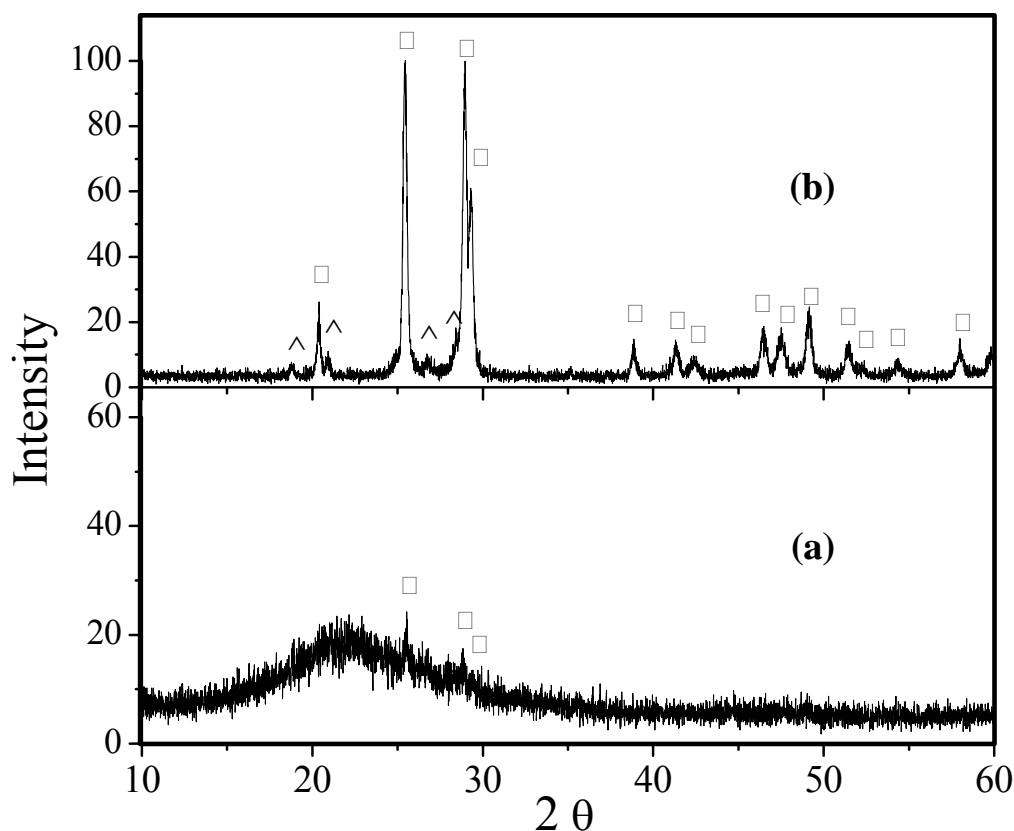


Figure 7. XRD patterns of activated MoVPNb oxide catalysts; (a) diluted with SiO_2 , and (b) in absence of diluent. Diffraction peaks are marked as follows: MoOPO_4 (\square) and VOMoO_4 (\wedge).

phase. Additional peaks at about 19° , 20.9° , 26.8° , 28.5° 2θ could be assigned to a phase related to VOMoO_4 (ICSD 27315), presenting a value of the lattice parameter a slightly different from that usually observed for this phase (**Figure 7b**). No M1-phase formation was obtained by replacement of Te by P.

Again, SiO_2 prevents crystallization of the phases present in the corresponding undiluted system (**Figure 7a**).

c) Mo-V-Bi-Nb oxides diluted with Cr_2O_3

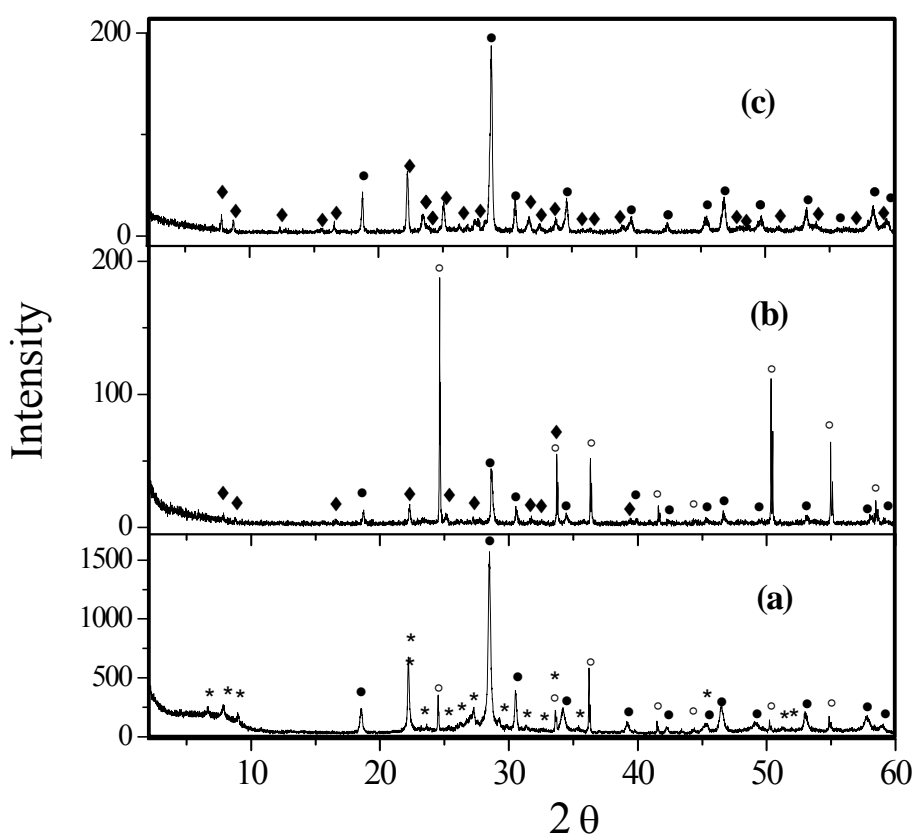


Figure 8. XRD patterns of MoVBiNb oxide catalysts synthesized for 24 h; (a) precursor BiCr-24, (b) activated BiCr-24 catalyst and (c) Bi-24 catalyst in absence of diluent. Diffraction peaks are marked as follows: M1 (*), Cr_2O_3 (°), $\text{Bi}_{0.82}(\text{V}_{0.45}\text{Mo}_{0.55})\text{O}_4$ (●), $\text{Mo}_{5-x}(\text{V},\text{Nb})_x\text{O}_{14}$ (◆).

For the Mo-V-Bi-Nb mixed oxide, the only synthesis time applied was 24 h. The XRD

patterns of the BiCr-24 precursor show the typical peaks of M1 in the lower 2θ interval (6.6° , 7.9° and 9.0° 2θ) and the peak at 22° and 45° 2θ , which are also typical for this phase (**Figure 8a**). Moreover, the crystalline phase, $\text{Bi}_{0.82}(\text{V}_{0.45}\text{Mo}_{0.55})\text{O}_4$ (ICSD 24939), is also present before the heat treatment. This phase is also observed in the bulk structure of the activated BiCr-24 material together with the $\text{Mo}_{5-x}(\text{V},\text{Nb})_x\text{O}_{14}$ structure (ICSD 27202). However, the M1 phase is no longer observed after activation. It seems that the M1 phase decomposes during the thermal treatment. Formation of unknown phases cannot be excluded since additional XRD reflections between 26° and 28° 2θ are observed (**Figure 8b**). As expected, the characteristic peaks belonging to the diluent, Cr_2O_3 (ICSD 250078), **Figure 1c**, are observed in the precursor as well as in the activated BiCr-24 catalyst (**Figure 8a and 8b**).

Table 3

Lattice parameters, cell volume, and crystallite size of the phases present in the undiluted Bi-24 and diluted BiCr-24 catalysts and of pure Cr_2O_3 . The standard deviations of the values are indicated in brackets.

	Bi-24			BiCr-24		
	Lattice Parameters [nm]	Cell Volume [nm ³]	Crystallite size LVol-IB* [nm]	Lattice Parameters [nm]	Cell Volume [nm ³]	Crystallite size [nm]
Bi _{0.82} (V _{0.45} Mo _{0.55})O ₄	a=5.19666(32)	316.24(5)	46.43(88)	a=5.22234(43)	320.03(7)	49.2(21)
	b=5.19666(32)			b=5.22234(43)		
	c=11.7104(10)			c=11.7344(18)		
Mo _{5-x} (V,Nb) _x O ₁₄	a=22.8131(22)	2085.6(5)	45.1(31)	a=22.8226(45)	2088.4(9)	44.2(97)
	b=22.8131(22)			b=22.8226(45)		
	c=4.00742(48)			c=4.00946(92)		
Cr ₂ O ₃	Cr ₂ O ₃ -diluent			BiCr-24		
	a=4.95651(17)	289.31(2)	-	a=4.95878(14)	289.485(19)	-
	b=4.95651(17)			b=4.95878(14)		
	c=13.59805(52)			c=13.59396(42)		

The reference Bi-24 catalyst shows a phase composition identical to that of the diluted activated catalyst BiCr-24, with peaks due to $\text{Bi}_{0.82}(\text{V}_{0.45}\text{Mo}_{0.55})\text{O}_4$ and $\text{Mo}_{5-x}(\text{V},\text{Nb})_x\text{O}_{14}$, the only difference being the peaks belonging to the diluent Cr_2O_3 (**Figure 8c**).

Additional peaks between 26° and 28° 2θ are also observed in the undiluted catalyst. Also in this case, no M1-phase was obtained by replacement of Te by Bi. Dilution with chromia results in a significant increase of the cell volume of the $\text{Bi}_{0.82}(\text{V}_{0.45}\text{Mo}_{0.55})\text{O}_4$ structure. The changes in the lattice parameters of the $\text{Mo}_{5-x}(\text{V},\text{Nb})_x\text{O}_{14}$ structure is within the error of the measurement. The crystallites size of the $\text{Bi}_{0.82}(\text{V}_{0.45}\text{Mo}_{0.55})\text{O}_4$ and $\text{Mo}_{5-x}(\text{V},\text{Nb})_x\text{O}_{14}$ is comparable before and after dilution (**Table 3**).

3.2 Catalytic performance

Table 4 and 5 show the catalytic behavior of selected catalysts: TeA-series, PA-series, TeZ-series, and BiCr-24 in selective oxidation of propane to acrylic acid at 673 K and a contact time (W/F) between 560 and 704 $\text{g}_{\text{cat}} \cdot \text{h} \cdot \text{mol}_{\text{C}_3\text{H}_8}^{-1}$. The undiluted reference materials oxides, Te-24, P-24 and Bi-24 have also been tested under comparable conditions (same catalyst mass).

The consumption rate of propane and the formation rate of acrylic acid were normalized either to the BET surface area, or to the mass of active metal oxide. These values represent a “formal” approach, since no dispersion measurements are available. The catalytic performance of the catalysts prepared by hydrothermal synthesis for 24 hours are compared in **Figure 9** (normalized to the BET surface area) and **Figure 10** (normalized to the mass of active metal oxide). Despite differences with respect to catalyst composition (active metal oxides and diluents), phase composition, and surface area, all tested catalysts showed catalytic activity for propane oxidation and formation of acrylic acid (**Table 4 and 5**). As it is shown in **Figure 9**, the activity normalized to the surface area of the catalysts decreases as follows: Te-24 > P-24 > Bi-24 > TeZ-24 > BiCr-24 > TeA-24 > PA-24. The undiluted Mo-V-Te-Nb oxide catalyst is the most active

Table 4

Conversion of propane and selectivity to acrylic acid in the oxidation of propane over diluted and non-diluted catalysts. The rates of propane consumption and acrylic acid formation are normalized to the mass of the active Mo-V-X-Nb (X=Te, Bi, P) oxide

Notation	W/F* [g _{cat} ·h·mol _{C₃H₈} ⁻¹]	X _{C₃H₈} [%]	S _{AA} [%]	Rate [10 ⁻³ mmol·g _{AM} ⁻¹ ·h ⁻¹]	
				C ₃ H ₈ consumption	Formation of AA
TeA-1/6	704	5	94	142	134
TeA-1/2	704	4	99	114	113
TeA-2	560	8	83	286	237
TeA-24	704	7	83	199	165
PA-1/6	560	5	85	179	152
PA-1/2	704	4	99	114	113
PA-2	704	9	57	256	146
PA-24	560	5	82	179	146
TeZ-1/6	666	12	22	360	79
TeZ-1/2	666	16	29	480	139
TeZ-2	666	21	33	631	208
TeZ-24	560	24	32	857	274
BiCr-24	666	5	86	150	129
Te-24	666	19	38	285	108
P-24	666	17	26	255	66
Bi-24	704	9	75	128	96

* contact time (g_{cat}·h·mol_{C₃H₈}⁻¹)

T = 673 K; GHSV = 1200 h⁻¹ (STP: T = 273 K, p = 1 atm)

AM: active metal oxide

material. Diluted catalysts are less active than their undiluted counterparts. The higher specific surface area of the diluted catalysts involves not only the specific surface area of the corresponding active mixed metal oxide but also that of the diluent, which might be not completely covered by the active phase. Therefore, and irrespective of the variations with respect to elemental and phase compositions between diluted and undiluted catalysts, a lower activity per unit of surface area is calculated for the diluted systems. Especially in the case of PA-24, showing the lowest activity per unit of surface area, the

increase in BET surface area is about seventy times compared to that of the undiluted P-24.

Table 5

Specific surface area, propane consumption rate, and rate of acrylic acid formation normalized to the specific surface area of catalysts prepared at 24 h hydrothermal synthesis time

Notation	S_{BET} [m ² ·g ⁻¹]	W/F* [g _{cat} ·h·mol _{C₃H₈} ⁻¹]	Rate [10 ⁻³ mmol·m ⁻² ·h ⁻¹]	
			C ₃ H ₈ consumption	Formation of AA
TeA-24	27	704	3.7	3.1
PA-24	185	560	0.5	0.4
TeZ-24	11	560	39.0	12.5
BiCr-24	2	666	37.6	32.3
Te-24	1.5	666	190.2	72.3
P-24	2.6	666	98.2	25.6
Bi-24	2.1	704	60.9	45.7

* contact time (g_{cat}·h·mol_{C₃H₈}⁻¹)
T = 673 K; GHSV = 1200 h⁻¹ (STP: T = 273 K, p = 1 atm)

This shows that the extent of “dispersion” of the active phase is quite different for the catalysts studied and no conclusion about a specific effect of dilution can be drawn from these data. The morphology seems to be not that of a homogeneously dispersed shell of active phase on a diluent particle.

In **Figure 10**, the rate of propane consumption and the formation rate of acrylic acid calculated per mass of active mixed metal oxide are compared. TeZ-24 is the most active catalyst. Specifically, TeZ-24 is more active than Te-24 per mass of active mixed metal oxide. A large fraction of the enhanced activity is due to combustion which may occur on the ZrO₂ support or which may be related to the presence of the zirconium molybdate phase. TeZ-24 operates at a similar selectivity to acrylic acid compared to that of Te-24 (32 % vs. 38 %) at comparable propane conversion of ~ 20 % (**Table 4**). Consequently,

the formation rate of acrylic acid normalized to the mass of active mixed metal oxide is significantly higher for TeZ-24 than for Te-24 (**Table 4** and **Figure 10**). Moreover, TeZ-24 also shows an enhanced formation rate normalized to the mass of the catalyst (**Table 6**) as compared with the corresponding undiluted catalyst. With all other examples a similar, albeit less drastic beneficial effect of dilution is demonstrated from the data.

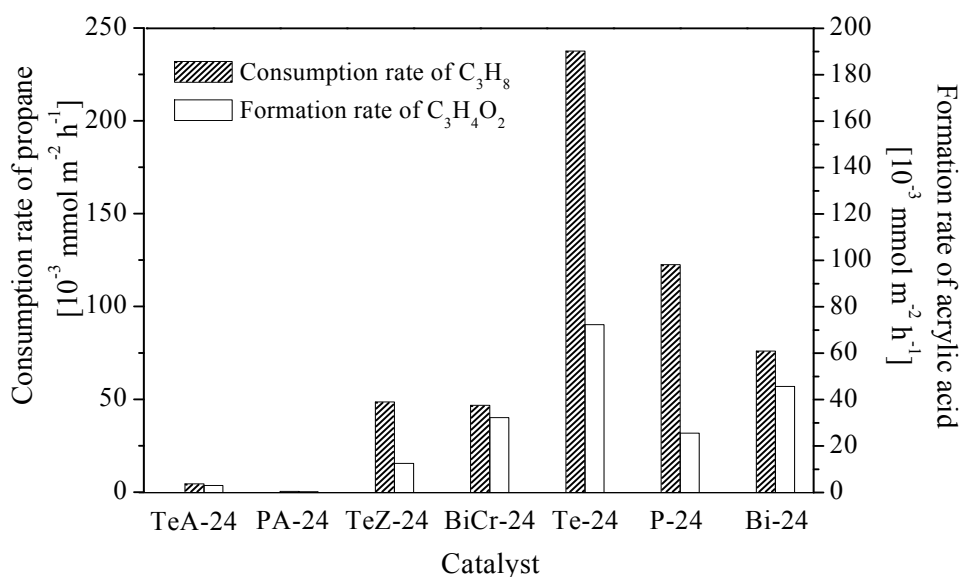


Figure 9. Rate of propane consumption, and rate of acrylic acid formation normalized to the specific surface area.

The influence of the hydrothermal synthesis time in preparation of the TeZ-catalysts on the catalytic performance is shown in **Figure 11**. Longer synthesis time in the autoclave leads to higher rates of propane consumption and acrylic acid formation calculated per mass of active metal oxides. However, the fraction of by-products is also much higher for the TeZ-24 catalyst than for the undiluted Te-system, which is not desirable. On the other hand, it should also be noted that the ratio $r_{AA}/r_{C_3H_8}$ increases with increasing hydrothermal synthesis time. Therefore, the application of longer synthesis times could lead to the formation of catalysts showing higher selectivities to acrylic acid.

In summary, the dilution of Mo-V-Bi-Nb mixed oxide with Cr_2O_3 slightly improves the activity and the acrylic acid formation rate per of active mixed metal oxide (**Figure 10**). Cr_2O_3 does not act as an oxidation catalyst by itself but, in fact, it seems to dilute the active component without much functional modification.

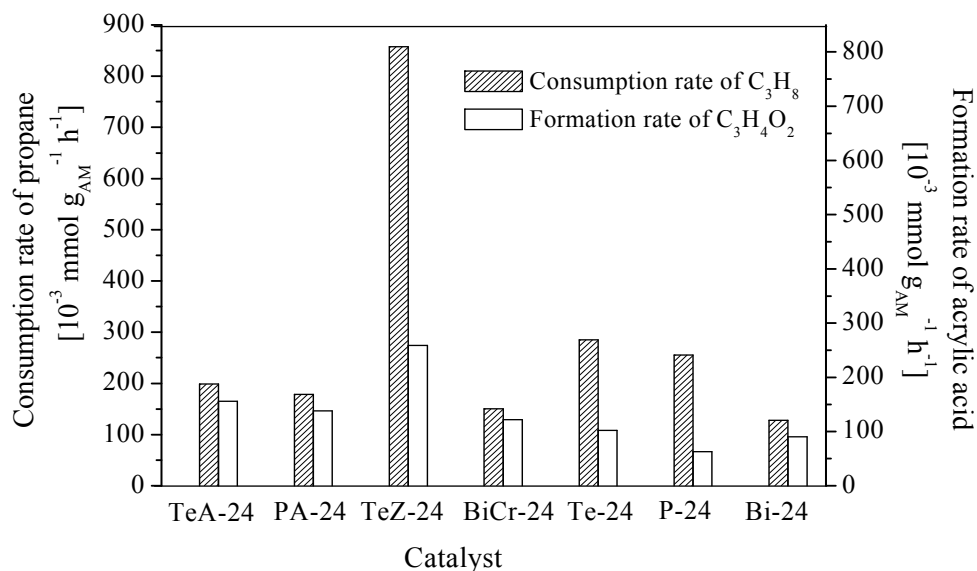


Figure 10. Rate of propane consumption, and rate of acrylic acid formation normalized to the mass of active mixed metal oxide.

The redox-inactive diluent SiO_2 is also beneficial for the acrylic acid productivity per mass of active mixed metal oxide. **Figure 10** reveals that in particular the selectivity to acrylic acid is improved for both, the Te and the P catalyst. Besides the dilution function, it is speculated that silica neutralizes some phase impurities such as molybdenum oxide that otherwise would catalyze total oxidation. From comparison of **Figure 9** and **Figure 10** it becomes apparent that the dispersion effect is small as compared to the “neutralization” effect, for which the high surface area may be instrumental.

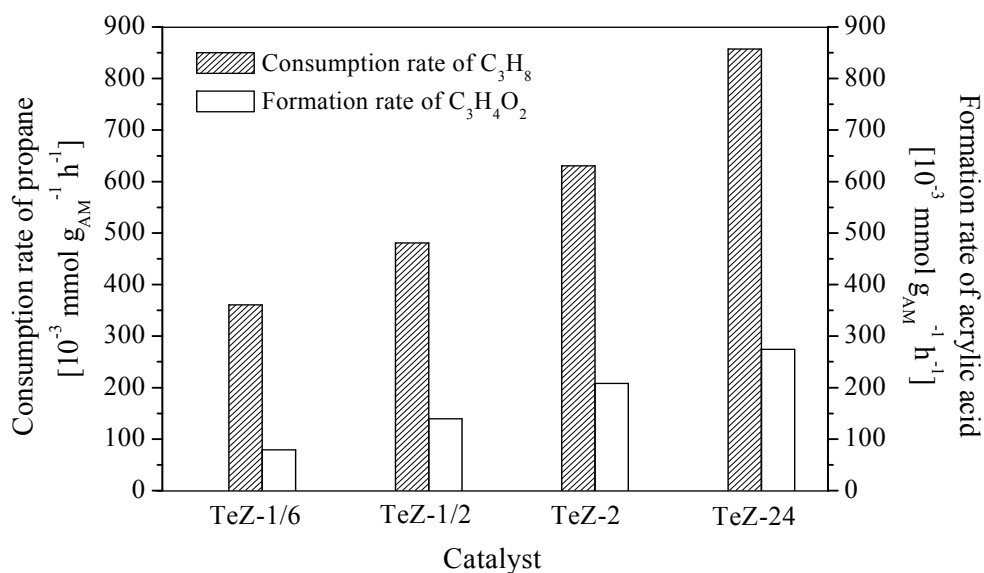


Figure 11. Rates of propane consumption, and rate of acrylic acid formation normalized to the mass of active metal oxide in the TeZ-series.

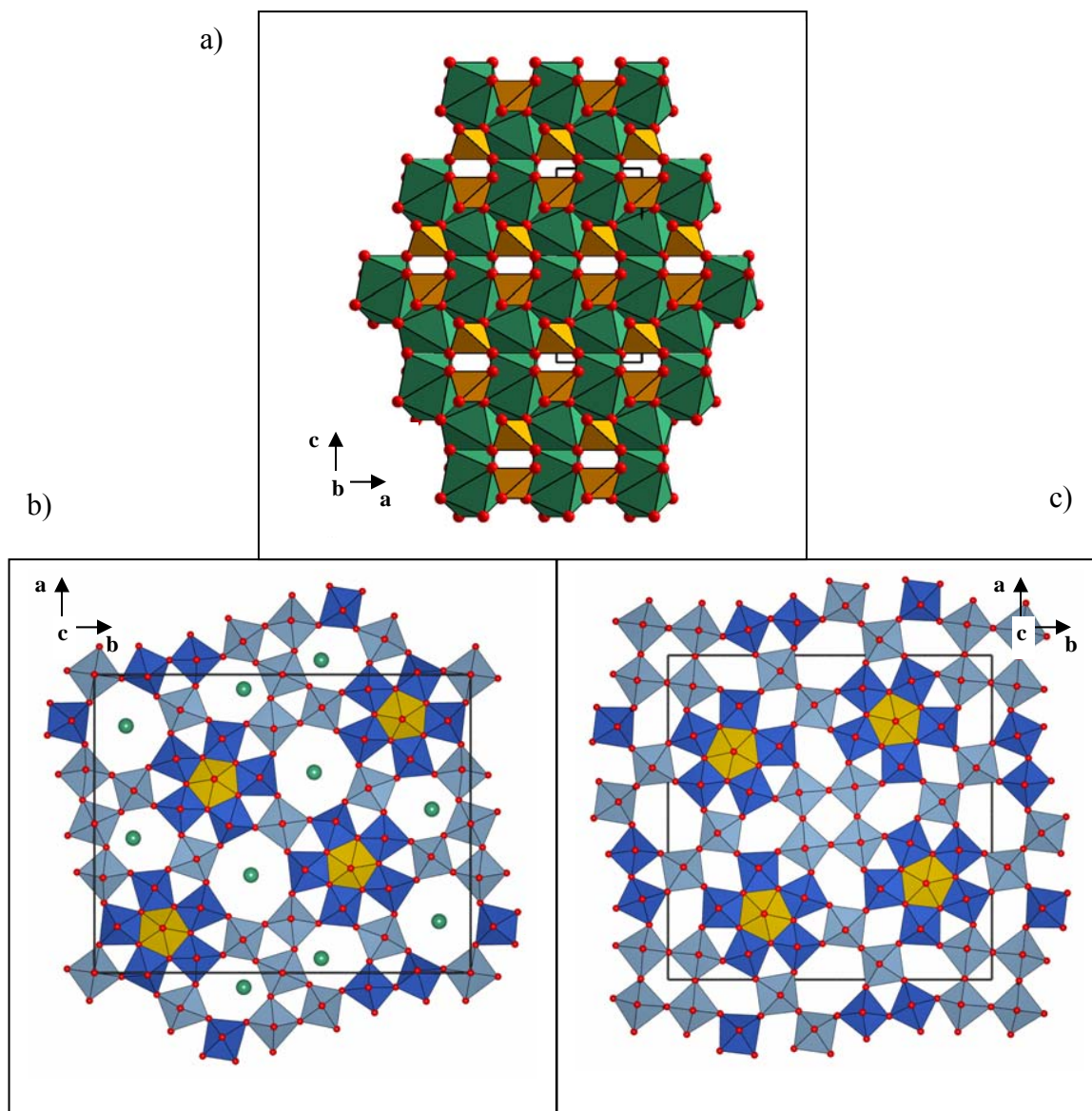
4 Discussion

In the present study, the effect of dilution of multi-metal oxides Mo-V-X-Nb (X=Te, P, Bi) with SiO₂ (Aerosil 300), ZrO₂ and Cr₂O₃ was studied with regards to phase compositions and the properties in selective oxidation of propane to acrylic acid.

The undiluted multi-metal oxide catalysts, Mo-V-X-Nb (X=Te, P, Bi), are composed of different crystalline phases. The classical Mo-V-Te-Nb oxide catalyst mainly consists of the M1 phase. Furthermore, α -MoO₃, and Mo_{5-x}(V,Nb)_xO₁₄ were identified as minority phases. On the other hand, no M1 was obtained in the activated catalyst, when Te was substituted by either P or Bi. A crystalline MoOPO₄ phase is identified as main component in the Mo-V-P-Nb oxide, whereas two crystalline phases, Bi_{0.82}(V_{0.45}Mo_{0.55})O₄ and Mo_{5-x}(V,Nb)_xO₁₄, constitute the bulk of the Mo-V-Bi-Nb oxide (**Scheme 1**). Despite of their different elemental and phase composition, comparable

formation rates of acrylic acid per mass of catalyst were found for these three structurally different undiluted catalysts in the screening experiments. This observation clearly indicates that the highly crystalline M1 phase is not necessarily required to convert propane into acrylic acid. Moreover, the Bi containing catalyst produces acrylic acid with similar rate compared to the Te containing catalyst (0.096 vs. 0.108 mmol·g⁻¹·h⁻¹) indicating that Te cannot be an essential ingredient for acrylic acid formation. These observations are not in contradiction to the extensive mechanistic considerations by Grasselli *et al.* [27], since all catalysts contain vanadium, which has been considered to be responsible for alkane activation. Furthermore, this is in line with the finding that also VPO catalysts [28, 29], comprising structural building blocks different from that of M1 or Mo₅O₁₄, effectively catalyze propane conversion. This implicates that the frequently used argument about the superior performance of M1 (see also below) is not a good support for the claimed chemical complexity of the active site as described on the (001) plane of M1, as no attempts were made to optimize the chemical potential of the reactants to the different material classes studied.

The Te containing catalyst, consisting mainly of the M1 phase, was diluted either with SiO₂ or with ZrO₂. Both additives cannot be considered as “inert” diluents, since different phase compositions of the diluted catalysts compared to the undiluted reference materials were obtained and the formation of the M1 phase was suppressed in both cases. Zirconia reacts with molybdenum by forming a Mo-Zr mixed oxide, which is more stable than M1. The phase α -Zr(MoO₄)₂ (ICSD 59144) was generated. The reaction between zirconia and molybdenum oxide may have occurred at the high activation temperature of 873 K that is necessary to crystallize the M1 phase from its nanostructured precursor. Increasing



Scheme 1. Schematic representation of the unit cells of (a) BiVO_4 (isostructural with $\text{Bi}_{0.82}(\text{V}_{0.45}\text{Mo}_{0.55})\text{O}_4$), (b) M1, and (c) Mo_5O_{14} .

fractions of such a nano-crystalline M1 precursor are probably formed with increasing hydrothermal synthesis time, as it becomes obvious from **Figure 4**. However, the data quality of the diffractograms that have been measured for the purpose of screening the phase composition does not allow to draw any conclusions on the impact of the hydrothermal synthesis on the microstructure of the diluent ZrO_2 .

Among all diluted catalysts, the dilution of the Te-system with ZrO_2 yielded a strong improvement in the propane consumption rate calculated per mass of active component as well as calculated per mass of the catalyst (**Table 4**). A discussion about dispersion of the active material is not appropriate, since the phases of the diluted and undiluted Mo-V-Te-Nb oxide catalysts differ and no reliable dispersion measurements were available. The enhanced propane consumption rate per mass catalyst of TeZ-24 might be due to the presence of the $\alpha\text{-Zr}(\text{MoO}_4)_2$ phase. This phase has been reported to be active in propane oxidative dehydrogenation (ODH) at 703 K [26]. Although the reaction conditions of the present study ($T = 673$ K and presence of 40 % steam in the feed) differ drastically from the ODH conditions, Zr-O-Mo sites may contribute to propane consumption. It is noted that the diluent $m\text{-ZrO}_2$ is inert under the reaction conditions applied. The formation rate of acrylic acid normalized to the mass of active metal oxide as well as normalized to the mass of the catalyst is higher for TeZ-24 compared to that of Te-24. This points to an additional function of the diluent that may be related to the weak peak at $22^\circ 2\theta$ observed in the XRD patterns of this catalyst. In the orthorhombic M1 structure, this peak indicates the presence of regular stacking of metal-oxygen polyhedra in [001] direction. The formation of M1 crystallites with a flat, disk-like morphology instead of the usual needle-like morphology may explain the very weak XRD signal of the M1 phase.

Zirconia was the most reactive diluent used here in the sense that a competitive formation of a stable compound (zirconium molybdate) with the essential constituent Mo prevented to a large extent the formation of the precursor to the desired M1 phase that may be present as minority phase in a distorted form in the active catalyst.

Silica as diluent exerts a different influence on the phase formation. With its large surface area and the supposed defect structure of the Aerosil material this diluent seems to bind Te such that it is not available for M1 formation leading to the “parent” structure Mo_5O_{14} and some MoO_3 (**Figure 3**). On the P-system that did not form the M1 phase in the undiluted state, an unknown effect on the phase formation was found for the silica diluent that did work as an agent preventing or retarding crystallization.

Chromia seems to be the most inert diluent in the series used here, as it did not notably interfere with the phase inventory. The comparison of the lattice parameters of the crystalline phases in the pure and in the diluted form gives, however, clear evidence for a modification of the defect state of one of these phases, namely $\text{Bi}_{0.82}(\text{V}_{0.45}\text{Mo}_{0.55})\text{O}_4$ (**Table 3**). It is assumed that chromium oxide did not interfere with the precursor formation in the autoclave but modified the defect state of the oxygen sub-lattice in the activated $\text{Bi}_{0.82}(\text{V}_{0.45}\text{Mo}_{0.55})\text{O}_4$ phase.

In summary, it became clear that the concept of diluting crystalline, phase-pure M1 by an “inert” oxide is not realizable. However, in all cases, some indication of dispersion was found. This effect is strongly superimposed by structural modifications of the active phase due to the presence of the diluent. Either capturing of a structural ingredient, or spriting of the intended guest species for the M1 channel structure, or modification of the defect disposition of a non-M1 active phase were effective means of catalyst modification.

The diversity of modifications hampers a meaningful comparative discussion of the results. It is obvious, however, that the M1 phase is not the only carrier of the active sites.

The results of this study are considered as path-finding experiments and suggest directions of further improvement of the systems.

As it is facile to improve a poor performance and very difficult to further optimize a highly advanced system, it is useful to validate the state of the art in propane oxidation to acrylic acid before investing into the necessary substantial optimisation of the systems presented here. To this end a survey of literature data presented in **Table 6** was collected from those sources allowing a comparison of rates. Regarding the yield of acrylic acid, it appears that the classical Mo-V-Te system is by far the best choice reaching up to 50 % yield. This compares reasonably to the patent literature where maximum yields slightly above 50 % yield [44] were claimed. It further occurs that no other catalyst system comes close to that performance. The comparison is only semi-quantitative as the experimental conditions and hence the reactant chemical potentials were significantly different in the studies and no attempts are documented that for any of the systems an optimization of the process conditions was carried out.

In this situation it seems appropriate to relate the discussion to the rates of acrylic acid formation spreading for the catalysts described in **Table 6** over about two orders of magnitude with an average of about $0.5 \text{ mmol}_{\text{AA}}/\text{g}_{\text{cat}}\cdot\text{h}$. This value indicates a still low productivity of all the complex MMO systems. The large spread in rates for nominally iso-structural M1 systems claimed as active materials in the studies indicates that either activity is not an intrinsic property of M1 but of its defect disposition. Alternatively, the presence of known or undetected additional phases affects the performance, a conjecture being likely in view of the many reaction steps and consecutive processes possibly involved in the target transformation of propane to acrylic acid.

It is informative to compare the rates found in **Table 6** to values quoted for another complex alkane transformation, namely the formation of maleic anhydride from butane over VPP systems also active in propane oxidation. Under comparable process conditions (GHSV = 1500 h⁻¹, feed: n-C₄H₁₀/O₂/He = 1.6/18/80.4, T = 673 K) a performance of 65 % conversion at a selectivity of 69 % maleic anhydride was reported [45] relating to a rate of maleic anhydride formation of 0.97 mmol_{MA}/g_{cat}·h. This comparison reveals that purely from the rates achieved, the very best MMO systems for propane oxidation are just as good as the highly optimized VPP system.

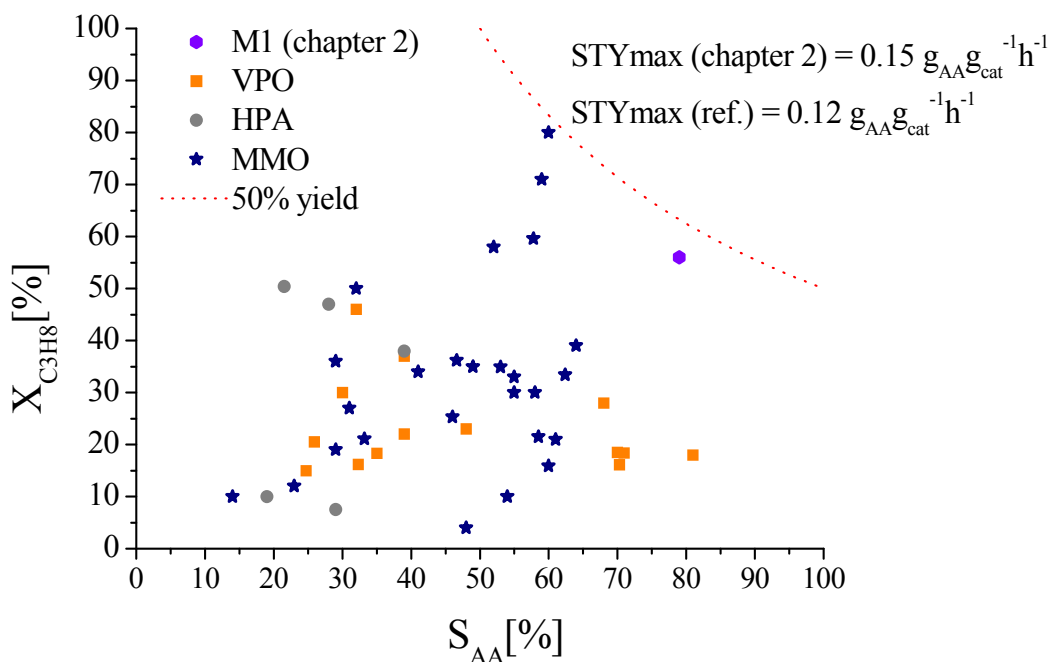


Figure 12. Conversion of propane versus selectivity of acrylic acid of the catalysts prepared in this work and the catalysts reported in the literature.

In **Figure 12** the reference data and the present results are compared in a conversion-selectivity diagram showing for reference the 50 % yield trajectory. The situation for propane activation looks less promising from this diagram. It occurs that almost all

systems reported have a serious selectivity problem if we consider the selectivity for maleic anhydride of about 70 % as reference. It becomes clear that the high-rate systems from **Table 6** are all unacceptable from their selectivity. VPP systems and the catalysts from the present study form a family of highly selective albeit poorly active catalysts. It is remarkable that they all are not of the M1 structure. Few data points near the 50 % yield trajectory relate all to phase-pure M1 catalysts. It may be concluded that phase-pure M1 is indeed the best existing catalyst system. Its performance is, however, very severely affected by phase impurities being they X-ray crystalline or not. Also the two nominal Mo-V-Te systems of the present study follow this observation. The argument that the highly selective systems are just good as their conversion is so low is not the only answer, as there are many Mo-V-Te systems in **Figure 12** with comparable low conversion but much worse selectivity. We conclude that it may be worthwhile to start an optimisation of non-M1 systems as they offer the prospect to highly selective propane oxidation systems.

The rate data for acrylic acid formation collected in this work and from reference data of the literature are graphically displayed in **Figure 13**. The lines labelled a-d are guides to the eye and may not be misunderstood as fits. Here a correlation of the rate per unit mass versus the rate per unit surface area is chosen. Would the catalysts all contain the same active sites in differing dispersions then we would expect a linear correlation. The spread of data as well as the poor statistics do not allow a conclusive interpretation of the data in **Figure 13** but some trends may be deduced. First we state that Te-free systems are not very productive. Second it becomes clear that the systems from the present study are reasonably active per unit surface area but inefficient per unit mass as expected from the

principle of dilution of active mass by inert materials. Line (c) may serve as extrapolation of the potential of this development. The reference systems with a comparable rate per unit surface area but with substantial better productivity per mass fall into an opening data field limited by the lines (a) and (b). The data statistics is not yet good enough to distinguish between families of correlations and an area of correlation maybe broadened by the spread in reaction conditions.

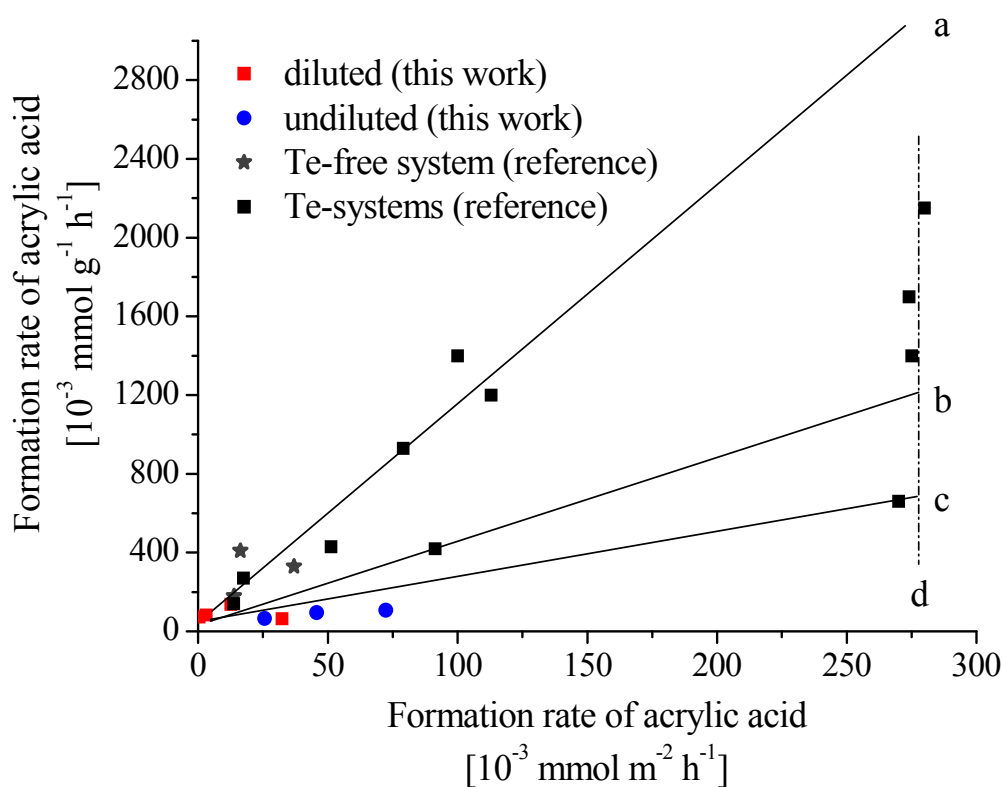


Figure 13. Formation rate of acrylic acid normalized to the catalyst mass versus formation rate of acrylic acid normalized to the surface area of the catalysts prepared in this work, and of catalysts reported in the literature.

Very markedly different is the family of data for highly pure M1 systems grouping around line (d). The fact that this line shows no variation of the area-specific activity suggests that this rate is an intrinsic property of the pure M1 system. The active sites

should thus be an integral component of the M1 phase. Their high-performance operation can only be realized if no interference is allowed of the initial synthesis of acrylic acid with consecutive oxidation processes. The formation rate for acrylic acid is the highest for all systems studied. The only variable in this family is the surface area of the bulk catalysts that exhibit no dispersion effect. It is conceivable that the intersection between lines (a) and (d) marks the maximum evolution of activity of the M1 system that can be obtained within the crystal chemistry of the Mo-V-Te system.

From this plot it seems less desirable to optimize the systems described in the results section of this paper but rather to concentrate on the optimisation of the clean and phase-pure M1 system. It is reassuring that the data points along line (d) designate systems from two different groups namely that of Ueda and of the authors of this study giving confidence that the performance level is an intrinsic property of the M1 phase without strong interferences of details of the preparation scheme of an individual research team.

5 Conclusion

Such a consequence of the analysis of the data from **Figure 13** needs to be contrasted with the shortcoming of the M1 system concerning its stability and lifetime as catalyst. This critical parameter for application is not reflected in **Figure 12** and **Figure 13**. It is known, however, that Te tends to volatilize setting free Mo-species and so degrading the catalyst under operation conditions. If this detrimental property of the M1 system cannot be removed then it may be a promising fallback strategy to develop the systems of the present study. Both the synthesis parameters (hydrothermal synthesis and activation) and the process conditions need to be optimized before a discussion on the potential of the highly selective non-M1 systems can be started.

The present work has shown again that the M1 phase in pure form is an excellent catalyst for the target reaction that cannot be rivalled by other systems. The work further showed the critical role of crystalline phases in the hydrothermal precursor that tend to strongly interfere with the formation of the target phase. This observations may form the basis of another explanation for the “synergy effect” [46] claimed for M1/M2 phase mixtures obtained from high throughput synthesis. Here, M2 may acts as “weak” diluent, such as Cr_2O_3 in the present study, dispersing the active M1 without interfering with the precursor chemistry of the M1 contribution due to its compositional and structural similarity with the M1 phase. The present study has opened up some alternative synthesis pathways to possibly more stable albeit still worse performing catalyst systems. A critical analysis of the publicly reported performance data of the target reaction reveals that it may be useful both from selectivity arguments and from challenge of a stable catalyst system to invest in optimization of the present alternative catalyst formulations rather than to only further improve the performance of phase-pure M1. M1, however, seems to be intrinsically active for the reaction rendering it the preferred target for fundamental studies on the mode of operation of propane oxidation over MMO catalysts.

Table 6 Catalytic performance of catalysts for the selective oxidation of propane to acrylic acid

Catalyst	Feed	Flow rate	Cat[g]/ V _{cat} [ml]	T [°C]	X _{C3} [%]	S _{AA} [%]	Y _{AA} [%]	Formation rate [mmol _{AA} /g _{cat} h]	Reference
V ₁ P _{1.15} Te _{0.1-0.15} O	C3/O ₂ /H ₂ O=1.86/76/22.15	C3+O ₂ =274ml/min H ₂ O=0.195 mol/h	40/-	390	30	30	10.5	0.0418	28
V ₁ P _{1.1} O	C3/O ₂ /H ₂ O=1.08/35.18/63.73	6.9 s	10/10	420	46.8	32	14.54	0.036	29
(PyH) ₃ PMo ₁₂ O ₄₀	C3/O ₂ /H ₂ O/N ₂ =20/10/20/50	50ml/min	3/-	340	7.5	29	2	0.178	30, 31
H _{1.26} CS _{2.5} Fe _{0.08} PVMo ₁₁ O ₄₀	C3/O ₂ /N ₂ =30/40/30 (vol%)	15cm ³ /min	1/-	380	47	28	13	1.5	32
MoV _{0.3} Te _{0.23} Nb _{0.12} O _n	C3/O ₂ /inert/H ₂ O(ml/min)=0.6/2/7.4/8.8	1.9s	0.61/-	380	80	61	49	1.08	3
MoV _{0.44} Te _{0.10} O _n	C3/O ₂ /H ₂ O/N ₂ = 8/10/45/37	20 ml/min	0.5/-	380	36.2	46.6	17	1.4	33
MoV _{0.25} Te _{0.11} Nb _{0.12} O _n	C3/O ₂ /H ₂ O/N ₂ = 8/10/45/37	20 ml/min	0.5/-	380	33.4	62.4	21	1.7	33
Te-Ni-Mo-O	C3/O ₂ /H ₂ O/N ₂ = 12/8/40/40	1500 ml (g _{cat} h) ⁻¹	1/-	420	30	55	17	1.4	34
MoV _{0.45} Te _{0.17} Nb _{0.12} O _n	C3/O ₂ /H ₂ O/He=4/8/30/58	205 g _{cat} h(mol _{C3}) ⁻¹	0.3-3/-	380	35.2	54.3	19.1	0.93	35
MoV _{0.26} Te _{0.11} Nb _{0.12} O _n	C3/O ₂ /H ₂ O/N ₂ /Ne=5/10/45/35/5	30ml/min	0.5/-	380	33	55	18.15	0.43	36
MoV _{0.28} Sb _{0.13} Nb _{0.15} O _n	C3/O ₂ /H ₂ O/N ₂ /Ne=5/10/45/35/5	30ml/min	0.5/-	380	35	49	17.15	0.41	36
MoV _{0.30} Te _{0.23} Nb _{0.11} O _n	C3/O ₂ /H ₂ O/N ₂ /Ne=5/10/45/35/5	30ml/min	0.5/-	380	30	58	17.4	0.42	36
MoV _{0.30} Sb _{0.15} Nb _{0.10} O _n	C3/O ₂ /H ₂ O/N ₂ /Ne=5/10/45/35/5	30ml/min	0.5/-	380	34	41	14	0.33	36
MoV _{0.36} Te _{0.17} Nb _{0.12} O _n	C3/O ₂ /H ₂ O/He=4/8/30/58	100g _{cat} h(mol _{C3}) ⁻¹	-/-	400	21.5	58.5	12.6	1.2	37
MoV _{0.3} Te _{0.23} Nb _{0.12} O _n	C3/O ₂ /H ₂ O/N ₂ =2/6/50/42	20-80 Ncm ³ /s	215-340/-	360	38	65	24.7	0.908	38
MoV _{0.17} Te _{0.22} Nb _{0.15} O _n	C3/O ₂ /H ₂ O/He=4/8/30/58	50cm ³ min ⁻¹	0.5-2.5/-	380	21.1	33.2	7	0.14	39
MoV _{0.25} Te _{0.23} Nb _{0.10} O _n	C3/O ₂ /H ₂ O/N ₂ /He=6/10/43/36/5	50cm ³ min ⁻¹	0.5-2.5/-	380	58	52	30	0.27	39
Mo ₁₂ W ₂ Bi ₁ Co _{5.5} Fe ₃ Si _{1.6} K _{0.08} O _n	C3/O ₂ =80/20	56 l/h	200/-	430	10	14	1.4	0.035	40
MoV _{0.3} Sb _{0.25} Nb _{1.12} O _n	C3/air/H ₂ O=3.3/50/46.7	2.4 s	35/30	390	36	29	10.44	0.20	41
MoV _{0.25} Te _{0.23} Nb _{0.124} O _n	C3/O ₂ /N ₂ /H ₂ O=2.8/6.4/50.8/40	1200 h ⁻¹	0.5/0.5	400	56	79	44.0	0.66	42
MoV _{0.25} Te _{0.23} Nb _{0.124} O _n (P-123)	C3/O ₂ /N ₂ /H ₂ O=2.8/6.4/50.8/40	1200 h ⁻¹	0.5/0.5	400	24	24	5.6	0.0864	43
MoV _{0.25} Te _{0.23} Nb _{0.124} O _n (P-123)	C3/O ₂ /N ₂ /H ₂ O=2.8/6.4/50.8/40	4800h ⁻¹	0.5/0.5	400	4	100	4	0.24	43
MoV _{0.25} Te _{0.23} Nb _{0.124} O _n (S ₀)	C3/O ₂ /N ₂ /H ₂ O=2.8/6.4/50.8/40	4800h ⁻¹	0.5/0.5	400	18	27	4.8	0.288	43
Mo ₁ V _{0.3} Te _{0.23} Nb _{0.125} /SiO ₂	C3/O ₂ /N ₂ /H ₂ O=2.65/19.76/47.78/29.81	1200 h ⁻¹	0.5/0.5	400	7	83	5.81	0.083	this work
Mo ₁ V _{0.3} Te _{0.23} Nb _{0.125} /ZrO ₂	C3/O ₂ /N ₂ /H ₂ O= 3.33/6.66/60/30	1200 h ⁻¹	0.5/0.5	400	24	32	7.68	0.137	this work
Mo ₁ V _{0.3} Bi _{0.23} Nb _{0.125} /Cr ₂ O ₃	C3/O ₂ /N ₂ /H ₂ O= 2.8/6.4/50.8/40	1200 h ⁻¹	0.5/0.5	400	5	86	4.3	0.065	this work
Mo ₁ V _{0.3} P _{0.27} Nb _{0.125} /SiO ₂	C3/O ₂ /N ₂ /H ₂ O= 3.33/6.66/60/30	1200 h ⁻¹	0.5/0.5	400	5	82	4.1	0.073	this work
Mo ₁ V _{0.3} Te _{0.23} Nb _{0.125}	C3/O ₂ /N ₂ /H ₂ O= 2.8/6.4/50.8/40	1200 h ⁻¹	0.5/0.5	400	19	38	7.22	0.108	this work
Mo ₁ V _{0.3} Bi _{0.23} Nb _{0.125}	C3/O ₂ /N ₂ /H ₂ O= 2.65/19.76/47.78/29.81	1200 h ⁻¹	0.5/0.5	400	9	75	6.75	0.096	this work
Mo ₁ V _{0.3} P _{0.27} Nb _{0.125}	C3/O ₂ /N ₂ /H ₂ O= 2.8/6.4/50.8/40	1200 h ⁻¹	0.5/0.5	400	17	26	4.42	0.066	this work

6 Acknowledgments

The authors thank Mrs. Gisela Lorenz, and Mrs. Edith Kitzelmann for technical assistance and Dr. Olaf Timpe for helpful discussions.

7 References

- [1] M. M. Lin, *Applied Catalysis A: General* 207 (2001), 1-2, 1.
- [2] F. Borgmeier, A. Tenten, H. Hibst, E. K. J. Mueller, S. Unverricht, G. Cox, WO0206199 (2002); BASF.
- [3] T. Ushikubo, H. Nakamura, Y. Koyasu, S. Wajiki, US Patent 5 380 933 (1995); Mitsubishi Kasei Corporation.
- [4] M. Tanimoto, H. Yunoki, H. Hironaka, N. Kimura, US 6 632 965 B1 (2003); Nippon Shokubai.
- [5] F. Borgmeier, J. Petzoldt, H. Hibst, A. Tenten, WO 2002083615 A1 (2002); BASF.
- [6] T. Ushikubo, K. Oshima, A. Kayou, M. Hatano, *Studies in Surface Science and Catalysis* 112 (1997), 473.
- [7] M. Baca, A. Pigamo, J. L. Dubois, J. M. M. Millet, *Topics in Catalysis* 23 (2003), 39.
- [8] W. Ueda, D. Vitry, T. Katou, *Catalysis Today* 96 (2004), 235.
- [9] J. Holmberg, S. Hansen, R. K. Grasselli, A. Andersson, *Topics in Catalysis* 38 (2006), 1-3, 17.
- [10] T. Katou, D. Vitry, W. Ueda, *Chemical Letters* 32 (2003), 1028.
- [11] W. Ueda, D. Vitry, T. Kato, N. Watanabe, Y. Endo, *Research on Chemical Intermediates* 32 (2006), 3-4, 217.
- [12] W. Ueda, D. Vitry, T. Katou, *Catalysis Today* 99 (2005), 43.
- [13] W. Ueda, N. F. Chen, K. Oshihara, *Chemical Communications* (1999), 517.
- [14] W. Ueda, K. Oshihara, *Applied Catalysis A: General* 200 (2000), 135.
- [15] N. Watanabe, W. Ueda, *Industrial & Engineering Chemistry Research* 45 (2006), 607.

- [16] J. Holmberg, R. Häggblad, A. Andersson, *Journal of Catalysis* 243 (2006), 2, 350.
- [17] J. B. Wagner, O. Timpe, F. A. Hamid, A. Trunschke, U. Wild, D. S. Su, R. K. Widi, S. B. A. Hamid, R. Schlögl, *Topics in Catalysis* 38 (2006), 51.
- [18] B. Solsona, M. I. Vázquez, F. Ivars, A. Dejoz, P. Concepción, J. M. López-Nieto, *Journal of Catalysis* 252 (2007), 2, 271.
- [19] L. Chen, J. Liang, H. Lin, W. Weng, H. Wang, J. C. Védrine, *Applied Catalysis A: General* 293 (2005), 49.
- [20] P. DeSanto Jr., D. J. Buttrey, R. K. Grasselli, C. G. Lugmair, A. F. Volpe Jr., B. H. Toby, T. Vogt, *Zeitschrift für Kristallographie* 219 (2004), 152.
- [21] H. Hibst, F. Rosowski, G. Cox, *Catalysis Today* 117 (2006), 234.
- [22] G. A. Zenkovets, G. N. Kryukova, V. Yu. Gavrilov, S. V. Tsybulya, V. A. Anufrienko, T. A. Larina, D. F. Khabibulin, O. B. Lapina, E. Rödel, A. Trunschke, T. Ressler, R. Schlögl, *Materials Chemistry and Physics* 103 (2007), 2-3, 295.
- [23] E. Roedel, PhD Thesis, TU Berlin, 2006.
- [24] L. Kihlberg, *Ark. Kem.* 21 (1963), 40427.
- [25] *Preparation of phase-pure M1 MoVTenb oxide catalysts by hydrothermal synthesis – Influence of reaction parameters on structure and morphology.*
A. Celaya Sanfiz, T. W. Hansen, E. Rödel, O. Timpe, A. Trunschke, R. Schlögl, (accepted for publication in *Topics in Catalysis*)
- [26] K. Chen, S. Xie, E. Iglesia, A. T. Bell, *Journal of Catalysis* 189 (2000), 421.
- [27] R. K. Grasselli, *Catalysis Today* 99 (2005), 23.
- [28] M. Ai, *Journal of Catalysis* 101 (1986), 389.
- [29] Z. Wang, W. Wei, G. Liu, G. Mao, D. Kuang, *Acta Petroleum Sinica* 14 (1998), 21.
- [30] W. Ueda, Y. Suzuki, *Chemical Letters* (1995), 7, 541.
- [31] W. Li, K. Oshihara, W. Ueda, *Applied Catalysis A: General* 182 (1999), 357.
- [32] N. Mizuno, M. Tateishi, M. Iwamoto, *Applied Catalysis A: General* 128 (1995), L165.
- [33] D. Vitry, Y. Moriwaka, J. L. Dubois, W. Ueda, *Applied Catalysis A: General* 251 (2003), 411.

- [34] N. Fujikawa, K. Wakui, K. Tomita, N. Ooue. *Catalysis Today* 71 (2001), 83.
- [35] P. Botella, J. M. López-Nieto, B. Solsona, A. Mifsud, F. Márquez, *Journal of Catalysis* 209 (2002), 445.
- [36] M. Baca, M. Aouine, J. L. Dubois, J. M. M. Millet, *Journal of Catalysis* 233 (2005), 234.
- [37] J. M. Oliver, J. M. López-Nieto, P. Botella, *Catalysis Today* 96 (2004), 241.
- [38] E. Balcells, F. Borgmeier, I. Grisstede, H.-G. Lintz, F. Rosowski, *Applied Catalysis A: General* 266 (2004), 211.
- [39] P. Botella, P. Concepción, J. M. López-Nieto, Y. Moreno, *Catalysis Today* 99 (2005), 51.
- [40] H. Jachow, A. Tenten, S. Unverricht, H. Arnold, US 6 541 664 (2003); BASF.
- [41] H. Hibst, F. Borgmeier, F. Rosowski, K. J. Müller-Engel, DE 10 2004 027 999 A1 (2005); BASF.
- [42] *Investigation of catalytic behavior of M1-phase catalyst in the selective oxidation of propane to acrylic acid. Correlation approach between catalytic performance and surface/bulk properties.*
A. Celaya Sanfiz, T. W. Hansen, P. Schnörch, D. Teschner, A. Trunschke, R. Schlögl, M. H. Looi, S. B. A. Hamid, (in preparation).
- [43] *A novel synthetic route to mesostructured MoVTeNb mixed oxide.*
A. Sakthivel, A. Trunschke, T. Hansen, A. Celaya Sanfiz, O. Timpe, F. Girgsdies, R. E. Jentoft, F. Mothar, R. Schlögl, (in preparation).
- [44] F. Borgmeier, F. Rosowski, H. Martan, K. J. Müller-Engel DE 10 344 265 A1 (2004); BASF.
- [45] M. Abon, K. E. Bere, A. Tuel, P. Delichere, *Journal of catalysis* 156 (1995), 28.
- [46] J. Holmberg, R. K. Grasselli, A. Andersson, *Applied Catalysis A: General* 270 (2004), 121.

CONCLUSION AND OUTLOOK

Hydrothermal synthesis of phase-pure M1 MoVTeNbO_x catalysts was systematically investigated in the present work achieving a better understanding of the formation mechanism of the M1 phase, and an improved control over the final catalyst structure. Moreover, links between bulk and surface properties of the M1 phase and its catalytic behavior in the selective oxidation of propane to acrylic acid are discussed.

Preparation of phase-pure M1 was shown to be not trivial. Hydrothermal synthesis enables access to the chemical and structural complex M1 phase. However, precise control of the preparation parameters is required. Phase-pure M1 synthesis was achieved in this work by applying a preparative stoichiometry of the metals of $\text{Mo}_1\text{V}_{0.25}\text{Te}_{0.23}\text{Nb}_{0.12}$ and a molybdenum concentration of 0.25 M. Depending on the technical parameters of the autoclave used, optimization of hydrothermal conditions, particularly, temperature and synthesis time is necessary to obtain M1 precursors. SEM-EDX analysis, Raman and UV/VIS spectroscopy show that the metals (Mo, V, Te and Nb) are inhomogeneously distributed in the initial aqueous suspension of the metal salt solution and initially formed precipitates, which is introduced into the autoclave. However, the precursor materials obtained after the hydrothermal reaction already exhibit the chemical composition of phase-pure M1. M1 precursors show a fairly homogeneous spatial distribution of the elements with a remarkably high Nb content and a long-range order of metal-oxygen polyhedra in the crystallographic c direction (XRD, EXAFS). Obviously, the phase-purity of the Mo-V-Te-Nb oxide is determined by prearrangement of structural elements established in course of the hydrothermal process, being the essential step in the

preparation of phase-pure M1. Further crystallization of the precursor occurs during the subsequent heat treatment in an inert gas at 823-923 K.

It was shown that the presence of ammonium containing phases in the precursor leads to the formation of phase mixtures after activation (XRD, TG/MS).

No phase cooperation between M1 and M2 phase was found in this work. Phase-pure M1 catalysts showed a better catalytic performance in the selective oxidation of propane to acrylic acid than mixtures of phases. The catalytic performance of phase-pure M1 synthesized in this work is comparable to that reported in the literature and in patents. M1 converts propane with about 75 % selectivity into acrylic acid whereas the propane conversion is mainly dependent on the specific surface area. The M1 phase is characterized by a certain flexibility with respect to the chemical composition. However, any systematic correlation between the bulk concentration of a specific element and the catalytic properties was not observed within the variations studied in the present work. Moreover, it could be shown that M1 can be prepared with different morphology. The aspect ratio of the needle-like crystals has been changed by applying different pretreatment temperatures. However, it seems that the unique catalytic properties of the M1 phase are not related to the surface area of the crystallographic *ab* plane. Moreover, it was shown that M1 catalysts with different composition of the topmost surface layer (LEIS) show similar catalytic behavior. These observations are in agreement with a dynamic nature of the active moiety on the surface of M1 under reaction conditions. The surface of M1, which was confirmed to be covered by an approximately 0.7 nm thick, structurally disordered layer (TEM), was investigated by *in-situ* XPS in presence of different gas mixtures at pressures below 1 mbar, and at high temperatures (623 K).

These experiments indicated the re-distribution of the elements at the catalyst surface in response to changes in the composition of the gas phase. The tellurium content at the surface increases in presence of steam in the feed. The *ex-situ* comparison of spent catalysts also revealed an increased Te concentration at the surface, the higher the activity the higher the Te concentration. Furthermore, phase-pure M1 showed a reasonable stability under reaction conditions, which is of a great importance for its potential industrial application.

Additionally, new synthesis routes to multi-metal oxide catalysts were also proposed. Metal substitution and/or addition of suitable diluents to the Mo-V-X-Nb (X=Te, P, Bi) oxides were prepared and investigated in the selective oxidation of propane to acrylic acid. The results underlined the exceptional role that is attributed to the M1 phase but also proved that M1 is not necessarily required for acrylic acid formation. This supports the hypothesis presented in the present work that the active ensembles are generated on the surface of the catalyst under reaction conditions. Contrary to findings previously reported, the arrangement of atoms like in the crystalline structure of the M1 phase should not be considered as structural holder of the active centers, but more likely as their precursor.

The lack of a comprehensive understanding of the catalytic behaviour of these catalysts will render impossible a further improvement of the Mo-V-Te-Nb mixed oxide catalysts and/or the development of new solid catalysts suitable for acrylic acid production starting from propane. Hence, *in-situ* methods, as for example *in-situ* Raman, *in-situ* IR and *in-situ* XRD, should be applied under conditions of propane oxidation in presence of C₃H₈, O₂, N₂ and H₂O at T = 673 K and p = 1 bar with the purpose of getting a realistic view of

the catalyst bulk and surface in contact with the gas phase. Stability of phase-pure M1 should also be confirmed in a long-term catalytic test experiment. It is important to monitor possible sintering of the M1 crystallites or phase transformation during time on stream by *in-situ* XRD. Additionally, further development of the new potential synthesis routes of the multi-metal oxides presented in this work (diluted and undiluted Mo-V-X-Nb (X=Te, P, Bi) oxides), together with the optimization of the reaction conditions for these alternative catalysts, are of high interest.

APPENDIX

Curriculum Vitae

Almudena Celaya Sanfiz

Persönliche Angaben:

Geburtsdatum: 16-März-1978
 Geburtsort: Incio (Lugo)
 Staatsangehörigkeit: spanisch

Akademische Ausbildung:

seit 01/2004	Dissertation: „Synthesis and Investigation of phase-pure M1 MoVTenbO _x Catalysts for Selective Oxidation of Propane to Acrylic Acid“, Fritz-Haber-Institut der Max-Planck Gesellschaft , Berlin, unter der Leitung von Prof. Dr. R. Schlögl und Dr. A. Trunschke.
10/2000-10/2001	Studienaustausch (Erasmus-Programm) mit der Universität Kaiserslautern . Fachrichtung Chemieingenieurwesen: neuntes und zehntes Semester. Diplomarbeit: „Simulation von Sorptionszyklen in halbtechnischen Aktivkohleschüttungen“; Note: Sehr Gut mit Auszeichnung; Lehrstuhl für Thermische Verfahrenstechnik von Prof. Dipl.-Ing. Dr. techn. Hans-Jörg Bart.
10/1996-10/2000	Studium an der Universität Oviedo (Spanien) . Fachrichtung Chemieingenieurwesen: Erstes bis achtes Semester.

Schulausbildung:

1991 – 1996	Gymnasium “Instituto Marqués de Casariego”, Tapia de Casariego (Spanien). Abitur mit der Gesamtnote Sehr Gut mit Auszeichnung.
1981 – 1991	Grundschule „Colegio Principe de Asturias“, Tapia de Casariego (Spanien). Grundschulabschluss mit der Gesamtnote Sehr Gut

Sprachkenntnisse:

Spanisch	Muttersprache
Deutsch	Fließend in Wort und Schrift. DSH (Deutsche Sprachprüfung für den Hochschulzugang).
Englisch	Fließend in Wort und Schrift. Zertifikat der offiziellen Sprachschule in Spanien (10 Semester). Irland: zwei 4-wöchige Sommerkurse.
Griechisch	Grundkenntnisse

Berufserfahrung:

09/2002 – 12/2003	Wissenschaftliche Mitarbeiterin am Forschungszentrum Karlsruhe, Institut für Technische Chemie, Abteilung Thermische Abfallbehandlung ; im Rahmen eines EU-Projektes mit dem Thema: „Konzepte modularer Kleinkraftwerke zur dezentralen Kraft-Wärme-Nutzung mit biogenen Festbrennstoffen“.
01/2002 – 07/2002	Wissenschaftliche Hilfskraft am Lehrstuhl für Thermische Verfahrenstechnik von Prof. Dipl.-Ing. Dr. techn. Hans-Jörg Bart.
01/2001 – 07/2001	Wissenschaftliche Hilfskraft am Lehrstuhl für Thermische Verfahrenstechnik von Prof. Dipl.-Ing. Dr. techn. Hans-Jörg Bart.

Berlin 2008

Publication Index

Articles

A novel synthetic route to mesostructured MoVTaNb mixed oxide

A. Sakthivel¹, A. Trunschke¹, T. W. Hansen¹, A. Celaya Sanfiz¹, O. Timpe¹, F. Girgsdies¹, R. E. Jentoft¹, F. Mothar¹, R. Schlögl¹; in preparation.

Preparation of phase-pure M1 MoVTaNb oxide catalysts by hydrothermal synthesis – Influence of reaction parameters on structure and morphology

A. Celaya Sanfiz¹, T. W. Hansen¹, F. Girgsdies¹, O. Timpe¹, E. Rödel¹, R. Ressler², A. Trunschke¹, R. Schlögl¹; accepted for publication in Topics in Catalysis.

Investigation of catalytic behavior of M1-phase catalyst in the selective oxidation of propane to acrylic acid. Correlation approach between catalytic performance and surface/bulk properties.

A. Celaya Sanfiz¹, T. W. Hansen¹, F. Girgsdies¹, P. Schnörch¹, D. Teschner¹, A. Trunschke¹, R. Schlögl¹, M. H. Looi³, S. B. A. Hamid³; in preparation.

How important is the (001) plane of M1 for selective oxidation of propane to acrylic acid.

A. Celaya Sanfiz¹, T. W. Hansen¹, A. Sakthivel¹, A. Trunschke¹, R. Schlögl¹, A. Knoester⁴, H. H. Brongersma⁴, M. H. Looi³, S. B. A. Hamid³, *Journal of Catalysis* 258 (2008), 35.

New synthesis routes of MMO catalysts by dilution of Mo-V-X-Nb (X=Te, Bi, and P) mixed oxides with SiO₂, Cr₂O₃ or ZrO₂ for the oxidation of propane to acrylic acid.

A. Celaya Sanfiz¹, F. Girgsdies¹, A. Trunschke¹, R. Schlögl¹, M. H. Looi³, S. B. A. Hamid³; in preparation.

¹ Fritz Haber Institute of the Max Planck Society, Department of Inorganic Chemistry, 14195 Berlin, Germany.

² Technische Universität Berlin, Institute of Chemistry, 10623 Berlin, Germany.

³ COMBICAT, University Malaya, 50603 Kuala Lumpur, Malaysia.

⁴ Calipso B.V., 5600 MB Eindhoven, The Netherlands.

Posters

Preparation and Characterization of Mo-V-M-Nb-O (M=Te, P, Bi) Catalysts prepared by Hydrothermal Synthesis

A. Celaya Sanfiz, J.B. Wagner, A. Trunschke, R. Schlögl, S.T. Lee, M.H. Looi, S.B.A. Hamid, XXXVIII. Jahrestreffen Deutscher Katalytiker, March 16-18, **2005**, Weimar/Germany.

Oxidación Selectiva de Propano a Ácido Acrílico sobre Catalizadores de Óxidos de Mo-V-Te-Nb preparados por el Método Hidrotermal

A. Celaya Sanfiz, J.B. Wagner, A. Trunschke, R. Schlögl, S.T. Lee, M.H. Looi, S.B.A. Hamid, SECAT'05, Reunión de la Sociedad Española de Catálisis, June 27-29, **2005**, Madrid/Spain.

Mo-V-Te-Nb-O Mixed Metal Oxides –“Diluted” and “Undiluted”- Prepared by Hydrothermal Synthesis for Selective Oxidation of Propane to Acrylic Acid

A. Celaya Sanfiz, J.B. Wagner, A. Trunschke, R. Schlögl, S.T. Lee, M. H. Looi, S.B.A. Hamid, EuropaCat-VII, August 28-September 01, **2005**, Sofia/Bulgaria.

Selective Oxidation of Propane to Acrylic Acid on Mo-V-Te-Nb-O Mixed Oxides Catalysts Prepared by Hydrothermal Synthesis

A. Celaya Sanfiz, J.B. Wagner, A. Trunschke, R. Schlögl, S.T. Lee, M. H. Looi, S.B.A. Hamid, 5WCOC, The World Congress of Oxidation of Catalysis, September 25-30, **2005**, Sapporo/Japan.

The Effect of Thermal Pre-treatment Parameters on Structural and Catalytic Properties of MoVTenbO_x Catalysts

A. Celaya-Sanfiz, A. Blume, O. Timpe, R. Jentoft, F. Girgsdies, A. Trunschke, R. Schlögl, XXXIX. Jahrestreffen Deutscher Katalytiker, March 15-17, **2006**, Weimar/Germany.

Microstructure, Bulk and Surface Properties of Single-phase MoVTenb Oxide Catalysts

A. Celaya Sanfiz, F. Girgsdies, T. W. Hansen, P. Schnörch, E. Rödel, A. Trunschke, R. Schlögl, M. H. Looi, S. B. A. Hamid, 40 Jahrestreffen Deutscher Katalytiker, March 14-16, **2007**, Weimar/Germany.

Synthesis of Single-phase M1 MoVTenbO_x Catalysts – Optimization of Hydrothermal Reaction Conditions

A. Celaya Sanfiz, F. Girgsdies, T. W. Hansen, E. Rödel, P. Schnörch, A. Trunschke, R. Schlögl, EuropaCat-VIII, August 26-31, **2007**, Turku/Finland.

Selective Oxidation of Propane over MoVTeNb Oxide Catalysts Prepared by Hydrothermal Synthesis

A. Celaya Sanfiz, F. Girgsdies, T. W. Hansen, P. Schnörch, D. Teschner, A. Trunschke, R. Schlögl, M. H. Looi, S. B. A. Hamid, 41 Jahrestreffen Deutscher Katalytiker, February 27-29, **2008**, Weimar/Germany.
